journal of the international meteor organization

WGN

47:1
february 2019

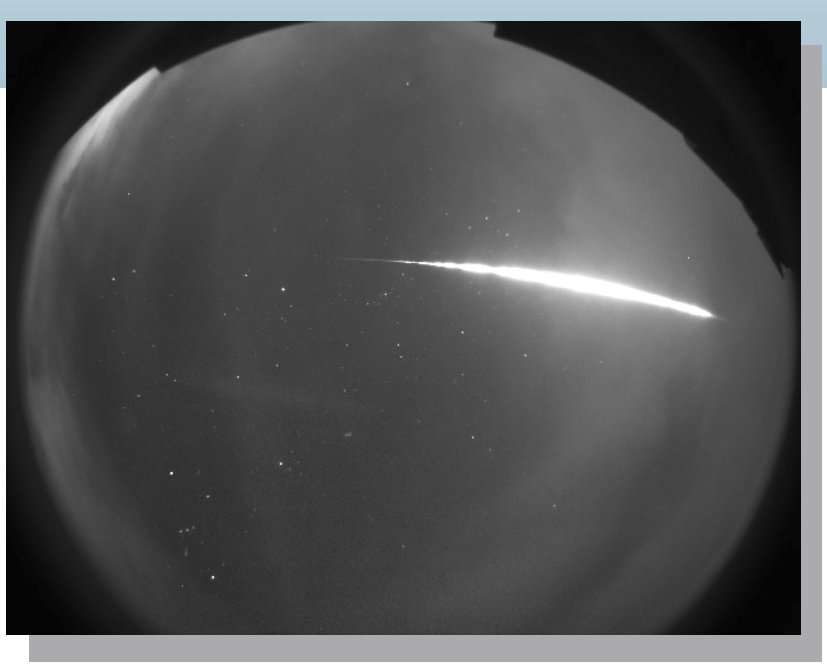

ISSN 1016-3115

WGN Vol. 47, No. 1, February 2019, pp. 1 – 42

Administrative

Conferences

Meteor showers

Meteor observations

Preliminary results

Front cover photo

Impressive fireball photographed on 2019 January 30 at $15^{h}48^{m}$ UT from Severskaya, Krasnodar Krai, Russia. Photo courtesy: Oleg Milantiev.

Writing for WGN

This Journal welcomes papers submitted for publication. All papers are reviewed for scientific content, and edited for English and style. Instructions for authors can be found in WGN **45:1**, 1–5, and at `http://www.imo.net/docs/writingforwgn.pdf` .

Copyright

Legal address

International Meteor Organization, Jozef Mattheessensstraat 60, 2540 Hove, Belgium.

Janus

Cis Verbeeck[1]

Welcome to the first WGN issue of 2019!

2018 was an interesting year, and featured a few interesting shower returns. An abundance of bright Perseid meteors observed during a short interval around 18^h30^m UT on August 12 clearly confirmed Peter Jenniskens's prediction of a Perseid filament (see below). And in the night of October 8-9, a month after the associated comet 21P/Giacobini-Zinner reached its perihelion, European observers noticed a sharp increase of activity of the Draconids, with ZHRs ranging to about 100 or more. The Draconid outburst was particularly rich in faint meteors. Preliminary analysis of data from the IMO Video Network suggests a population index $r = 3.4$ (which would be the largest r-value ever measured), and shows evidence for three distinct peaks in flux density. It will be interesting to study the video and visual observations of the Draconids in more detail.

The IMC 2018 took place in Pezinok, Slovakia, and was organized by the Modra Observatory of the Comenius University in Bratislava. The conference was a big success and drew 127 participants from 28 countries. As always, the public was a mixture of amateurs with a substantial minority of professional meteor scientists. The distribution of talks at an IMC reflects how hot various subfields of meteor science are, and what the main trends are.

While there were not many talks on visual observations, Jürgen Rendtel exploited IMO's unique long-record track of visual observations to study the evolution of Geminid activity from about 1900 till present. Another highlight was the Visual Workshop which preceded the IMC, and where the participants analyzed the Perseid 2018 observations and detected clear signs of a Perseid filament of many bright meteors (Rendtel et al., 2019), close to the time predicted by Peter Jenniskens (2006, table 5d on pages 659ff). This is the first time that a global analysis of visual observations was performed with Kristina Veljković's meteor analysis software MetFns. This very fruitful and relatively easy way of working opens the way to many new global analyses of meteor showers, since the participants of the workshop have now grasped the intricate considerations involved in global shower analysis, which were previously only known to a few experts. Moreover, the Proceedings of the IMC 2018 will feature a paper that aims to provide insight into the trial and error procedure used in the analysis of the Perseids 2018. This means YOU can start the global analysis of a meteor shower yourself! Both the VMDB and MetFns are freely available via the IMO website. If you are interested in performing a global analysis yourself, we recommend contacting `visual@imo.net`, so you can participate in a joint global analysis before you venture on your own.

It is clear from the talks at the IMC 2018 that video observations are ever more ubiquitous, spawning significant and indeed impressive results. Since video technology quickly evolves, resulting in many different technical solutions, standardization unfortunately is much more difficult. Still, the possibilities offered by video observations are amazing. Consideration of the influence of various observing parameters such as camera pointing direction and field of view led Sirko Molau to investigate the optimal viewing direction for video observation, dependent on amongst others the limiting magnitude and the population index of the meteor shower.

Radio observations of meteors are an inherently indirect and rather complicated way of studying meteors. Though no standard data format is currently employed for radio observations and there is no IMO database for radio observations, the Radio Meteor Observing Bulletin (RMOB) has gathered radio data worldwide since 1993. At present, no single standardized reduction method for radio data is in use, but promising advances have been made in the past years, for example by Ogawa and Steyaert (Ogawa & Steyaert, 2017) and the BRAMS team (Verbeeck et al., 2018). I expect this field to grow to a more mature state in the years to come.

Since a few years, meteor spectroscopy is gaining interest, thanks to the availability of sensitive video cameras and relatively cheap gratings. The Spectroscopic Workshop, which preceded the IMC, brought together both professionals and amateurs to discuss the scientific use and needs of spectroscopic meteor observations, with a focus on calibration and which spectral resolution is needed to contribute to our scientific understanding.

Fireballs and meteorites are becoming an increasingly large topic as fireball networks, hunting for new meteorites, grow and gain in quality. Finding a new fireball with a known orbit is very valuable, as there are not more than a few tens of meteorite recoveries that also have an accurate orbit. The chain comets/asteroids/meteoroids/meteors/meteorites was addressed in several IMC talks and is an exciting avenue as many pieces of the puzzle fit together in this kind of approach. Complementary to the fireball networks, IMO's fireball form and

[1] Bogaertsheide 5, 2560 Kessel, Belgium.
Email: `cis.verbeeck@scarlet.be`

IMO bibcode WGN-471-verbeeck-janus NASA-ADS bibcode 2019JIMO...47....1V

page (`http://fireballs.imo.net/members/imo/`) builds on the contributions by the general public as eye witnesses of bright fireball events, sometimes with smartphone images or videos. IMO's fireball page is most often the fastest source for information about a fireball, and intends to be a comprehensive page gathering all information about specific fireball events. What is often still missing, is the footage from fireball cameras and networks. I call upon you to register your network at `https://www.amsmeteors.org/members/cam_uni_api`. Once you have gotten an API key, it should be quite easy to upload images/videos of a fireball, such as in `https://www.imo.net/members/imo_video/view?video_id=87`.

In 2018, there were 8 bright fireballs with more than 200 reports. You can find more information in Table 1 and 2, and I encourage you to check out our new *International Fireball Program* widget on the IMO website (or `https://www.imo.net/observations/fireballs/fireball-report-program/`) for more detailed statistics and visualizations.

Table 1 – Number of fireball reports in 2017 and 2018 (total number of reports, number of reports entered via IMO form or customized form (non-AMS), and percentage of reports entered via IMO form or customized form).

Year	# reports	# IMO reports	IMO contribution (%)
2017	28 306	8 129	29%
2018	23 787	7 960	33%

Table 2 – Number of fireball events in 2017 and 2018 (total number of events, number of events entered via IMO form or customized form (non-AMS), and percentage of events entered via IMO form or customized form).

Year	# events	# IMO events	IMO contribution (%)
2017	6 170	2 010	33%
2018	6 762	2 729	40%

I am happy to say that since the inception of the new IMO website in 2016, IMO membership has increased from 291 in 2016 to 323 in 2017 to 353 in 2018. I wish to thank Mike Hankey and Vincent Perlerin for their great achievements in developing and maintaining the IMO website, and Karl Antier for his excellent job as webmaster. Likewise, I am grateful to all IMO officers, contributing in various ways to the achievement of IMO as an organization solely borne by volunteers.

The IMC 2019 in Bollmansruh, Germany on October 3-6 will present another great opportunity to meet meteor workers worldwide, to share your passion with fellow meteor enthusiasts, and to return home full of new ideas and plans. I hope to meet you there! Another highlight will be the Meteoroids conference in Bratislava, Slovakia, June 17-21, where most of the participants are professional meteor scientists.

I wish you a great, healthy and happy 2019 with clear skies and a lot of fun and success with your meteor work!

References

Jenniskens P. (2006). *Meteor showers and their parent comets.* Cambridge Univ. Press.

Ogawa H. and Steyaert C. (2017). "Major and daytime meteor showers using global radio meteor observations covering the period 2001–2016". *WGN, Journal of the IMO*, **45:5**, 98–106.

Rendtel J., Veljković K., Weiland T., Verbeeck C., and Knöfel A. (2019). "Perseids 2018 — analysis of global visual data". *WGN, Journal of the IMO*, **47:1**, 18–25.

Verbeeck C., Lamy H., Calders S., Tétard C., and Martínez Picar A. (2018). "Overview of major shower observations 2016–2017 by the BRAMS network". In *Proceedings of the International Meteor Conference 2017, Petnica, Serbia, September 21–24.* pages 138–144.

Janus *was a Roman god with two faces, one looking to the past and one to the future, called upon at the beginning of any enterprise. Today he is often a symbol of re-appraisal at the start of the year.*

Conferences

Thirty-Eighth International Meteor Conference, Bollmannsruh, Germany, 2019 October 3–6

Rainer Arlt, Jürgen Rendtel, Ina Rendtel, André Knöfel, Sirko Molau, Roland Winkler

1 Venue

The 38th International Meteor Conference (IMC) will be held in Bollmannsruh, Germany, a countryside place not far from Berlin. The venue is a youth hostel by a lake, which hosted the IMC already in 2003. The hostel is called KiEZ Bollmannsruh and can as such be found on Google maps. Alternatively, the address is Bollmannsruh 13, 14778 Päwesin, Germany, or it can be found at the geographical coordinates 52.506° N, 12.679° E. We were able to rent the entire place for October 3–6. Earlier dates were not available in 2019. The hostel offers accommodation in bungalows, a conference hall as well as a few smaller seminar rooms. Note that the relatively remote location brings along rather poor connectivity to the internet.

The web page of the hostel is `http://kiez-bollmannsruh.de/`. The area is a 25-acre place for recreation with surrounding forests and fields for extensive hikes. For the brave, swimming in the lake is possible, but water temperatures will have dropped to about 15°C by October.

2 Location

Bollmannsruh is situated in the western part of the German state of Brandenburg and actually close to the eponymous city of Brandenburg. The oldest settlements at its location date back to the 8th century, while a bishopric was founded in the 10th century. The city was first mentioned to have town privilege as early as 1170 CE.

From the motorway A2, it takes about half an hour by car to reach Bollmannsruh. There is a large parking area in front of the KiEZ grounds. Brandenburg has a train station with trains directly to Berlin Hauptbahnhof (main station). The trains are called RE1.

The two airports of Berlin are called Tegel (TXL) and Schönefeld (SXF). Budget airlines tend to prefer Schönefeld as their destination. The new airport of Berlin will not yet be operational in 2019. Tegel connects to Berlin main station with a bus, while Schönefeld is connected by a city train (S-Bahn). The RE1 is the relevant train also for people arriving by train; coming from northern, eastern and southern Europe, they change to RE1 in Berlin, while people coming from western Europe may also change to RE1 in Magdeburg. We will arrange for cars shuttling to Brandenburg main station on Thursday and Sunday.

You may consider combining the trip to the IMC with a visit to the nature reserve “Westhavelland” offering very dark skies, which you can reach by car in about 45 minutes. The new Moon on September 28 favours the nights before the IMC.

[1]Arbeitskreis Meteore e.V., Germany. Email: `rarlt@aip.de`

Figure 1 – Main building of KiEZ in Bollmannsruh, where the conference hall is located.

Figure 2 – Bungalows with two rooms each, sharing a bathroom.

3 Programme and events

The scientific programme will start in the morning of Friday, 2019 October 4, and will end on Sunday noon, October 6. All oral presentations will be given in the main conference hall; there will be no parallel sessions. We will also arrange for ample poster space, but it may not be in the immediate proximity of the conference hall.

The Saturday afternoon is reserved for an excursion to Potsdam in order to visit the "Telegraph hill" hosting the historical buildings of the Astrophysical Observatory of Potsdam, founded in 1874. With the advent of spectroscopy, it was the first observatory addressing physical questions of celestial bodies, such as their composition and physical processes they imply, in contrast to positional astronomy and celestial mechanics. The observatory includes the Einstein Tower, a still operational solar telescope housed in an impressionistic structure of 1920s. The hill hosts several scientific institutes as well as a replica of the optical telegraph that gave the hill its name.

Figure 3 – Lakeside of the IMC location.

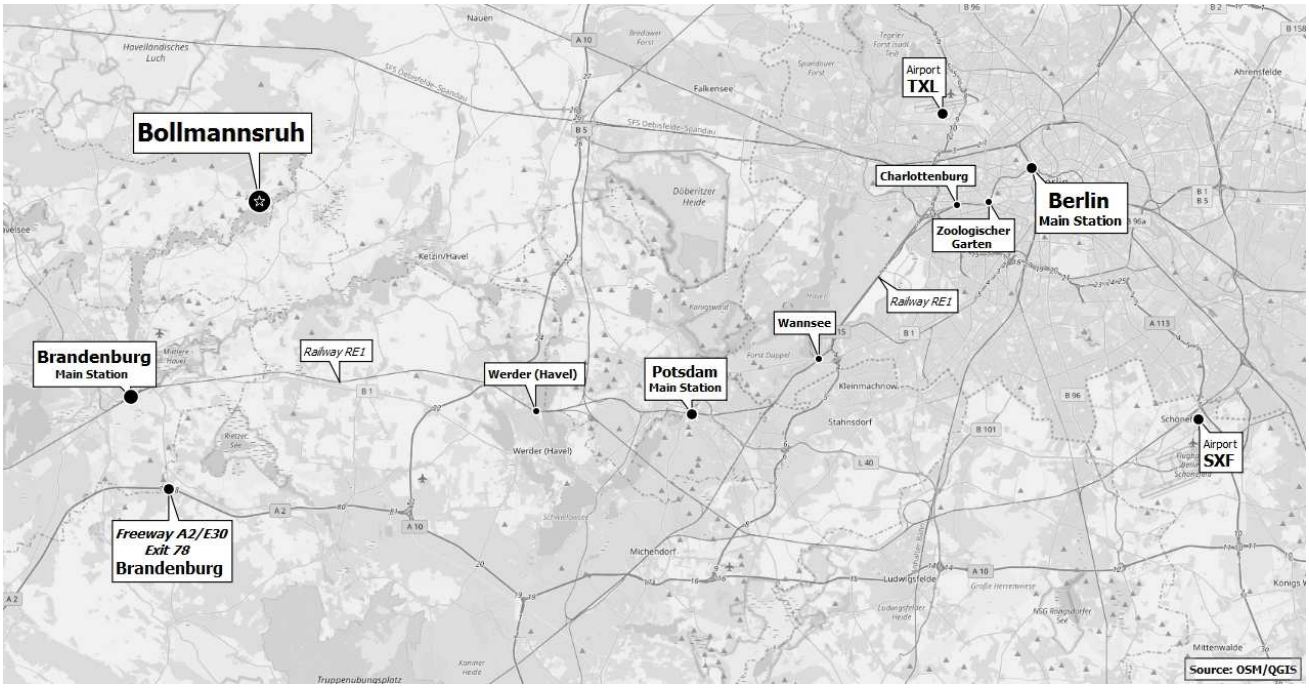

Figure 4 – Map with the IMC location west of Berlin.

4 Registration and payment

The early-bird registration fee is 160 EUR for accommodation in two-bed rooms, while a limited number of rooms with single occupancy is available for the early-bird registration fee of 190 EUR. Registration fees after 2019 June 30 will be 180 and 210 EUR, respectively.

There is also a hotel in the vicinity of the conference venue.
(`https://www.hotel-bollmannsruh.de/home.html`) Booking the hotel (or any other location) is on your own; we request a conference fee of 90 EUR in this case (which includes also the meals during the day and the excursion). Please visit `http://imc2019.imo.net` for further details and a registration page.

The local organising committee consists of members of the Arbeitskreis Meteore (AKM), the German society for meteors and atmospheric phenomena. The IMC 2019 will be kindly supported by the Vereinigung für Sternfreunde (VdS), the largest German society for astronomy.

IMO bibcode WGN-471-arlt-imcsecann NASA-ADS bibcode 2019JIMO...47....3A

Figure 5 – The Great Refractor at Telegraph Hill in Potsdam will probably be the highlight of the excursion on Saturday.

Figure 6 – The Einstein Tower is located very close to the Great Refractor and serves as a solar observatory.

Meteor showers

Showers of the IAU Meteor Data Center in the video data of SonotaCo: a simple and clear criterion for grading meteor showers

Masahiro Koseki[1]

We investigated radiant distributions of all listed meteor showers in the IAUMDC meteor shower database (SD) of 2018 January 18 version (IAUMDC, 2018) including those with pro-tempore status using SonotaCo net video meteors. The distributions show that the radiant density around the solar longitude of the peak shower activity can indicate the plausibility of a meteor showers existence. It is essential to express radiant points in $(\lambda - \lambda_s, \beta)$ coordinates because the radiant shift is almost cancelled in these coordinates.
The radiant density ratios (DR) within 3° to between 3° to 6° from the center of the radiant concentration can be a very simple criterion for the confirmation of a meteor shower activity without knowing the velocity difference. We calculate DR values of all established showers and several notable showers of the working status in SD except for daytime showers. It became clear that DR should be larger than 2 during 10° in the solar longitude of the observations in order to confirm the activity.
The DR is a very simple measure but can be a useful tool to confirm the detection of a meteor shower activity. We found out several entries in the working status are clearly confirmed by DR, though there are many problematic entries in the established showers.

Received 2018 November 13

1 Introduction

We viewed major showers through video data in both SonotaCo net and CAMS, and recognized that radiant distributions are simple and therefore a very useful tool for analyzing shower activity (Koseki, 2018). The SonotaCo net published meteor data on the web for 2007–2016 (SonotaCo, 2017). CAMS data are now available only from 2010 October 21 to 2013 March 29 (Jenniskens et al., 2016). It is, therefore, suggested that the research of the radiant distribution on all SD showers using SonotaCo net 2007–2016 data would be very interesting. We call SonotaCo net 2007–16 data simply video data hereafter, if not noted otherwise.

We included all nighttime established showers and several working status showers in the video data search and try to present a new simple criterion for the meteor shower research. It was almost impossible to set a criterion for analyzing the inconsistency using SD itself. Problems are caused by the reported data themselves and also because there are many problems in the SD.

The author had analyzed the SD by using D_{SH} (Southworth & Hawkins, 1963) and identified many inconsistent data (Koseki, 2016). The differences are caused mainly by the shower definition of each research and not so much by observational devices, though there are some cases affected by observational conditions such as weather conditions and missing the maximum. It is, therefore, necessary to execute the preliminary search on the SD.

[1]The Nippon Meteor Society, 4-3-5 Annaka-shi, Gunma-ken, 379-0116 JAPAN. Email: geh04301@nifty.ne.jp

IMO bibcode WGN-471-koseki-grading
NASA-ADS bibcode 2019JIMO...47....7K

2 Preliminary search

We made radiant point (RP) distributions on $(\lambda - \lambda_s, \beta)$ coordinates for all SD showers both for established and working, excluding only those with insufficient entries (lacking radiant data). The SD has several entries for one shower and, therefore, it is necessary to select the representative data by following procedures. We use IAUMDC No. + Code + AdNo to indicate the individual record in order to clarify the different entry and indicate the representative entry by this abbreviation.

1. Video data is the preferred because SonotaCo net data itself represents video observations.

2. The entry based on the most abundant data is the most preferable.

3. If there is no video results, the first entry is the preferred one.

We select video data during 15° in solar longitude around the maximum of each representative entry and plot on the x-y-plane by $(\lambda - \lambda_s, \beta)$ coordinates. It is very natural that the intensity of meteor activities are widely different; we can easily point out the meteor activity in case of major showers (Figure 1a: η-Aquariids (31 ETA)), but cannot recognize clear concentrations for even established showers in all cases (Figure 1b: Northern δ-Cancrids (96 NCC)). On the other hand, some working showers show distinct activity (Figure 1c and 1d: ζ-Cassiopeiids (444 ZCS) and August γ-Cepheids (523 AGC), respectively). The $\lambda - \lambda_s$ of the selected radiant runs along the y-axis and intervals on axes marked in degrees and $\lambda - \lambda_s$ increases to the left in these figures.

It is interesting to mention some unique showers. The τ-Herculids (61 THE) and the Corvids (63 COR)

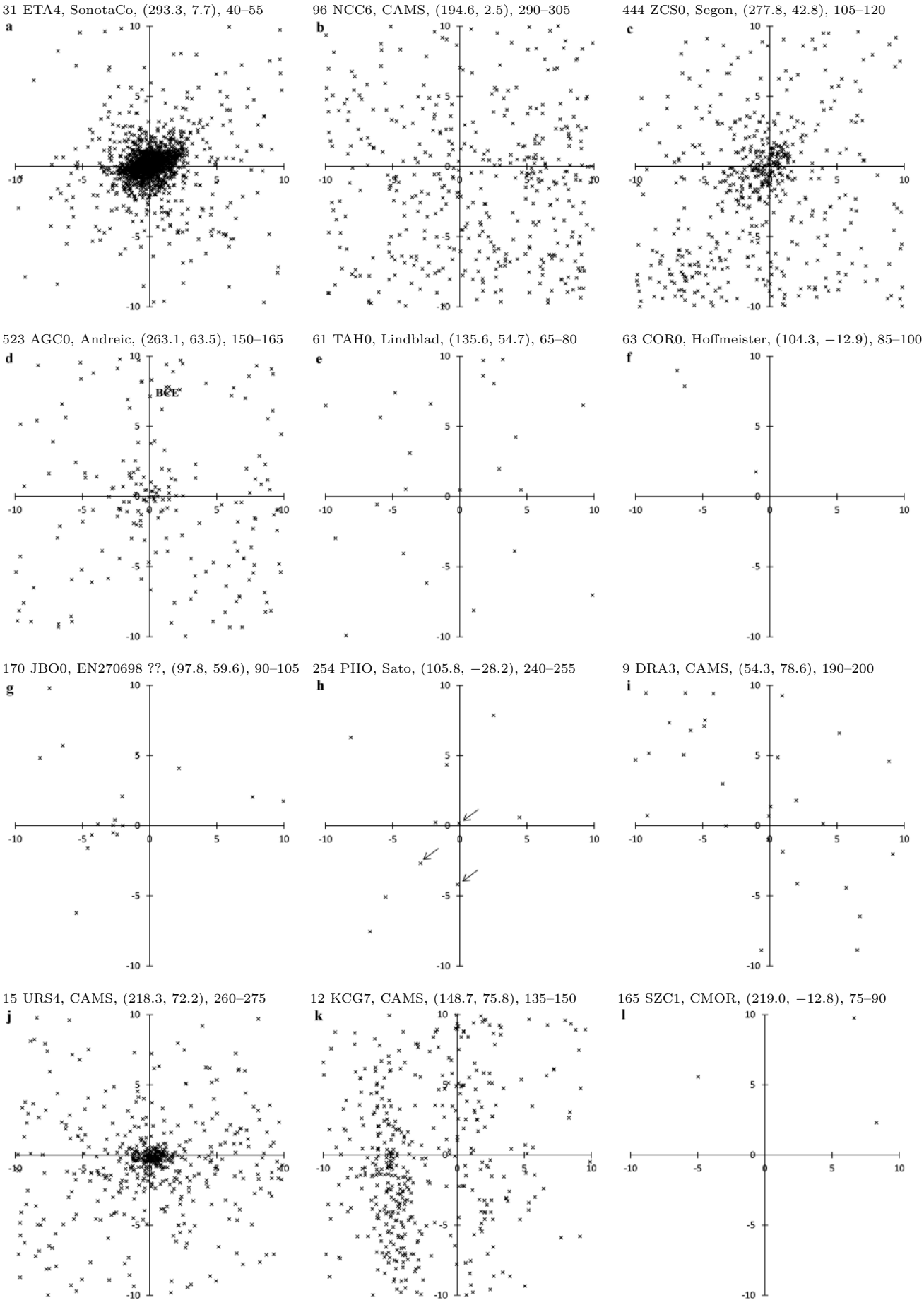

Figure 1 – Radiant distributions in right ascension and declination constructed in the preliminary survey (Section 2). For each of figures (a to l) we provide the shower code, the source, the radiant point in $(\lambda - \lambda_s, \beta)$ and $\Delta\lambda_s$ (the solar longitude of the considered period).

are probably meteor showers with only one observed return. There is no sign of them in SonotaCo net data (Figure 1e and 1f), though SD has two uncertain entries each. Their orbits would be changed by the perturbations and might appear again but their radiant might change also. 170 JBO (June Bootids) and 254 PHO (Phoenicids) are somewhat different. JBO were observed by SonotaCo net 2010 (Figure 1g); the center of this figure is based on a fireball radiant EN270698 and the radiants on the left of the center are recorded in 2010 observations, that is JBO. PHO are thought to be originated from comet 289P/Blanpain and lost, but Sato et al. (2017) detected activity in 2014, though the radiant point shifted largely. SonotaCo net recorded three PHO meteors from Japan (Figure 1h) in 2013 and 2014; this figure is produced by Sato's estimated RP (Sato & Watanabe, 2010). The 9 DRA (Draconids) have a periodic nature known as well and not leave a clear trace in SonotaCo net (Figure 1i). 15 URS (Ursids) are thought as one of the periodic showers but SonotaCo net recognized them annually. Particularly abundant URS were captured in 2011 (Figure 1j).

The radiant density would play an important role to evaluate the meteor shower significance. We recognized the validity of the ratio of radiant number within 3° to the outer area for distinguishing meteor shower activity from sporadic background even if the observational conditions are different (Koseki, 2018). But there are many entries in SD showing curious figures; the distribution core does not coincide with the location of the entry (Figure 1k: 12 KCG, κ-Cygnids) or there is no sign of the meteor shower activity and so on (see Figure 1l, though CAMS insists meteor activity (165 SZC2, Southern June Aquilids) apart from SZC1 $\Delta\lambda_s = 23.5$ as SZC). It is clear that we need to select a more plausible entry to study the criterion in the Section 4.1.

3 Views of SD showers through video data

3.1 Selection of the most plausible entry for each shower

It became clear we should select the most representative entry of each shower when we study the radiant distributions of SD showers. We checked problematic entries in the SD and selected the most plausible entry by following steps for showers having multiple entries.

1. Calculate median values of RPs and the solar longitude of the maximum activity for all entries of the shower. The mean values are less important for this process, because there are several far apart entries. We select the entry nearest to the median values of the both as the preliminary representative.

2. Check the distribution of the shower radiants of all entries of the shower. We draw the distribution of the shower radiants of every entry around the preliminary representative and calculate the distance from it. If there is more suitable candidate that can be situated at the center of the distribution and reduce the distance of the farthest, we would consider it the representative.

3. Check the activity maximum solar longitude of all entries of the shower. If the selected entry is far from the median of the maximum, we would change it with the next candidate in the second step.

Table 1 – Radiant distribution of Perseids and Geminids. R is the distance from the radiant in degrees. S is the area (square degrees) between R of this line and $R-1°$; when $R = 1$, the area is the circle around the radiant. n and D are the number of radiants and the density between R and $R-1$.

		Perseids		Geminids	
R	S	n	D	n	D
1	3.14	3561	1133.53	11452	3645.38
2	9.42	4380	464.79	3997	424.15
3	15.70	2017	128.45	1502	95.65
4	21.98	831	37.81	777	35.35
5	28.24	385	13.63	496	17.56
6	34.50	209	6.06	372	10.78
7	40.75	149	3.66	258	6.33
8	46.99	106	2.26	175	3.72
9	53.21	95	1.79	157	2.95
10	59.42	65	1.09	109	1.83

We found the problematic showers by this procedure and by the preliminary search of the Section 2. We will study some detail in the Section 6. There are many showers showing clear radiant concentration naturally, though some of them are of working status. We will mention such showers in the Section 3.4.

3.2 Basic idea of the simple criterion

Preliminarily drawn radiant distributions show the many radiants, the majority of which are distributed within 3° from the center. The radiant distributions of Perseids and Geminids seem to be widely spread and there are many radiants over 3° in appearance (Figure 2a and 2b). When we examine the radiant density per square degrees, it is very clear the density decreases rapidly with the distance from the center (Table 1). If we select other weak dispersed showers having elongated radiant area, for example KCG (see Figure 1k), the radiant density would descend with the distance from the center (Figure 3).

The author introduced the ratio of radiant number within 3° (N3) to the number between 3° and 10° (N10) to compensate for the influences of the observational circumstances: weather, background sporadic activity (Koseki, 2018). This idea has worked well and revealed more clear activity profiles (see Figure 17b for 5 SDA and Figure 27c for CAMS 2 STA and 17 NTA in Koseki (2018)). The preliminary survey mentioned above shows another shower activity hinders the radiant distribution when we adopt outer area as 3° to 10°. Therefore, it is better to use 3° to 6° instead of 10° as outer reference area. And, we calculate the radiant density per square degrees for both areas ($D3$

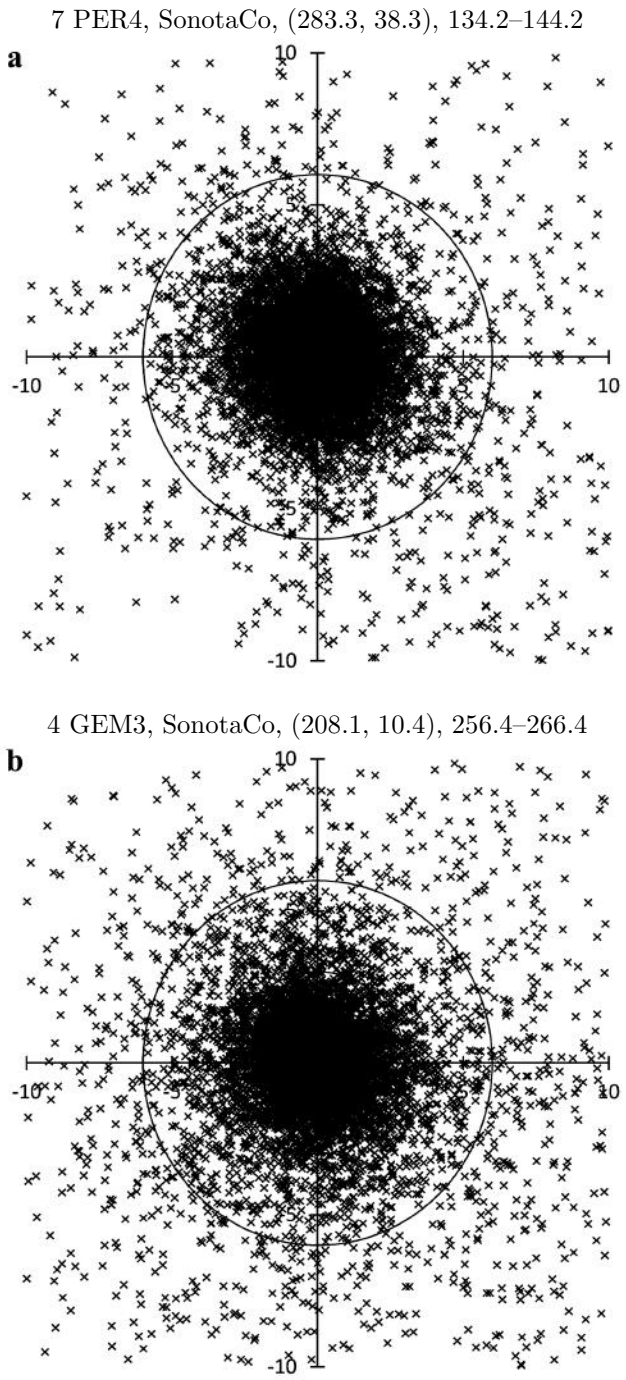

Figure 2 – Radiant distributions in right ascension and declination and circles of $r = 3°$ and $6°$. For the showers we provide the same data as in Figure 1.

and $D6$ respectively) and use the ratio $D3/D6$; for an example, $D3 = (n1 + n2 + n3)/(S1 + S2 + S3)$ and $D6 = (n4 + n5 + n6)/(S1 + S2 + S3)$ in Table 1 (here the number 1–6 in $n1$–$n6$ and $S1$–$S6$ means R of the table).

The major part of the radiants can be recorded within 5° to both sides from the maximum and the recorded number of meteors decreases also apart from the maximum (Figure 3 of Koseki (2012a)). We shorten the period by 5° compared with the former mentioned preliminary search and select data within 5° both sides from the maximum; the distribution would change little though.

We intend to propose a simple criterion.

1. The RP should be expressed by $(\lambda - \lambda_s, \beta)$.
2. The ratio of D3/D6 should be higher than 2; we name this ratio simply DR (Density Ratio).
3. The meteor number N3 recorded before and after the maximum 5 degrees in solar longitude should be not less than 10.

It is noteworthy to note that RP should be expressed on $(\lambda - \lambda_s, \beta)$ coordinates. If we represented it on (α, δ) coordinates, we had to correct the radiant motion. We can disregard such drift when the shower radiant on $(\lambda - \lambda_s, \beta)$ coordinates of $\Delta\lambda_s < 10$. If we limit the data within $\Delta\lambda_s < 10$, we can ignore the change of the geocentric velocity also, though we simply use the radiant distributions. The velocity distribution is discussed in the next section.

The radiant density decreases with the distance from the center (listed radiant), even if the form of the distribution and the intensity of the activities are different. Therefore the ratio of the radiant density of inner area to outer area should be larger than 1 for the existent activity. It is proper to suppose the ratio of DR fluctuates by chance and the probable limit is about 2.

The third condition might be different in the other surveys and the 10 radiants correspond to about 0.005% in SonotaCo net data.

3.3 The results of the DR survey on SD

We calculated DR and N3 for 95 established showers in SD excluding 17 Southern and Daytime showers: XSA, ACE, MKA, PPU, APS, NOC, OCE, SMA, ZPE, BTA, XRI, BHY, ZCA, KLE, PHO, EPR, DLT (Table 2). We surveyed 78 working status showers recognized interesting by the preliminary search in SD also (Table 3).

Showers in Tables 2 and 3 are listed in descending order of DR and show that ETA is the highest. When a shower radiant is located in a scarce sporadic background, the DR becomes higher naturally (see Figure 1a). As we see radiant distributions visually in the preliminary search, we can express the sense on the concentration by DR here objectively. Major showers having clear concentration get high DRs and working showers are lower.

A meteoroid stream is not a solid body as an asteroid but is a flow of meteoroids. Such a flow has a rather clear boundary if it is young, that is, released from a parent body recently but will be blurred/scattered with time. A meteor shower activity would become lower as time goes by and its boundary also changes from clear to unclear.

The distribution of the DR values shown in Table 2 and 3 states clearly that there is no boundary between established showers and working status. The parameter provides no basis to distinguish the former from the latter. Dividing showers into two ranks is somewhat like a dualism. Nature does not consist of only two elements but is diverse.

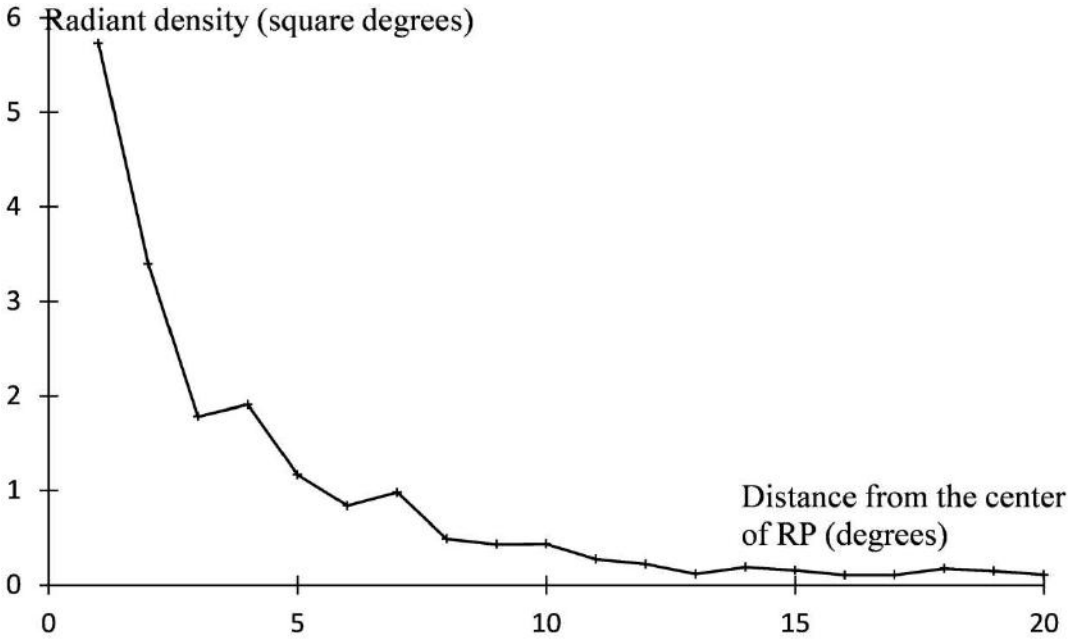

Figure 3 – Radiant density distribution for the 12 KCG4 (SonotaCo, $(\lambda - \lambda_s, \beta) = (161.5, 71.9)$, $\Delta\lambda_s = 135.7$–145.7). This radiant point is different from that given in Figure 1k and is located at the center of the distribution.

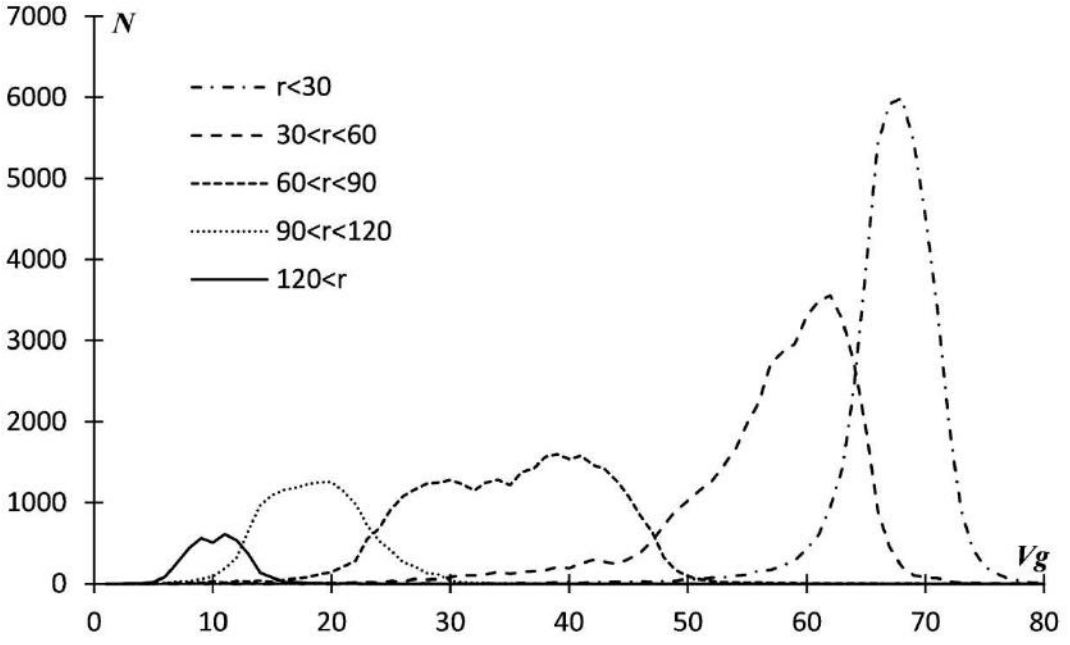

Figure 4 – The geocentric velocity distributions of sporadic meteors of the video data. r denotes the distance from the apex.

3.4 Showers with working status

Strong and conspicuous meteor activities had been noticed by visual observations and registered in SD formerly. Meteor activities reported to SD recently are weak quite naturally and some of them are questionable. DR values of working status showers are small in general but several notable showers exist (Table 3). Showers selected in Table 3 have attractive radiant distributions in the preliminary survey (see the Section 2) and, therefore, the remains are more unclear and should be reexamined.

4 Discussions

We suggest a very simple criterion for the shower/stream confirmation. Several conditions need to be considered.

1. We have not considered the difference in velocity yet.

2. We limit the duration of activity $\Delta\lambda_s < 10$, though there are many showers the maximum activity differs within one shower from researchers to researchers widely: $\Delta\lambda_s > 10$.

Table 2 – Distribution of DR for the established showers. The Code refers to the IAUMDC. The quantities DR and N3 are described in detail in the text.

Code	DR	N3	Code	DR	N3
31 ETA4	33.44	1573	530 ECV3	4.11	70
4 GEM3	30.89	16951	323 XCB4	4.00	28
8 ORI4	23.78	7465	526 SLD1	3.92	51
6 LYR5	23.54	644	221 DSX2	3.85	9
171 ARI3	22.98	23	506 FEV2	3.85	81
7 PER4	20.95	9958	23 EGE3	3.77	219
16 HYD2	19.31	1617	343 HVI3	3.75	35
13 LEO6	17.21	2194	510 JRC1	3.66	22
17 NTA4	16.98	867	170 JBO0	3.60	6
20 COM1	15.51	1195	21 AVB4	3.53	20
5 SDA7	15.17	1356	11 EVI2	3.41	83
335 XVI0	14.47	111	372 PPS2	3.32	51
22 LMI3	14.24	190	512 RPU2	3.12	25
1 CAP6	11.77	381	339 PSU2	3.12	132
19 MON3	11.58	676	18 AND1	3.09	35
208 SPE1	10.27	483	9 DRA3	3.00	5
184 GDR0	10.25	65	63 COR1	3.00	1
15 URS4	9.94	242	330 SSE2	3.00	4
250 NOO3	9.58	617	338 OER0	3.00	41
533 JXA3	9.22	40	337 NUE0	2.83	122
333 OCU1	8.84	115	348 ARC1	2.61	20
341 XUM2	8.73	102	388 CTA1	2.56	65
175 JPE2	8.62	138	390 THA1	2.49	64
2 STA3	8.47	975	69 SSG1	2.47	14
281 OCT3	8.14	38	246 AMO1	2.40	73
10 QUA3	7.75	1976	257 ORS3	2.33	141
431 JIP1	7.36	27	12 KCG4	2.25	78
411 CAN1	7.08	52	549 FAN1	2.21	45
428 DSV2	6.72	121	326 EPG1	1.87	5
346 XHE1	6.71	47	151 EAU0	1.80	9
404 GUM2	6.59	33	529 EHY1	1.76	187
191 ERI1	6.49	169	27 KSE2	1.73	15
206 AUR4	5.99	76	183 PAU2	1.71	32
319 JLE4	5.77	52	252 ALY2	1.60	8
445 KUM1	5.69	169	334 DAD0	1.50	58
165 SZC3	5.57	26	362 JMC2	1.50	5
331 AHY1	5.34	114	96 NCC6	1.36	35
145 ELY4	5.12	94	97 SCC3	1.28	29
320 OSE2	5.00	5	187 PCA3	1.12	3
569 OHY0	4.85	55	327 BEQ0	1.00	1
524 LUM1	4.72	52	321 TCB1	0.95	12
336 DKD0	4.64	181	242 XDR0	0.89	8
33 NIA6	4.50	51	328 ALA1	0.88	5
26 NDA4	4.48	145	322 LBO2	0.87	18
164 NZC3	4.42	31	197 AUD0	0.78	11
110 AAN4	4.36	16	61 TAH0	0.50	1
427 FED1	4.28	20	233 OCC0	0.00	0
446 DPC0	4.12	22			

Table 3 – Additional DR values for the working status showers. Code, DR and N3 are the same as in Table 1.

Code	DR	N3	Code	DR	N3
860 PAN0	11.99	12	575 SAU0	2.52	32
523 AGC0	9.47	60	644 JLL0	2.50	55
514 OMC1	7.99	24	836 ABH0	2.50	20
598 TCT0	7.61	33	531 GAQ0	2.45	40
517 ALO0	7.49	30	571 TSB0	2.44	13
450 AED0	6.99	42	919 ICN0	2.43	17
507 UAN0	6.99	28	417 ETT0	2.40	36
520 MBC0	6.74	27	515 OLE0	2.40	36
444 ZCS0	6.62	159	594 RSE0	2.38	27
81 SLY2	6.27	69	713 CCR0	2.37	15
642 PCE0	5.88	51	493 DEC0	2.32	51
667 JTP0	5.69	38	602 KCR1	2.31	50
519 BAQ0	5.59	28	614 JOS0	2.30	23
462 JGP0	5.30	53	416 SIC0	2.30	36
340 TPY0	5.02	77	430 POR0	2.27	87
882 PLE0	5.00	15	638 DZT0	2.25	103
497 DAB3	4.63	34	839 PSR0	2.18	16
500 JPV2	4.47	79	825 XIE0	2.16	13
370 MIC0	4.06	23	215 NPI2	2.14	50
893 EOP0	4.04	31	216 SPI0	2.14	50
90 JCO1	3.96	119	1002 SVE0	2.14	20
136 SLE2	3.84	32	535 THC0	2.09	16
483 NAS0	3.72	36	556 PTA0	2.05	28
841 DHE0	3.66	22	558 TSM0	2.01	53
502 DRV0	3.56	95	651 OAV0	1.98	41
410 DPI0	3.30	11	717 LAU0	1.93	58
645 PHC0	3.29	34	818 OAG1	1.91	21
878 OEA0	3.16	20	567 XHY0	1.83	44
563 DOU0	3.03	89	885 DEV0	1.78	63
658 EDR0	3.00	13	439 ASX0	1.72	35
415 AUP0	2.94	51	479 SOO0	1.70	71
465 AXC0	2.86	61	440 NLM0	1.65	61
505 AIC0	2.86	81	515 OLE1	1.65	39
873 OMI0	2.76	23	593 TOL0	1.62	54
480 TCA0	2.71	85	481 OML0	1.59	73
429 ACB0	2.68	76	722 FLE0	1.52	76
644 JLL1	2.60	59	874 PXS0	1.43	78
488 NSU0	2.54	45	601 ICT0	1.24	41
527 UUM0	2.53	43	531 GAQ2	0.73	10

3. Though we limit the studied duration as $\Delta\lambda_s < 10$, there might be changes in RP and velocity.

We need to check these conditions.

4.1 V_g distributions

Figure 4 shows the velocity distribution of sporadic meteors of the video data along the elongation from the apex (ε) dividing them into 30° bins. We exclude every shower meteors defined by SonotaCo net in this figure for the elimination of the large contributions from the showers. It is very natural that the observed velocity strongly depends on the elongation, because of the geometry between the meteoroid orbit and the Earth's defines the possible range of the geocentric velocity.

We can easily show the geocentric velocity dependence on the geometry by calculating the geocentric velocity (V_g) for hypothetical showers; we set the heliocentric velocity $V_h = 30$ (km/s) for $a = 1$ au, that is, the Earth and the near Earth objects (NEO) and $V_h = 42$ (km/s) for objects having a parabolic orbit (Figure 5).

We study the geometric dependence in case of 7 PER and 4 GEM in detail. The radiant point of PER is near $\varepsilon = 40°$ and calculated geocentric velocities are 46 km/s

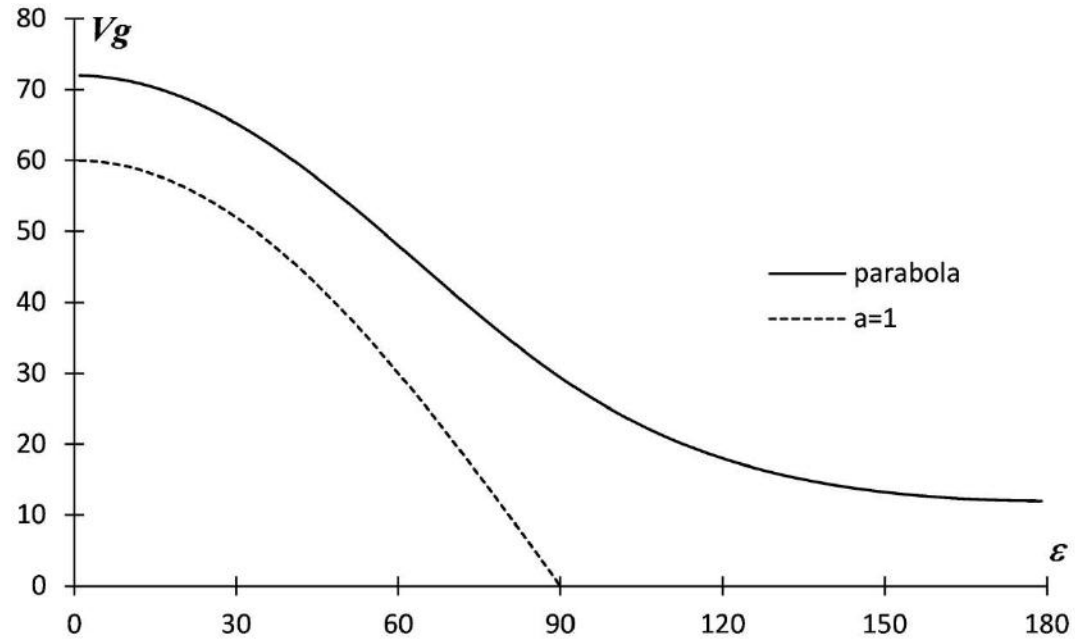

Figure 5 – The geocentric velocity distributions of hypothetical showers. ε is the elongation, that is, the distance from the apex.

for a NEO and 60 km/s for a parabola. GEM is near $\varepsilon = 60°$ and 30 km/s for a NEO and 48 km/s for a parabola.

Figure 6a shows the velocity distribution within 10° from PER: $(\lambda - \lambda_s, \beta) = (283.3, 38.3)$. We add the velocity distributions of three reference periods in the same area; $\lambda_s = 164.2 - 174.2$ is for the neighbor, $\lambda_s = 14.2 - 24.2$ and $254.2 - 264.2$ are for the non-relevant meteors. The reference distributions are similar to the PER itself and show clearly that meteors radiated from the same elongation have identical velocity. The distribution of PER seems to spread over the parabolic limit; $V_g = 46 - 60$ km/s for hypothetical showers but this is caused by the observational errors (see the 2σ bar in the figure).

Figure 6b shows the velocity distribution within 10° from GEM: $(\lambda - \lambda_s, \beta) = (208.1, 10.4)$ with three reference distributions in the same way. The velocity distribution of three reference periods coincide well with both original distribution and well within the listed limit in case of GEM: $V_g = 30 - 48$ km/s. It seems to be very difficult to distinguish different meteor activities within these narrow geometric limits, because the standard deviation of geocentric velocity is pretty large: $2\sigma = 3.96$ for PER and $2\sigma = 3.70$ for GEM.

4.2 Duration of meteor activities

We limit the period of the research as $\Delta\lambda_s < 10$ but the duration of the showers are different each other. Figure 3 of Koseki (2012a) shows estimated activity profiles and 1 CAP is the longest in that figure; half width at half maximum is about 6°. We can, therefore, identify a meteor activity with another shower recognized $\Delta\lambda_s < 10$ and distinguish a meteor shower from another observations $\Delta\lambda_s > 10$. It is the limitation of $\Delta\lambda_s < 10$ is proper to distinguish different activities and to unite meteors as a single shower by setting the limit as $\Delta\lambda_s = 10$.

Table 4 – The shift of RP and the velocity described as $y = ax + b$ where x is the solar longitude (λ_s) of the observation. The RP shift is plotted in $(\lambda - \lambda_s, \beta)$ coordinates. All data is derived from the SonotaCo net own shower definition.

	$\lambda - \lambda_s$		β		V_g	
	a	b	a	b	a	b
ETA	−0.23	303.99	0.05	5.44	0.05	63.38
CAP	−0.45	235.87	0.10	−2.82	−0.19	46.44
SDA	−0.29	245.77	−0.09	3.92	−0.20	65.54
PER	0.01	282.06	−0.06	47.30	0.02	56.88
STA	−0.30	258.32	−0.06	7.92	−0.10	48.38
NTA	−0.27	253.18	0.02	−1.94	−0.13	57.90
ORI	−0.27	303.22	0.10	−27.87	−0.06	79.12
GEM	−0.10	235.07	−0.06	27.06	0.04	22.79

4.3 The shift of RP and V_g within the duration

If we select $\Delta\lambda_s = 10$, we could neglect the shift of the radiant (and more, of the velocity). Table 4 gives the shift of radiants on (x, y) plane and of the velocity based on SonotaCo's shower definition; a and b in the table indicate when we express the shift as $y = ax + b$, b is the value for $x(\lambda_s) = 0$. PER seems to be a stationary shower in $(\lambda - \lambda_s, \beta)$ coordinates. Ecliptic showers, such as STA, move slowly along the ecliptic latitude line. In general, we can approve the presumption of this search by this table; it is very useful to express RPs on $(\lambda - \lambda_s, \beta)$ coordinates.

5 Validity of DR

This proposal is only a preliminary one. There are many shortcomings, for example:

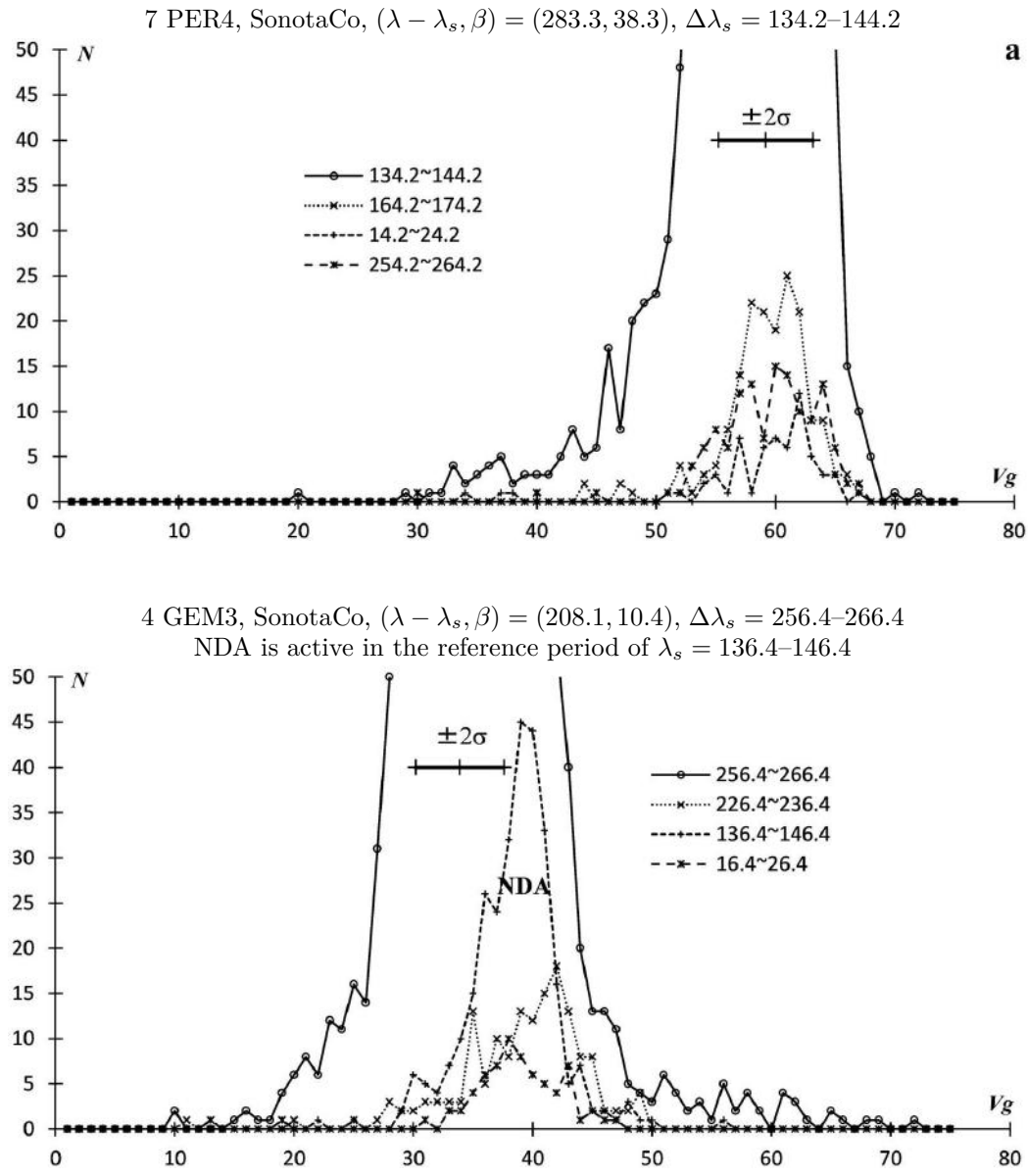

Figure 6 – Distribution of the recorded meteors over the geocentric velocity with three distributions of the reference period as described in detail in the text.

1. This is based on optical and only on video observations. Daytime showers need to be treated separately, because radar observations provide a different view on meteor activity.

2. For 529 EHY1 (η-Hydrids) we find 187 meteors within 3° and a clear concentration, but DR is only 1.76 (Table 2), because a very strong meteor shower 16 HYD (σ-Hydrids) has a radiant close to it. 257 ORS3 (Southern χ-Orionids) is near to 2 STA (Southern Taurids) and DR is 2.33. There are a few cases disturbed by strong neighboring shower.

3. 12 KCG4 (κ-Cygnids) has an elongated radiant area (Figure 1k) and DR is 2.25. A radiant area is not round always but elongated in some cases.

D-criteria (such as Southworth and Hawkins, 1963) are expressed in a four dimensional space and usable for such difficult cases, but the distance between data cannot be drawn on the two dimensional sheet. Orbit based criteria are distorted by observational errors and it is difficult to take such distortion into consideration of the criterion. Sekanina (1970) introduced the ratio between the number of stream and background meteors between $D = 0$ and $D = s\sqrt{2}$; the cumulative number ratio of stream meteors to sporadic meteors at D of the most frequent stream number. Simplicity is the unique advantage of DR, because the contamination from the background activity and the observational errors can be ignored in the DR calculation.

The reports on detections of "new showers" from the corners of the world are mainly by video. The DR criterion is useful to check whether such reports could be recognized objectively. The DR criterion is useful in most cases, though special caution is necessary for extreme cases: when "a new shower" is located in close vicinity to the center of a more active shower.

Table 5 – STAs in SD. The solar longitude of the peak activity (LaSun) does not match the node (ω) in several cases. Columns with apostrophe for 2 STA0 (last column) are re-calculated from the node.

	LaSun	node	$\lambda - \lambda_s$	β	DR	N3	$\lambda - \lambda'_s$	β'	DR′	N3′
2 STA0	224	37.3	186.5	−5.0	0.71	149	193.2	−5.0	8.51	741
2 STA1	207.6	27.6	193.8	−5.2	5.85	392	193.8	−5.2		
2 STA2	196.5	16.0	195.2	−4.3	5.40	288	195.7	−4.3		
2 STA3	219.7		191.5	−4.8	8.47	975				
2 STA4	196	16.0	195.6	−4.2	5.89	279	195.6	−4.2		
2 STA5	216.0	34.4	193.0	−4.8	7.83	601	194.6	−4.8		
2 STA6	211.3	31.3	192.3	−5.6	3.38	292	192.3	−5.6		

6 Problematic showers in the SD

6.1 2 STA (Southern Taurids)

Tables 2 and 3 list the DR and N3 for the representative entry and, therefore, these values change widely if we select other entries. For example, STAs in the SD are a confused case (Table 5). The DR of 2 STA0 is extraordinary; DR under unity indicates that there is no meteor activity. LaSun (the solar longitude of the maximum activity) of 2 STA0 is different from its node by 6.7°; LaSun should be the descending node $\omega + 180$, because the STA appear at the ascending node of the orbit. The recalculated orbit of 2 STA0 based on LaSun disagrees with the listed orbit in SD, and the recalculated RP of the 2 STA0 based on the orbit agrees well with listed values except for LaSun in SD. LsSun of 2 STA0 might be inserted from an unknown source. If we change LaSun from its node, the re-calculated DR and N3 for the 2 STA0 of Table 5 seem to be proper.

The most important difference in STAs of the SD is the diverted time of the maximum. Figure 7 shows the activity profile of selected STA meteors within 3° from the estimated point (see STA of Table 4) and LaSuns of STA entries in SD. The author suggested that STA is composed of two branch activities (Koseki, 2012b); STA worked here is mainly from S_F part (the maximum $\lambda_s = 223$) and another S_E part reaches its maximum at $\lambda_s = 203$. 5 of 7 STA entries are between the two maxima including 2 STA0 and 2 are earlier than the S_E part (both 2 STA2 and 2 STA4 are from radar observations). Visual observers recognize STA is active in late October, that is the S_E part, and know STA become active again and reach its maximum early November, that is the S_F part. It is clear STA entries in SD indicate the time of the maximum activity neither S_E nor S_F.

Some recent entries in the SD insist the existence of other shower activities in the heart of the major showers, for examples, 626 LCT0 (λ-Cetids) and 626 LCT1 are located 0.36° and 0.81° from 2 STA5.

123 of the representative entries (see Section 3.1) in all 1031 showers in SD have close neighbor(s) within 3° from its RP. In contrast to this, 42 showers in them have distant member(s) located farther than 10° from its RP. 69 showers including working status have longer ΔLaSun > 10 among themselves.

It is impossible to divide meteor showers / meteoroid streams into two categories established and work-

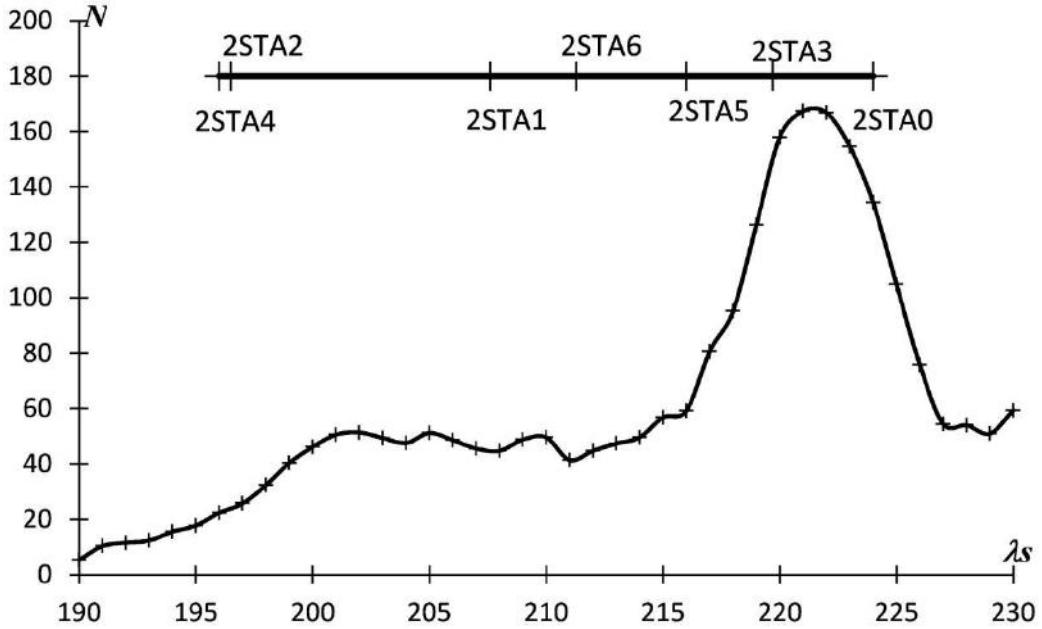

Figure 7 – The STA activity profile (number of recorded meteors) over the solar longitude with the maximum activity of SD showers.

ing clearly. And, moreover, there are many different meteor shower definitions. It is natural there are showers too widespread and no clear concentration, and, on the other hand, conglomerates of several activities.

6.2 Other synthetic problems in SD

The IAU three-letter code became neither convenient nor intelligible for observers/researchers now, because too many "showers" have an own code. There is no border or threshold between "established" and "working" as shown Table 2 and 3 and there are too many uncertain entries that are unsettled by DR. The larger part of working showers have no recognizable concentration in the radiant maps given in the preliminary search.

NDA in IAUMDC is far from original Northern δ-Aquariids (26 NDA) regarding the date and the position (Wright et al., 1957). We find that DR of the 33 NIA6 is 4.50 and large enough compared with other ANT activities, though 33 NIA6 is different from the traditional activity (Wright et al., 1957). DR of 21 AVB4 (α-Virginids) is 3.53 but 21 AVB4 is another difficult case; 21 AVB4 is far from the "traditional" α-Virginids (McCrosky & Posen, 1959).

The so-called "Andromedids" are now located at the boundary of Pisces and Triangulum. The suffix *id* means "belonging to, connected with, member of a group or class, descendent of" from Latin *-ides* or from Greek *-ides*. It seems to be better to call this shower the Bielids, which means the descendent of Comet Biela, rather than Andromedids, daughters of Princess Andromeda. The nomenclature should not interdict to call such meteor shower as the descendent of the parent body.

The orbit of 289P/Blanpain has been transformed and consequently its meteors radiate from Sculptor not from Phoenix (Sato & Watanabe, 2010). 254 PHO (Phoenicids) in the SD refers only the historical record. If we keep this in the SD, the Great Bielid records should be kept in SD as well. The orbit of 26P/Grigg-Skjellerup also has been perturbed in a way that its debris radiate from Puppis now. Short period comets are frequently perturbed by Jupiter and meteor showers produced by some of them might be shifted from one constellation to another. When a radiant moved, is it better to keep its historical names or give a new names? It might be one manner to call them by their parent body.

6.3 Suggestions to modify the SD

We would like to suggest following modifications of meteor showers/meteoroid streams list.

1. AdNo (for given shower-number of a set of parameters) would start at 1 not 0 as is the reference column.

2. Code (IAU 3 letter code) would not be given for a working status and especially not for *pro tempore*.

3. Shower name would not be given for a working status also.

4. Activity should express the year(s) of the observations always, because one line concerns the observations of the specific year(s). The term "annual" is not suitable for the listed data.

5. Shower status(es) would be eliminated and the DR value would be shown for new coming showers.

6. Ecliptic longitude of the Sun at the peak shower activity (LaSun) would be listed only when the research shows the peak shower activity distinguishing from the mean from their observations.

7. Radiant position should be given both (α, δ) and $(\lambda - \lambda_s, \beta)$.

8. Radiant daily motion should be given (x, y) centered at $(\lambda - \lambda_s, \beta)$.

9. Group (IAU numerical code of the main complex group) and CG (serial number of the member of the complex group) should be eliminated, because these are based on some researchers personal view.

10. A "parent body" should be mentioned only if the researcher(s) themselves insist. Code and shower name should be given, when the working group of IAUMDC would judge it properly. Problems in already existing "established" and "working" showers as shown above remain. These inconsistencies might be solved by further studies and cooperative works of the working group members with enthusiastic researchers.

7 Conclusions

We propose a very simple criterion for a meteor activity discrimination; the ratio of the radiant density per square degrees within 3° from the initial radiant to one of the area between 3° and 6° (DR). The DR is very simple but proves to be useful. The DR can show the certainty of every entry of the SD objectively; showers under DR < 2 should be re-examined.

The research applying DR on the IAU Shower Database (SD) shows that there is no proper reason for establishing two categories in the SD. We discussed several problematic entries in SD the and give suggestions to improve the SD.

SonotaCo net video data were used for calculations of DR in this paper, and it became clear that they are useful as a standard reference for a meteor shower research.

References

IAUMDC (2018). "IAU Meteor Data Center website". `https://www.ta3.sk/IAUC22DB/MDC2007/` .

Jenniskens P., Nénon Q., Albers J., Gural P. S., Haberman B., Holman D., Morales R., Grigsby B. J., Samuels D., and Johannink C. (2016). "The established meteor showers as observed by CAMS". *Icarus*, **266**, 331–354.

Koseki M. (2012a). "A simple model of spatial structure of meteoroid streams". *WGN, the Journal of the IMO*, **40:5**, 162–165.

Koseki M. (2012b). "Three components of 'Taurids'". *WGN, Journal of the IMO*, **40:4**, 129–138.

Koseki M. (2016). "Research on the IAU meteor shower database". *WGN, the Journal of the IMO*, **44:5**, 151–169.

Koseki M. (2018). "Different definitions make a meteor shower distorted.—The views from SonotaCo net and CAMS". *WGN, the Journal of the IMO*, **46:4**, 119–135.

McCrosky R. E. and Posen A. (1959). "New photographic meteor shower". *Astron. J.*, **64**, 25–27.

Sato M. and Watanabe J. (2010). "Forecast for Phoenicids in 2008, 2014, and 2019". *Publications of the Astronomical Society of Japan*, **62:33**, 509–513. (also `https://doi.org/10.1093/pasj/62.3.509`).

Sato M., Watanabe J., Tsuchiya C., Moorhead A., Moser D., Brown P., and Cooke W. (2017). "Detection of the Phoenicids meteor shower in 2014". *Planetary and Space Science*, **143**, 132–137.

Sekanina Z. (1970). "Statistical model of meteor streams. I. Analysis of the model". *Icarus*, **13**, 459–474.

SonotaCo (2017). `http://sonotaco.jp/doc/SNM/` .

Southworth R. B. and Hawkins G. S. (1963). "Statistics of meteor streams". *Smithsonian Contributions to Astrophysics*, **7**, 261–285.

Wright F. W., Jacchia L. G., and Whipple F. L. (1957). "Photographic ι-Aquarid meteors and evidence for the northern δ Aquarids". *Astron. J.*, **62**, 225–233.

Handling Editor: Jürgen Rendtel

Meteor observations

Perseids 2018 – Analysis of Global Visual Data

Jürgen Rendtel[1], *Kristina Veljković*[2], *Thomas Weiland*[3], *Cis Verbeeck*[4], *André Knöfel*[5]

The results presented here have been obtained in the Visual Workshop held during the IMC 2018 in Pezinok-Modra. The Workshop included a verification of data stored in IMO's current Visual Meteor Database (VMDB), was an application of the MetFns procedures and was meant as a training session. While there were no dust trail encounters expected in 2018, a stream filament was calculated to appear on August 12, close to $20^{\rm h}$ UT. The visual data (27650 Perseids reported by 201 observers within 1265.39 hours between August 5 and 21) show a clear signature of the filament, consisting of a minimum in the population index $r = 1.60 \pm 0.08$ at $\lambda_\odot = 139\,^\circ\!.797$ (2018 August 12, $19^{\rm h}47^{\rm m}$ UT) and a peak ZHR $= 134 \pm 13$ at $\lambda_\odot \approx 139\,^\circ\!.773$ (2018 August 12, $19^{\rm h}11^{\rm m}$ UT). During the main (nodal) maximum the population index r varied between 1.75 and 1.95; the ZHR reached values in the range 80–90 in the period $\lambda_\odot = 139\,^\circ\!.8$ to $140\,^\circ\!.2$. The filament encounter is most obvious in the number density profile for larger meteoroids (≥ 10 mg) at $\lambda_\odot = 139\,^\circ\!.78 \pm 0\,^\circ\!.02$ (2018 August 12, $19^{\rm h}21^{\rm m}$ UT).

Received 2018 December 8

1 Introduction

Numerous analyses of visual data obtained during shower encounters and collected in the IMO's Visual Meteor DataBase (VMDB) have been published over years. It is important to continue these series as they may reveal details of the long-term evolution of meteor showers. Further, it is important to have overlapping periods with analyses of similar data obtained e.g. by video observations in order to ensure calibration and thus allow to compare such series. Last but not least, the expertise gained over more than two decades in selection of parameters for such analyses should be forwarded to more colleagues.

The Visual Workshop held during the IMC 2018 was a good opportunity to discuss procedures and evaluate various effects but also to test the newly available MetFns software package[a] which will be described in a separate paper in the Proceedings of the International Meteor Conference 2018 (Rendtel et al., forthcoming). The hands-on analysis was made from the data sample available at this time, just about two weeks after the Perseid peak. All incoming data submitted by the observers listed in the next section by end-September is included here. The programs were run with the same parameter settings, but applied to the increased data sample.

[1]Leibniz-Institut für Astrophysik, An der Sternwarte 16, 14480 Potsdam and International Meteor Organization, Eschenweg 16, 14476 Potsdam, Germany. Email: jrendtel@web.de

[2]Petnica Meteor Group, Petnica, 14104 Valjevo, Serbia. Email: mackikac@gmail.com

[3]Ospelgasse 12-14/6/19, 1200 Wien, Austria. Email: thomas.weiland@aon.at

[4]Royal Observatory of Belgium, Ringlaan 3, 1180 Brussels, Belgium. Email: cis.verbeeck@scarlet.be

[5]Am Observatorium 2, 15848 Lindenberg, Germany. Email: aknoefel@minorplanets.de

IMO bibcode WGN-471-rendtel-per2018
NASA-ADS bibcode 2019JIMO...47...18R

[a]https://cran.r-project.org/package=MetFns

2 Visual Perseid data 2018

The maximum period of the 2018 Perseids was free from moonlight interference and a huge number of observers submitted their reports in due time. Here we concentrate on the period $\lambda_\odot = 133\,^\circ\!.09 - 147\,^\circ\!.90$ (August 05, $20^{\rm h}$ UT – August 21, $06^{\rm h}$ UT), but also include the neighbouring intervals to compare the results with previous returns and for calibration, if necessary. Of course, there is further data available for the long pre-maximum period in July/August and also after the maximum until August 24. In total, the sample we used for the above given period includes data of 27650 Perseids noted by 201 observers from 32 countries (Australia, Austria, Belgium, Brazil, Bulgaria, Canada, China, Croatia, Cyprus, Czechia, France, Germany, Greece, Hungary, Iran, Israel, Italy, Japan, Norway, Poland, Romania, Russia, Serbia, Slovakia, Slovenia, South Korea, Spain, Switzerland, Taiwan, Ukraine, United Kingdom, United States) within 1265.39 hours effective time. The following observers contributing to the visual data compilation during the 2018 Perseids:

Ioan Adam, Rainer Arlt, Pierre Bader, Fodor Balazs, Ognjen Bašić, Orlando Benitez Sanchez, Felix Bettonvil, Dina Blagojević, Maša Bogojević, Steve Brown, Viktor Buchenko, Rada Burmazović, Dvid Buzgo, María Delfina Carvajal Balagué, Roman Cecil, Mikhail Chubarets, Ilie Cosovanu, Magdalena Cosovanu, Tibor Csorgei, Patrik Dančo, Thomas Daniëls, Katie Demetriou, Peter Detterline, José Vicente Diaz Martinez, Polina Dimitrieva, Sofia Dimitrieva, Yiyang Ding, Chiara Dzudziová, Janko Durić, Yuankeqin Dong, Shlomi Eini, Reza Ensandoost, Frank Enzlein, Tomasz Fajfer, Kai Gaarder, Daniela Gavronova, Iglika Genova, Slaveya Georgieva, Christoph Gerber, William Godley, Mitja Govedič, Shy Halatzi, Torsten Hansen, Amir Hasanzadeh, Davood Hemmati, Gabriel Hickel, Adam Horanic, Jasmina Horvat, Lukas Hreha, John Hsueh, Glenn Hughes, Moran Idan, Miloš Igrutinović, Elitsa Ilieva, Gerardo Jiménez López, Carl Johannink, Karoly Jonas, Penko Jordanov, Han-sub Jung, Javor Kac, Václav Kalaš, Omri Katz, Jakub Kazimír, Ghasem Keshavarz, Iva Kirova, André Knöfel, Zdenek Komarek, Jakub Koukal, Maciej Kwinta, Viliam Ledžinský, Viera Lenčišová, Anna Levin, Gang Li, Zhou Lijie,

Michael Linnolt, Ole Lit, Hartwig Lüthen, Časlav Lukić, Eduard Lungu, Robert Lunsford, Matea Mašinović, Anđela Mahmutović, Adam Marsh, Jacqueline Marsh, Ken Marsh, Marindah Marsh, Pierre Martin, Antonio Martínez Picar, Bruce McCurdy, Fabrizio Melandri, Frederic Merlin, Polák Michal, Bojana Mićić, Peter Mikloš, Tanja Miković, Isidora Milivojević, Koen Miskotte, Shai Mizrachi, Jan Mocek, Alireza Mohammadi, Amir Hossein Mohammadizadegan, Sirko Molau, Yulia Moralyiska, Arash Nabizadeh Haghighi, Raphael Ner, Zvi Ner, Rafael Neumann, Stariy Nicolay, Ana Nikolić, Mohammad Nilforoushan, Katarina Ninković, Vladimir Obradović, Francisco Ocaña González, Zuzana Ontkovicova, Matěj Otýs, Boris Pankovčin, Igor Parnahaj, Debora Pavela, Dunja Pavlović, Nina Perović, R. Suyin Perret-Gentil, Katarina Petrović, Pedro Pérez Corujo, Julia Piatnicova, Jakub Popovič, Lazar Popović, Sasha Prokofyev, Alireza Rahimi, Ella Ratz, Marie-Hélène Raymonde, Ina Rendtel, Jürgen Rendtel, Janko Richter, Stephen Riley, Dalida Rittossa, Safiria Rittossa, Bohus Rosko, Boris Rosko, Terrence Ross, Hana Rottenbornová, Xu Ruihan, Jan Sadiv, Mirco Saner, Branislav Savić, Stefan Schmeissner, Kai Schultze, Diana Sekulić, Ben Sharp, Ali Sharvandi, Fangzheng Shi, Wei Shi, Costantino Sigismondi, Andrzej Skoczewski, David Spontak, Teodora Srećković, Sergey Stariy, Toni Stipeč, Wesley Stone, Petra Strunk, Vojtěch Suchánek, Ádám Szabó, Richard Taibi, Hanjie Tan, Tamara Tchenak, Alexandru Tehanciuc, Iurascu Teodor, Csilla Tepliczky, Aleksa Teić, Snežana Todorović, Tomáš Toma, Yasuhiro Tonomura, Oliver Tošković, Stafie Tudorel, Shigeo Uchiyama, Andras Uhrin, Peter van Leuteren, Hendrik Vandenbruaene, Anatoliy Vasylenko, Janna Vasylenko, Alexandru Vatamanu, Kristina Veljković, Dita Vetrovcova, Martin Vincencik, Erik Vincler, Katarina Vrhovac, Dušan Vukadinović, Thomas Weiland, Ariel Westfried, Frank Wächter, Sabine Wächter, Roland Winkler, Oliver Wusk, Quanzhi Ye, Wang Yihe, Zlatin Yovev, Yueyang Yu, Khalil Zarei, Zohre Zarghami, Geng Zhao, Przemysław Żołądek, Andrej Zrnić.

3 Data analysis

3.1 Temporal distribution

A first step is to get an overview of the temporal distribution of the data to detect critical periods which may not have sufficient data for detailed analyses (Figure 1). Here we apply a constant $r = 2.20$ and include all available reports. Once such periods are identified, the analysis first concentrates on the variations of the population index profile, allowing the proper corrections for the ZHR in the later steps.

3.2 Population index profile

Because we need a certain sample of shower meteors to derive a population index r, the temporal resolution of the r-profile is lower than for rate data. We use the method described by Arlt (2003), obtaining values of r from the difference between the average shower meteor magnitude and the limiting magnitude per interval. The result for the entire period between August 5 and 15 is shown in Figure 2. The interval lengths and required minimum number of shower meteors per bin have been adapted to the available samples and varies during the period. This holds in particular for the period around the rate maximum (Figure 3).

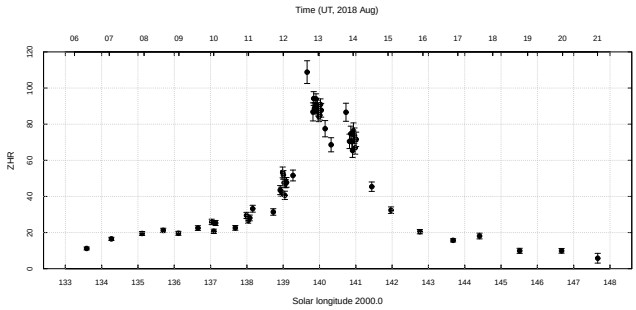

Figure 1 – First rough ZHR profile applying a constant $r = 2.20$ to identify the temporal distribution of the available data and obvious peculiarities which require special attention.

An obvious remarkable feature is the very low value of $r = 1.60 \pm 0.08$ at $\lambda_\odot = 139\overset{\circ}{.}797$, corresponding to 2018 August 12, $19^{\rm h}47^{\rm m}$. This is also illustrated by notes about a considerable fraction of bright Perseids from observers starting at European dusk. We carefully checked the values around this position, as it coincides with a predicted filament encounter (Jenniskens, 2006; Table 5d on pages 659ff) on August 12 near $20^{\rm h}$ UT. Unfortunately, this occurred at the beginning of the European observing window and there are fewer observations in the preceding period. Observers in southeast Europe had dark sky at this time, but the radiant is very low until about $22^{\rm h}$ local time. Those further north in central Europe see a higher radiant elevation, but can start only past $21^{\rm h}$ local time due to twilight. Nevertheless, the low r in this bin is defined by a reasonable sample (14 intervals, 102 Perseids). We are not able to determine any further details, however. Later in the night, the r-profile is smooth with "typical" values of r, but constantly rising values up to $r = 1.96 \pm 0.10$ at $\lambda_\odot = 140\overset{\circ}{.}18$ (2018 August 13, $05^{\rm h}20^{\rm m}$ UT). This is close to the transition between European and North American longitudes since the most western European observers (Iberian peninsula) face dawn around $04^{\rm h}$ UT. As the profile is smooth in this period, there are no indications for an artefact here.

Several observers again mentioned a larger fraction of bright Perseids at a late position on August 13 around $02^{\rm h}$ UT, i.e. in the descending branch of the activity profile. There is just one bin with r being lower than the two adjacent bins ($\lambda_\odot = 140\overset{\circ}{.}029$, i.e. August 13, $01^{\rm h}35^{\rm m}$ UT); see Figure 3. Another dip occurs a day later at $\lambda_\odot = 140\overset{\circ}{.}991$ (2018 August 14, $01^{\rm h}37^{\rm m}$ UT). Both bins are not at an "edge" of a (geographic) observing window and base on 69 and 37 intervals containing 940 and 606 Perseids, respectively. We need to check these bins in the subsequent steps of our analysis.

3.3 ZHR profile

The outer regions of the Perseids before August 12 and after August 14 (Figure 4) are close to the average profile (see, e.g. Figure 2.26 on p. 32 in Rendtel, 2014). During the maximum period (Figure 5) we find one high peak and a few further variations. The nodal crossing time was announced between $\lambda_\odot = 139\overset{\circ}{.}8$ and $140\overset{\circ}{.}3$,

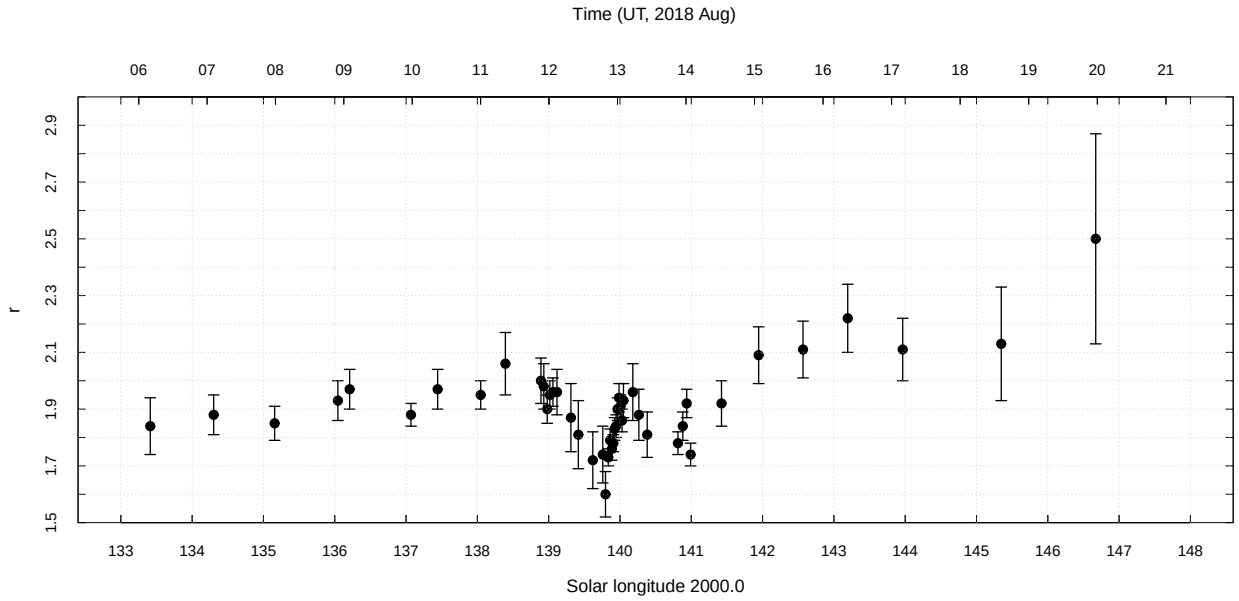

Figure 2 – Profile of the population index r for the entire period studied in this analysis. Details of the central region are shown in Figure 3 and are discussed below.

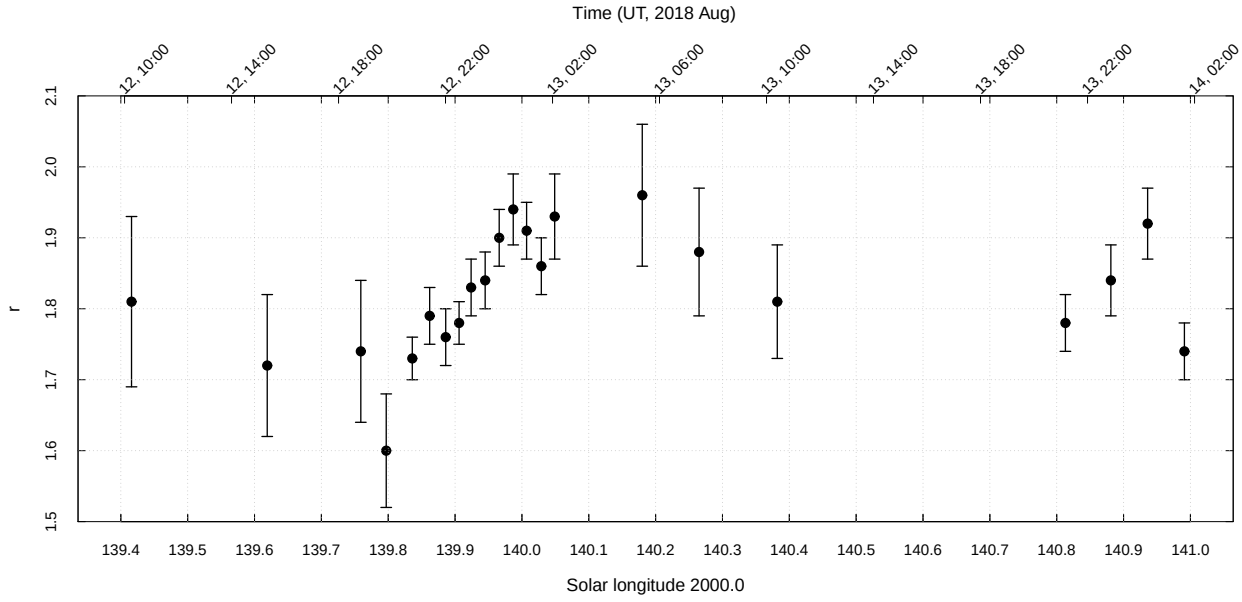

Figure 3 – Profile of the population index r for the near maximum period. Although not covered by a large number of intervals, there is a clear minimum of r in the European evening time.

equivalent to 2018 August 12, $20^{\rm h}$ to August 13, $08^{\rm h}$ UT. This period is well covered by observations.

As mentioned above, a filament encounter was expected on August 12 shortly before $20^{\rm h}$ UT ($\lambda_\odot \approx 139\overset{\circ}{.}790$). Close to this position (at $\lambda_\odot = 139\overset{\circ}{.}797$, i.e. about 45 minutes later), we do not only find the minimum $r = 1.60$ but also a significantly enhanced rate with a peak of ZHR $= 134\pm13$ at $\lambda_\odot = 139\overset{\circ}{.}773\pm0\overset{\circ}{.}020$ (2018 August 12, $19^{\rm h}11^{\rm m}$ UT). The values are given in Table 1. Similar to the r-profile, the temporal resolution is not as high as for the subsequent intervals due to the distribution of the observer locations. Nevertheless, both the low r and the ZHR-enhancement are a strong signature of the filament encounter. Since we used only data obtained under good conditions (LM better than +5.5 mag), the high ZHR is no artefact. To the contrary, the lower r as compared to the neighbouring intervals ensures that we do not have an LM over-correction. Further, we checked the effect of the radiant elevation. Selecting only intervals with a radiant elevation $h_R \geq 25°$ reduces the sample, while including also intervals with the radiant between 15° and 25° ensures a larger sample but an increasing effect of the zenith correction. In our case, both ZHR values agree within the error margins 134 ± 13 vs. 132 ± 12. We once more deal with the time of the filament encounter in the number density analysis.

Further ZHR enhancements (single bins with ZHRs above their neighbours) are found at $\lambda_\odot = 139\overset{\circ}{.}847$ (August 12, $21^{\rm h}02^{\rm m}$; 91 intervals with 744 Perseids,

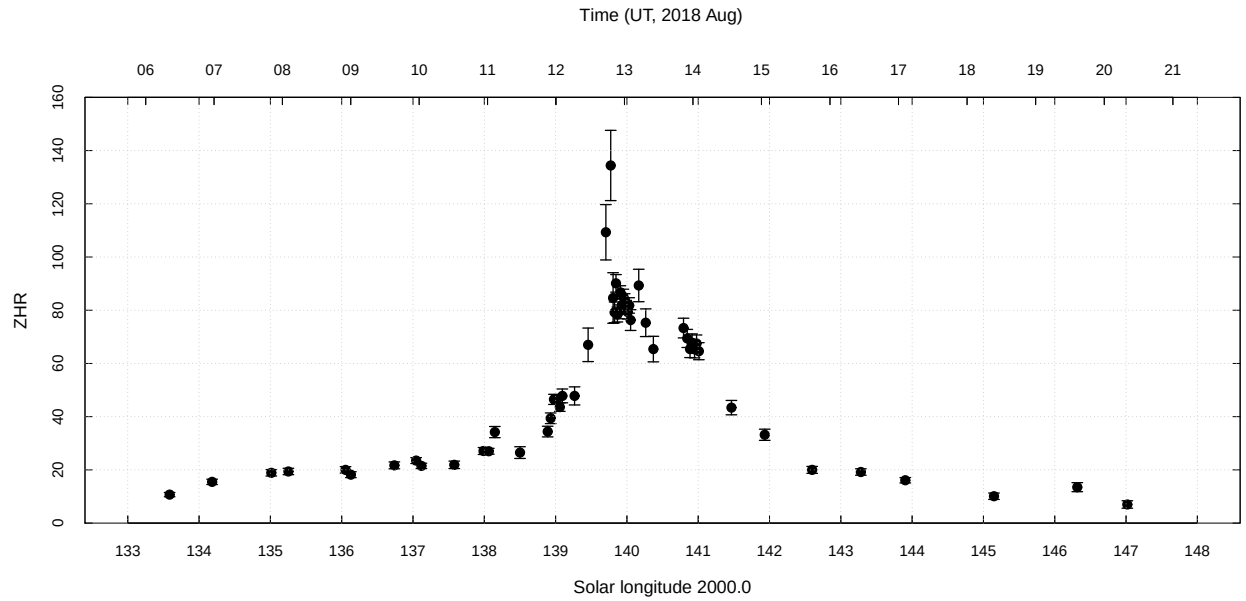

Figure 4 – ZHR-profile of the entire Perseid 2018 activity period studied in this analysis, using the r-profile calculated in the first step. Details of the central region are shown in Figure 5.

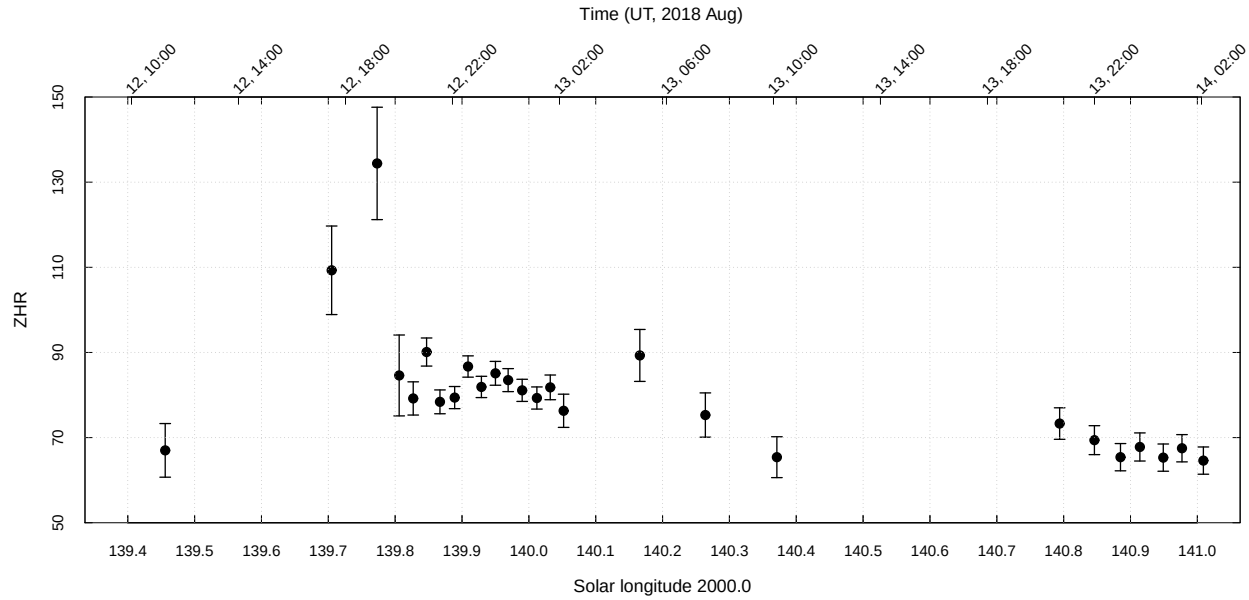

Figure 5 – Details of the ZHR-profile of the 2018 Perseid maximum period, using the previously determined population index values. Numerical values are given in Table 1.

Table 1 – Numerical values obtained for the analysis of the Perseid 2018 reports for each bin. The date/UT refers to the centre of the bin. 'Int.' and N(PER) are the number of count intervals and Perseid meteors, respectively, included in each bin. The given r per bin is interpolated from the r-profile obtained first and represents the value for the solar longitude. ND6.5 and ND10mg are the number densities for meteoroids causing meteors of at least +6.5 mag and meteoroids of $\geq$ 10 mg, respectively.

Sol. Long.	Aug.	UT	Int.	N(PER)	ZHR	r	ND6.5	ND10mg
133.587	06	08:24	56	184	10.7±0.8	1.85	6.9±0.5	0.3±0.04
134.183	06	23:20	42	250	15.5±1.0	1.88	10.7±0.7	0.4±0.05
135.013	07	20:07	49	252	18.9±1.2	1.85	12.2±0.8	0.5±0.05
135.253	08	02:07	35	256	19.4±1.2	1.85	12.5±0.8	0.5±0.05
136.054	08	22:10	46	261	20.0±1.2	1.93	15.5±0.9	0.5±0.05
136.129	09	00:03	42	278	18.2±1.1	1.95	14.7±0.9	0.4±0.05
136.739	09	15:19	45	263	21.7±1.3	1.90	15.7±0.9	0.5±0.05
137.044	09	22:56	75	439	23.5±1.1	1.88	16.2±0.8	0.6±0.05
137.118	10	00:48	69	461	21.5±1.0	1.89	15.2±0.7	0.5±0.05
137.579	10	12:19	41	259	21.9±1.4	1.97	18.5±1.2	0.5±0.05
137.989	10	22:35	61	444	27.1±1.3	1.94	21.4±1.0	0.6±0.05
138.063	11	00:26	83	579	27.0±1.1	1.95	21.8±0.9	0.6±0.04
138.148	11	02:33	19	268	34.2±2.1	1.98	29.5±1.8	0.8±0.05
138.501	11	11:23	15	141	26.5±2.2	2.06	27.0±2.2	0.6±0.05
138.889	11	21:05	67	302	34.4±2.0	2.00	30.9±1.8	0.8±0.05
138.931	11	22:08	66	381	39.4±2.0	1.98	34.0±1.7	0.9±0.05
138.977	11	23:17	64	574	46.5±1.9	1.90	33.6±1.4	1.1±0.04
139.017	12	00:17	115	980	46.3±1.5	1.95	37.4±1.2	1.1±0.04
139.059	12	01:20	93	787	43.6±1.6	1.96	36.0±1.3	1.0±0.05
139.095	12	02:14	31	344	47.8±2.6	1.96	39.5±2.1	1.1±0.1
139.266	12	06:31	22	203	47.8±3.4	1.90	34.6±2.5	1.1±0.1
139.456	12	11:16	11	112	67.0±6.3	1.77	35.5±3.3	1.7±0.2
139.705	12	17:29	7	111	109.3±10.4	1.84	68.8±6.5	2.7±0.3
139.773	12	19:11	7	104	134.4±13.2	1.67	54.9±5.4	3.6±0.4
139.806	12	20:00	13	79	84.6±9.5	1.61	29.3±3.3	2.3±0.3
139.827	12	20:32	70	408	79.2±3.9	1.69	34.2±1.7	2.1±0.1
139.847	12	21:02	91	744	90.1±3.3	1.77	47.8±1.8	2.3±0.1
139.867	12	21:32	90	801	78.4±2.8	1.79	43.7±1.6	2.0±0.1
139.889	12	22:05	102	938	79.4±2.6	1.76	41.1±1.3	2.0±0.1
139.909	12	22:35	114	1187	86.7±2.5	1.79	48.3±1.4	2.2±0.1
139.929	12	23:05	102	1094	81.9±2.5	1.83	50.3±1.5	2.0±0.1
139.950	12	23:36	80	952	85.1±2.8	1.85	54.8±1.8	2.1±0.1
139.969	13	00:05	86	982	83.5±2.7	1.91	61.7±2.0	2.0±0.1
139.990	13	00:36	89	970	81.1±2.6	1.94	64.1±2.1	1.9±0.1
140.012	13	01:09	89	960	79.3±2.6	1.89	56.0±1.8	1.9±0.1
140.032	13	01:39	62	815	81.8±2.9	1.86	53.9±1.9	2.0±0.1
140.052	13	02:09	35	388	76.3±3.9	1.94	60.3±3.1	1.8±0.1
140.166	13	05:00	18	213	89.3±6.1	1.98	77.0±5.3	2.1±0.1
140.264	13	07:27	20	206	75.3±5.2	1.88	52.0±3.6	1.8±0.1
140.371	13	10:08	21	184	65.4±4.8	1.82	39.2±2.9	1.6±0.1
140.794	13	20:42	43	400	73.3±3.7	1.77	38.9±2.0	1.9±0.1
140.846	13	22:00	40	411	69.4±3.4	1.80	39.7±1.9	1.8±0.1
140.885	13	22:58	39	412	65.4±3.2	1.85	42.1±2.1	1.6±0.1
140.914	13	23:42	36	410	67.8±3.3	1.91	50.1±2.4	1.6±0.1
140.949	14	00:34	36	411	65.3±3.2	1.90	47.2±2.3	1.6±0.1
140.977	14	01:16	31	432	67.5±3.2	1.80	38.6±1.8	1.7±0.1
141.009	14	02:04	31	414	64.6±3.2	1.67	26.4±1.3	1.7±0.1
141.466	14	13:29	38	251	43.4±2.7	1.98	37.4±2.3	1.0±0.1
141.933	15	01:09	30	258	33.2±2.1	2.09	35.9±2.3	0.7±0.05
142.598	15	17:46	40	256	20.0±1.3	2.12	22.9±1.5	0.4±0.04
143.281	16	10:49	33	253	19.2±1.2	2.22	26.6±1.7	0.4±0.04
143.904	17	02:22	37	250	16.1±1.0	2.12	18.5±1.1	0.3±0.03
145.148	18	09:25	14	73	10.1±1.2	2.10	11.1±1.3	0.2±0.02
146.316	19	14:34	6	63	13.5±1.7	2.38	24.7±3.1	0.2±0.03
147.018	20	08:04	4	24	7.0±1.4	2.61	18.3±3.7	0.1±0.02

ZHR = 90 ± 3) and at $\lambda_\odot = 140\overset{\circ}{.}166$ (August 13, 05^h00^m; 18 intervals with 213 Perseids, ZHR = 89 ± 6). There are no other known or expected encounter with dust trails within the meteoroid stream. Both ZHR enhancements mentioned here do not coincide with one of the r-minima discussed above.

3.4 Number density and flux

The ZHR describes the appearance of a meteor shower in the sky. A meteoroid stream is better characterised by its number density (ϱ, or ND) or the meteoroid flux density (Q), often shortened to flux. Both can derived from the data we obtained, using the procedure described by Koschack and Rendtel (1990). Considering all meteors up to the (entire) magnitude class +6 mag, we obtain the "total number density" for the visually covered magnitude range. According to the relations between mass and brightness quoted in (Koschack and Rendtel, 1990), a +6.5 mag Perseid is caused by a meteoroid of $5 \cdot 10^{-5}$ g (see Koschack and Rendtel, 1988, and the examples given in Table 2).

Table 2 – Meteor magnitudes and meteoroid masses for the Perseids according to Koschack and Rendtel (1990). Despite the model limitations, this gives an idea about the involved particle dimensions.

Mass (g)	Magnitude
100	−8.0
10	−5.7
1	−3.4
0.1	−1.1
0.01	+1.2
0.001	+3.5
0.00046	+6.5

The particle number density (ND) is the number of stream meteoroids within a cube with 1000 km edge length ($10^9 km^3$). This can be easily converted into the flux density by multiplying with the velocity of the stream meteoroids. The order of magnitude of ND is roughly a few (say 1–100 for most streams) $10^{-9} km^{-3}$. This indicates how 'empty' a region of a meteoroid stream is, even if the observer has the impression that the Earth crosses a densely populated region.

The procedure described by Koschack and Rendtel (1990) is based on several assumptions and approximations which allowed to apply the method for values of $r > 1.8$. This has been extended for the 1998 Leonid fireball storm by Arlt (1998). His approximation allows us to calculate number densities down to $r \approx 1.1$. Of course, one has to bear in mind that the 1990 number density paper gives several conditions. For example, during periods of lower r the effective field becomes larger and consequently the field centre should be higher than 50° in the sky. Further, all fits become less accurate the further the conditions deviate from the reference parameters. So the "real" error margins may be larger than those given here. Despite all this, our values definitively allow a comparison of the density along the Earth's passage through the stream.

In Figure 6, which shows the number density of all visually observable meteors ND6.5 (down to +6.5 magnitude, i.e. the entire "magnitude class +6" included), we find two peaks: the filament close to $\lambda_\odot = 139\overset{\circ}{.}7$ as well as a later peak at $\lambda_\odot = 140\overset{\circ}{.}16$. A less pronounced enhancement appears at the end of the main maximum profile at $\lambda_\odot = 140\overset{\circ}{.}92$ (two bins). The number density of $68.8 \cdot 10^{-9}$ $km^{-3}s^{-1}$ corresponds to a flux density of $14.6 \cdot 10^{-3}$ $km^{-2}h^{-1}$.

In a next step, we calculate the number density of meteoroids with at least 10 mg mass (ND10mg). For the fast Perseids (V_∞ = 59 km/s) this limit corresponds to +1.2 mag (Table 2). The result shown in Figure 7 demonstrates the difference between the different regions along the encounter, as it shows only one prominent peak. The highest number density of $3.5 \cdot 10^{-9}$ $km^{-3}s^{-1}$ corresponds to a flux density of $7.5 \cdot 10^{-4}$ $km^{-2}h^{-1}$ for the 10 mg particles. The filament obviously is composed of mainly larger meteoroids centered at $\lambda_\odot = 139\overset{\circ}{.}78$. Of course, this is already visible in the r-profile, but is shown here as a physical quantity.

The difference in the time of the peaks for ND6.5 (closer to $\lambda_\odot = 139\overset{\circ}{.}70$) and for ND10mg ($\lambda_\odot = 139\overset{\circ}{.}78$) could be interpreted as a mass sorting. However, the bins before the main peak period are not sufficiently well distributed over time so that this interpretation must remain rather a speculation.

The other two local maxima in ND6.5 do not occur in the ND10mg graph and thus underline that they do not represent any distinct region in the meteoroid stream but are fluctuations in the number density of the nodal maximum with no different particle population.

4 Discussion

There are different concepts of meteoroid stream filaments (discussion in Jenniskens 2006; pages 210ff). Several papers deal with filaments but lack a description what a filament actually is (e.g. Neslušan, Hajduková, Jakubík, 2013; Jakubík and Neslušan, 2015; Buček and Porubčan, 2014). Also, the IAU Commission F1 (Meteors, Meteorites and Interplanetary Dust) has no definition on their page `https://www.iau.org/public/themes/meteors_and_meteorites/`. Since we refer to the filament encounter list published by Jenniskens (2006), we also use his description of a filament, being a complex of several dust trails blended together due to planetary perturbations. According to an earlier publication (Jenniskens et al., 1998) the concentration of dust near the comet is kept in a mean motion resonance with Jupiter. Since it needs time to fill up a filament, such an accumulated structure is much older than the trails (tens of revolutions). Meteoroids in resonance with Jupiter additionally tend to be dispersed by Saturn (Jenniskens, 2006).

Jenniskens and Betlem (2002) claim for the Leonids, that a filament has a size which is about an order of magnitude larger than a typical dust trail dimension. This would imply roughly a filament crossing time of a few hours rather than one hour or less for a dust trail encounter.

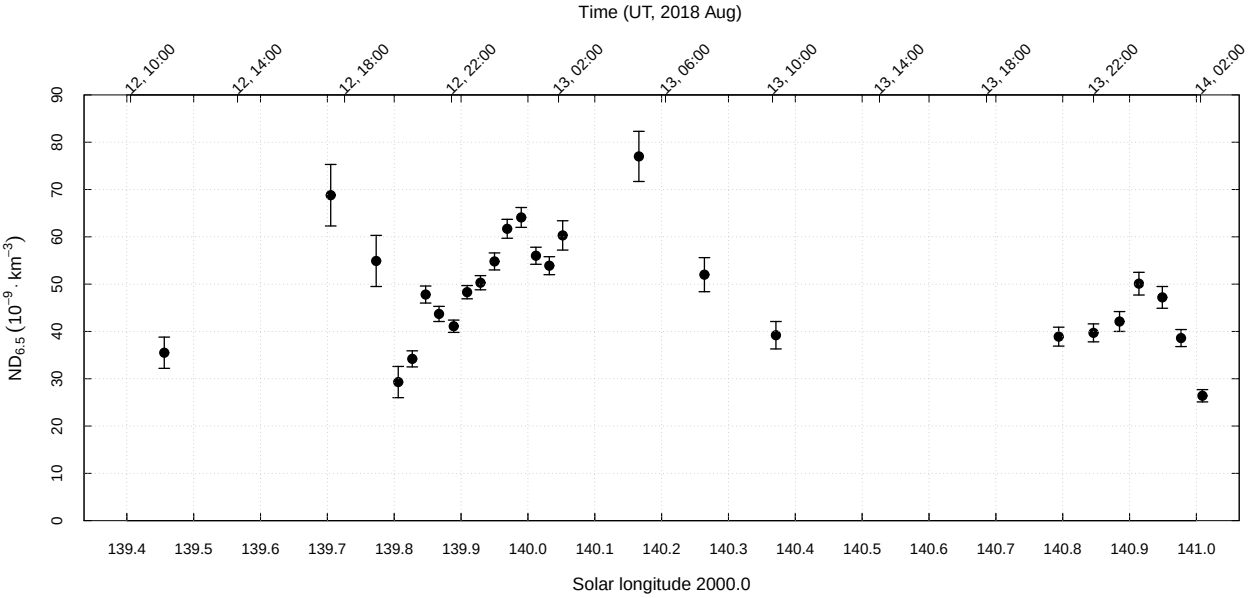

Figure 6 – Number density of meteoroids causing meteors of at least +6.5 mag during the 2018 Perseid maximum period. Using the procedures of Koschack and Rendtel (1990), a +6.5 mag Perseid is equivalent to a 0.45 mg meteoroid. This sample includes all visually accessable magnitude classes.

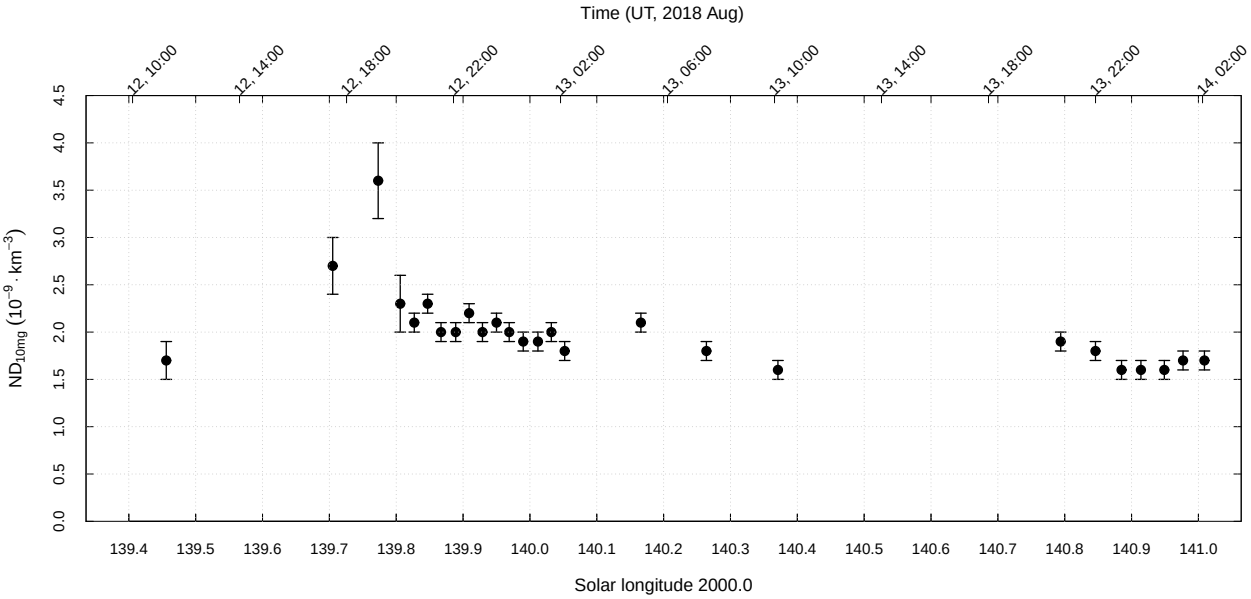

Figure 7 – Number density of meteoroids of at least 10 mg. For the Perseids this corresponds to meteors of +1.2 mag and brighter. It is obvious that the filament at $\lambda_\odot = 139\overset{\circ}{.}76$ is composed of larger meteoroids than the late peak at $\lambda_\odot = 140\overset{\circ}{.}16$.

For the Perseids, Jenniskens (2006) gives a width of $0\overset{\circ}{.}03 - 0\overset{\circ}{.}05$ for dust trails and the filament as well (Tables 5c and 5d). Longer durations have been observed for the dust trails in 1993 (about $0\overset{\circ}{.}11$) and the filament in 2004 (about $0\overset{\circ}{.}15$).

Filament encounters were observed on several occasions during the last decade or so. However, identification can be ambiguous with respect to other peaks, as filament predictions are uncertain by some hours (Jenniskens, 2006). Weiland (2019) claims that identification of resonant meteoroids is most effective by determination of the population index r in accordance with more or less prominent peaks in the activity profile. Obvious filament encounters in the past usually have been found to have $r < 1.80$ (Arlt, 1998; Jenniskens, 2006; Weiland, 2019; see also this work).

However, filament encounters may not necessarily show up as a distinct peak in the activity profile, as the 2015 data suggest. To the contrary, in 2016 a superposition of the filament with the AD 1079 dust trail appears to be present, resulting in a relatively sharp peak (Weiland, 2019). The 2007 return instead yielded only a moderate peak around the predicted time, though the population index was rather low (Rendtel, 2008).

Number density data allow best to distinguish between different meteoroid populations as we have shown here for the filament and the variations in the main (nodal) Perseid maximum 2018. The filament encounter is the most prominent structure in the number density profile for meteoroids of $\geq$ 10 mg Perseids (ND10mg profile, Figure 7).

5 Conclusions

Additional to the smooth general profiles of the population index r and the ZHR of the 2018 Perseid return, we find a strong signature of a filament encounter. This consists of a minimum in the population index $r = 1.60 \pm 0\overset{\circ}{.}08$ at $\lambda_\odot = 139\overset{\circ}{.}797$ (2018 August 12, $19^{\mathrm{h}}47^{\mathrm{m}}$ UT) and a peak ZHR $= 134 \pm 13$ at $\lambda_\odot \approx 139\overset{\circ}{.}773 \pm 0\overset{\circ}{.}20$ (2018 August 12, $19^{\mathrm{h}}11^{\mathrm{m}}$ UT). The filament encounter is most obvious in the number density profile for larger meteoroids with masses of $m \geq 10$ mg.

Further small rate enhancements are described as fluctuations within the stream. They appear only in the number density of all Perseids to +6.5 mag (ND6.5), but are not visible in the number density ND10mg of meteoroids with masses of at least 10 mg. Hence the size distribution at these locations do not differ from the main maximum region.

Visual observations can reveal details of the particle composition throughout the Perseids 2018, and the updated MetFns software package has allowed us to obtain these complete data. Hence we encourage to use the software for further analyses.

References

Arlt R. (1998). "Global analysis of the 1997 Perseids". *WGN, Journal of the IMO*, **26**, 61–71.

Arlt R. (2003). "Bulletin 19 of the International Leonid Watch: population index study of the 2002 Leonid meteors". *WGN, Journal of the IMO*, **31**, 77–87.

Buček M. and Porubčan V. (2014). "Taurid meteor complex". In Jopek T. J., Rietmeijer F. J. M., Watanabe J., and Williams I. P., editors, *Meteoroids 2013, Proceedings of the Astronomical Conference held at A.M. University, Poznan, Poland, Aug. 26–30, 2013*. pages 193–197.

Jakubík M. and Neslušan L. (2015). "Meteor complex of asteroid 3200 Phaethon: its features derived from theory and updated meteor data bases". *Mon. Not. R. Astron. Soc.*, **453**, 1186–1200.

Jenniskens P. (2006). *Meteor showers and their parent comets*. Cambridge Univ. Press.

Jenniskens P. and Betlem H. (2002). "Massive remnant of evolved cometary dust trail detected in the orbit of Halley-type comet 55P/Tempel-Tuttle". *Astrophys. J.*, **531**, 1161–1167.

Jenniskens P., Betlem H., de Lignie M., ter Kuile C., van Vliet M. C. A., van't Leven J., Koop M., Morales E., and Rice T. (1998). "On the unusual activity of the Perseid meteor shower (1989–96) and the dust trail of comet 109P/Swift-Tuttle". *Mon. Not. R. Astron. Soc.*, **301**, 941–954.

Koschack R. and Rendtel J. (1988). "Number density in meteor streams". *WGN, Journal of the IMO*, **16**, 149–157.

Koschack R. and Rendtel J. (1990). "Determination of spatial number density and mass index from visual meteor observations (II)". *WGN, Journal of the IMO*, **18**, 119–140.

Neslušan L., Hajduková, jr. M., and Jakubík M. (2013). "Meteor-shower complex of asteroid 2003 EH1 compared with that of comet 96P/Machholz". *Astron. Astrophys.*, **560**. id. A47 (10pp).

Rendtel J. (2008). "Filament and dust trail encounters and the mean Perseid maximum 2000-2007". *WGN, Journal of the IMO*, **36**, 68–76.

Rendtel J. (2014). *Meteor shower workbook 2014*. International Meteor Organization.

Rendtel J., Veljković K., Verbeeck C., Weiland T., and Knöfel A. (forthcoming). "Tricks of the trade: Global analysis of visual meteor observations using VMDB and MetFns — an example". In *Proceedings of the International Meteor Conference 2018 in Pezinok-Modra, Slovakia*.

Weiland T. (2019). "Young and old dust trails, filament, mean maximum peculiarities – evidence found in visual Perseid observations 2007–2016". *WGN, Journal of the IMO*, **47:1**, 26–37. (this issue).

Handling Editor: Javor Kac

This paper has been typeset from a LaTeX file prepared by the authors.

Young and old dust trails, filament, mean maximum peculiarities — evidence found in visual Perseid observations 2007–2016

Thomas Weiland[1]

Based on a data sample of nearly 3000 visual Perseids, gathered during the five most favourable returns within the examined 2007–2016 period, dust trail and filament encounters were identified from European longitudes. Detected peculiarities of the mean maximum complement this work. As a result, trail encounters of different age (2 to 12 revolutions of the parent comet 109P/Swift-Tuttle ago) become evident within $\sim 1°$ of solar longitude ($\lambda_\odot = 139\,\overset{\circ}{.}60$ to $140\,\overset{\circ}{.}59$). Corresponding ZHRs are ranging from ~ 95 to 170. Whereas in most cases population indices of dust trails do not vary with the age of the trail, significantly lower r-values (< 1.80) have been found for the 12-revolution trail and the filament.

Received 2018 November 14

1 Introduction

During the 1990s, the Perseids saw a series of outbursts, showing up as an additional peak preceding the mean maximum few hours to half a day, which established the fame of the Perseids as a dynamic meteor shower. This "new" peak was last seen in 1999, but in 2004, another short outburst few hours before the mean maximum was observed. Since then, various rate enhancements of varying strength were encountered at different positions of Earth's orbit, which could be attributed to dust trails formed by the parent comet 109P/Swift-Tuttle mainly during the last millennium and older dust kept in mean motion resonance by Jupiter respectively (Rendtel, 2014).

The following article tries to identify such encounters observed between 2007 and 2016, based on single visual observations performed by the author from different European longitudes (Austria; Crete, Greece; La Palma, Canary Islands, Spain). If applicable, peculiarities of the mean maximum are worked out and described, too.

2 Parent comet 109P/Swift-Tuttle

Comet 109P/Swift-Tuttle was independently discovered on 1862 July 16 by Lewis A. Swift and on 1862 July 19 by Horace P. Tuttle (1862 III). At the time, the concept of comets as a source of meteor showers was not widely accepted, but shortly thereafter, in 1866, Giovanni V. Schiaparelli proved the coincidence of the orbits of 109P/Swift-Tuttle and the Perseid stream.

109P/Swift-Tuttle is a short-period comet ($P \sim 135$ years), moving on a highly inclined ($i = 67°$) and thus stable, retrograde orbit. With a mean nucleus diameter of 26 km, it ranks as one of the biggest comets currently visiting the inner solar system. Prior to 1862, the comet was observed in 69 BC and AD 188 (Chinese records) and in 1737 by Ignatius Kegler in Beijing, China; the most recent perihelion return happened in late 1992. In 2126, the comet will pass a mere 0.153 AU from Earth and it will come even closer in 3044 and 4479. More than one thousand years ago, probably around the AD 698 return, 109P/Swift-Tuttle was forced by planetary perturbations into a 1:11-resonance with Jupiter (Jenniskens, 2006).

3 Dust trails, filament and the background component

The 1862 return of the comet was accompanied by enhanced Perseid rates of a few hundred per hour, but higher rates were also observed on various occasions later, even at times when the comet was near its aphelion, i.e. in 1921 (Jenniskens, 2006). With the last return of comet 109P/Swift-Tuttle rates rose to higher levels again, culminating in 1991–1994 with ZHRs of 200–300 (Rendtel, 2008). Initially, these outbursts were thought to be caused by young dust ejected from the comet one revolution ago, but detailed investigations turned out that for the major part resonant meteoroids of much older age (tens of revolutions ago) and trapped by Jupiter were responsible. The concentration of meteoroids kept in mean motion resonance near the comet was called a *filament* (Jenniskens et al., 1998), contrary to *dust trails*, which are mostly of younger age when crossing Earth's orbit. In this context the differentiation of Maslov (2018) of "young" dust trails (formed 1–7 revolutions ago) vs. "old" ones (at least 8 revolutions ago), is followed. Both, dust trails and the filament, superimpose the background component, which stems from different ejection periods and has seen lots of perturbations for thousands of years. Its densest concentration returns as the *mean maximum* every year. Perseid dust trails, although to a lesser degree perturbed as well, have a width of only $\sim 0\,\overset{\circ}{.}03 - 0\,\overset{\circ}{.}05$ in solar longitude (except 1993; $\sim 0\,\overset{\circ}{.}11$), comparable to the filament (except 2004; $\sim 0\,\overset{\circ}{.}15$) (Jenniskens, 2006; Tables 5c and 5d).

Apart from that, evidence has been found that Jupiter steers the stream roughly every 12 years (orbital period 11.86 years) to Earth by ~ 0.01 AU, leading to higher rates by a factor of ~ 1.5–2.0 (Maslov, 2018). This affects dust trails and the filament more than the mean maximum (Jenniskens, 2006). A similar effect is caused by Saturn roughly every 30 years (orbital period 29.46 years) (Maslov, 2018). These periodic shifts of the stream towards Earth would explain why higher rates could also occur, when the comet stays near its aphelion.

[1]Ospelgasse 12-14/6/19, 1200 Wien, Austria.
Email: thomas.weiland@aon.at

IMO bibcode WGN-471-weiland-perseids
NASA-ADS bibcode 2019JIMO...47...26W

Table 1 – Observing conditions and predictions 2007–2016 with respect to Central European longitudes.

Year	Mean Maximum	Visibility from Central Europe	k	Dust Trail	Filament	Visibility from Central Europe
2007	Aug 12, $\sim 06^h15^m$	no	+0.00			
	Aug 12			**22^h42^m** (1479) (V)		**yes**
	Aug 12			**22^h55^m** (1479) (S)		**yes**
	Aug 13			**00^h27^m** (1479) (L)		**yes**
	Aug 13				$\sim 04^h00^m$ (J)	no
2008	Aug 12, $\sim 12^h45^m$	no	+0.82			
	Aug 12			02^h57^m (1479) (S)		no
	Aug 12			05^h30^m (1479) (L)		no
	Aug 12				**$\sim 01^h00^m$** (J)	**yes**
2009	Aug 12, $\sim 18^h45^m$	no	−0.61			
	Aug 12			08^h01^m (1610) (S)		no
	Aug 12			08^h07^m (1610) (M)		no
2010	**Aug 13, $\sim 00^h45^m$**	**yes**	+0.13			
	Aug 12			14^h06^m (1479) (S)		no
	Aug 12			*16^h49^m* (1479) (V)		no
2011	Aug 13, $\sim 07^h15^m$	no	+1.00			
2012	Aug 12, $\sim 13^h15^m$	no	−0.25			
2013	Aug 12, $\sim 19^h30^m$	no	+0.32			
	Aug 12			15^h43^m (1079) (V)		no
2014	Aug 13, $\sim 01^h30^m$	yes	−0.92			
2015	Aug 13, $\sim 07^h45^m$	no	−0.02			
	Aug 12				**$\sim 23^h00^m$** (J)	**yes**
2016	Aug 12, $\sim 14^h15^m$	no	+0.67			
	Aug 11			**23^h23^m** (1479) (M)		**yes**
	Aug 12			**00^h32^m** (Combined 15 revs) (MSFC)		**yes**
	Aug 12			04^h36^m (1079) (MSFC)		no
	Aug 12			04^h43^m (1079) (V)		no
	Aug 12			13^h03^m (441) (MSFC)		no
	Aug 12				*$\sim 04^h00^m$–05^h00^m* (J)	no

4 Observing conditions and predictions 2007–2016

Because of the dispersion of the background component, Perseids can be observed from around Mid-July to late August ($\lambda_\odot \sim 115-155°$), which implies that every year sees a moon-free period for observing them. As for the mean maximum, however, favourable conditions for a defined observing place are recurring only every eight years (least common multiple of the leap year's misfit in combination with similar lunar phases).

For the 2007–2016 period, Table 1 gives a compilation of the mean maximum visibility with respect to Central European longitudes, together with the illumination of the moon (k) at the expected time in UT (from *IMO Meteor Shower Calendars*, 2007–2016).

Additionally, predictions of significant dust trail and filament encounters (ZHR ≥ 50) are noted and in bold, if they were theoretically observable from Central Europe. Sources: J = Peter Jenniskens; L = Esko Lyytinen; M = Mikhail Maslov; MSFC = Marshall Space Flight Center, NASA; S = Isao Sato; V = Jérémie Vaubaillon (from Jenniskens, 2006; Cooke et al., 2016; CBETs; Maslov, 2018). Later updates from CBETs with respect to Jenniskens (2006) are in Italics. Given times refer to UT.

Consequently, the years **2007, 2008, 2015** and **2016** look most promising for identifying possible dust trail and filament encounters from European longitudes within the given period. **2010** serves as a "reference year" to some extent, as the mean maximum fell within European night times with no disturbing moonlight.

5 Observing method and data analysis

Fieldwork was carried out as single visual observations. For determination of the limiting magnitudes direct vision in combination with averted view was performed.

Population indices were derived using the magnitude difference between the meteors and the limiting stellar magnitudes, based on table 7.2, p. 122 and the table on p. 124 in the *Handbook for Meteor Observers* (Rendtel & Arlt, 2014). Only intervals with minor moonlight interference and at least 30 meteors were considered.

ZHR calculations followed the procedure given in the *Handbook for Meteor Observers* (Rendtel & Arlt, 2014), based on individual population indices. The zenith exponent was assumed to be $\gamma = 1.0$. No perception coefficient was applied. In general, intervals allowed for ZHR calculations were restricted as follows: $T_{\text{eff}} \geq 0.50$ h, $F \leq 1.20$, $lm \geq 5.50$ and $h_{\text{Rad}} \geq 20°$. If not stated otherwise, observing periods with a total correction factor of $cf_{\text{tot}} \geq 5.00$ were discarded.

With respect to the 2010 "reference profile", only the period between August 06/07 and 15/16 ($\lambda_\odot \sim 135$–$145°$) was considered. During that time, the Perseids are regarded as a major shower (ZHR > 10).

Table 2 – Magnitude distribution and population index of 421 Perseids logged from 2007 August 06/07 to 15/16.

Date	lm	−6	−5	−4	−3	−2	−1	0	+1	+2	+3	+4	+5	+6	Σ	r
06/07	5.64	0	0	1	0	0	1	1	0	1	2	6	1	0	13	
07/08	5.62	0	0	0	1	0	0	2	2	6	0	4	2	0	17	
08/09	5.60	0	0	0	1	0	1	3	3	1	7	3	1	0	20	
12/13	5.79	0	1	4	2	9	5	19	7	17	27	30	9	0	130	2.05 ± 0.14
13/14	5.83	0	1	1	2	4	10	21	14	26	27	27	8	0	141	2.05 ± 0.13
14/15	5.80	0	0	0	0	4	5	7	6	11	12	17	5	0	67	
15/16	6.15	0	0	1	2	0	3	4	1	7	3	7	5	0	33	
Σ		0	2	7	8	17	25	57	33	69	78	94	31	0	421	
Mean	5.78															2.12 ± 0.08

6 Results

6.1 Extended mean maximum and possible young dust trail in 2007

6.1.1 Observation

Observations were carried out from August 06/07 until 15/16 (total effective observing time $T_{\text{eff}} = 26.02$ h) at Atzelsdorf, Lower Austria, Austria (16°33′11″E, 48°30′30″N, 220 m; GPS/WGS84). Because of interfering moonlight at the beginning of the period ($k \leq 0.39$) and somewhat hazy skies, limiting magnitudes were ranging between $lm = 5.50$ and 6.20 (average 5.78; Table 2). During the given period 730 meteors were logged, of which 421 were classified as Perseids (PER) and 250 as sporadics (SPO).

Despite the expected time of the mean maximum (August 13, $\sim 06^{\text{h}}15^{\text{m}}$ UT), both nights of August 12/13 and 13/14 yielded almost equal, albeit less than average hourly counts. Fireballs (meteors of magnitude −4 or brighter) turned up throughout the whole period, most abundant on August 12/13 (Table 2).

6.1.2 Magnitude distribution and population index

In general, the magnitude distribution of the 2007 Perseids fits a standard function, showing a maximum at magnitude class +4. Apart from that, a second peak becomes evident at magnitude class 0 (Figure 1; Table 2). Of the PER logged, 14% were brighter than magnitude 0 and 2% classified as fireballs.

Determination of the population index for the whole period yielded a mean value of $r = 2.12 \pm 0.08$ (Table 2). Going in line with similar activity observed on both nights of August 12/13 and 13/14 (Section 6.1.1), the corresponding mean population indices show the same value ($r = 2.05 \pm 0.14$ and $r = 2.05 \pm 0.13$ resp.; Table 2). For comparison, calculation of the population index of the sporadic background results in a mean r of 2.81 ± 0.20.

6.1.3 ZHR profile

At a glance, similar activity on both nights of August 12/13 and 13/14 (Section 6.1.1) is the most prominent feature of the 2007 Perseids, which is borne out by the ZHR profile as well (Figure 2). In return, maximum ZHRs barely seem to have reached the typical value of 100 (Rendtel, 2014), instead hovering around 60–70 for most of the observing time.

As for the night of August 12/13, the first observing hour ($21^{\text{h}}00^{\text{m}}$ to $22^{\text{h}}00^{\text{m}}$ UT) started out with a ZHR of 48 ± 13, almost doubling during the next interval ($22^{\text{h}}00^{\text{m}}$ to $23^{\text{h}}00^{\text{m}}$ UT; 92 ± 16). Then rates were going back again to 54 ± 12 ($23^{\text{h}}00^{\text{m}}$ to $00^{\text{h}}00^{\text{m}}$ UT) and 62 ± 12 ($00^{\text{h}}00^{\text{m}}$ to $01^{\text{h}}00^{\text{m}}$ UT) respectively. During the last observing hour ($01^{\text{h}}00^{\text{m}}$ to $02^{\text{h}}00^{\text{m}}$ UT) once more an increase of the ZHR to 91 ± 15 was seen.

Highest rates on August 13/14 were almost comparable to those of August 12/13, with maximum ZHRs at the beginning and the end of the night of 73 ± 17 and 75 ± 12 respectively (Figure 2).

To determine the maximum time on August 12/13, ZHR values based on 10-minute intervals and an average population index of $r = 2.05$ (Section 6.1.2) have been

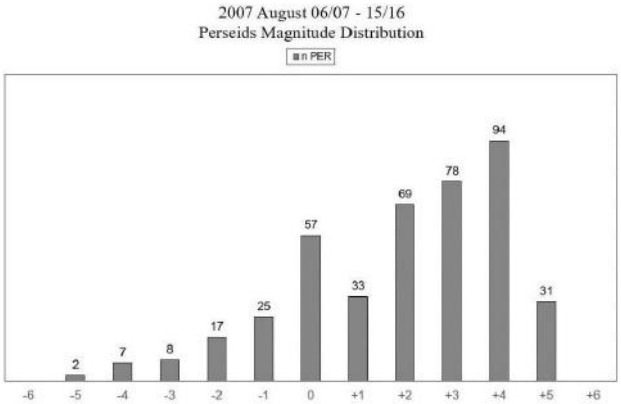

Figure 1 – Magnitude distribution of 421 Perseids logged from 2007 August 06/07 to 15/16.

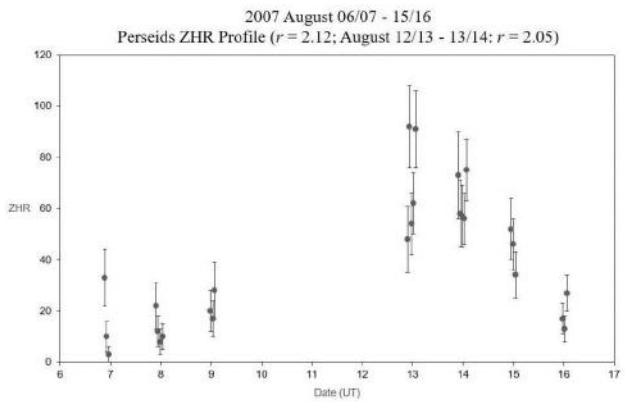

Figure 2 – Perseids ZHR profile from 2007 August 06/07 to 15/16.

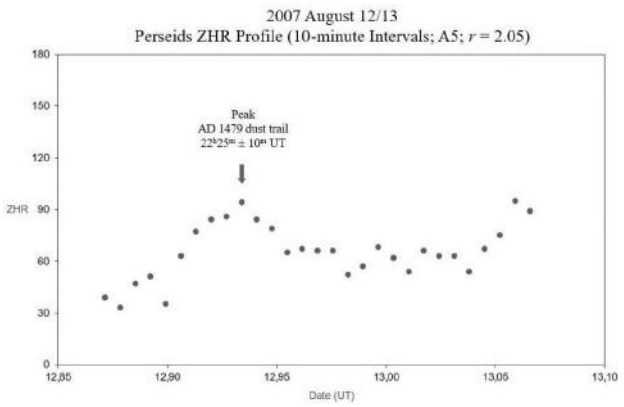

Figure 3 – Perseids ZHR profile of 2007 August 12/13 (10-minute intervals; A5).

calculated. In a further step, to smooth the profile, ZHR values were averaged using a sliding mean of five bins per step (A5), yielding an activity curve seen in Figure 3. This gives a clear peak at $22^{\rm h}25^{\rm m} \pm 10^{\rm m}$ UT with a ZHR $\sim$ 95 and a width of $\sim 0\,^{\circ}\!.05$ ($\sim$ 1.3 h). A second peak of comparable strength comes out at $01^{\rm h}25^{\rm m} \pm 10^{\rm m}$ UT.

6.1.4 Discussion

The average population index determined for the 2007 Perseids within the given period ($r = 2.12$) corresponds to values detected during earlier returns, whereas the mean r-value for August 12/13 (2.05) seems to be somewhat higher (Rendtel, 2014). Nevertheless, the average population index found for the sporadic background ($r = 2.81 \pm 0.20$) is in accordance with the mean value of $\sim$ 2.85 given for the period of $\lambda_{\odot} \sim 125$–$150°$ in Fig. 1.11, p. 14 of the *Handbook for Meteor Observers* (Rendtel & Arlt, 2014).

As for the times of the detected peaks (Section 6.1.3), no significantly deviant r-values were later determined for the interval of $22^{\rm h}00^{\rm m}$ to $23^{\rm h}00^{\rm m}$ UT (2.07 ± 0.35) and $01^{\rm h}00^{\rm m}$ to $02^{\rm h}00^{\rm m}$ UT (2.18 ± 0.34) respectively, giving no hint on either of them.

Apart from that, the first peak seen in Figure 3 matches in some way the times of the AD 1479 (4-rev) dust trail encounter predicted by Vaubaillon and Sato, but not by Lyytinen (Table 1). Maximum ZHR was at the order of 95 ($\sim$ 50% above the background component) with a width of $\sim 0\,^{\circ}\!.05$ ($\sim$ 1.3 h).

The second peak in Figure 3 is difficult to interpret, as the filament encounter was forecast to occur later that day (Table 1). With respect to the corresponding population index, which is significantly higher than for the filament found during previous returns ($r < 1.80$; cf. Arlt, 1998; Jenniskens, 2006), this explanation seems to be unlikely.

Furthermore, as both nights of August 12/13 and 13/14 yielded nearly identical ZHR-values (Section 6.1.3), one may assume a mean maximum of longer duration, going in hand with a below average peak value (< 100). This was indeed confirmed by Rendtel (2008).

In summary, it can be concluded that the 2007 return of the Perseids revealed two peculiar features: an extended, less than average mean maximum for the duration of at least 1.2 days ($\sim$ August 12.9 to 14.1; $\lambda_{\odot} \sim 139\,^{\circ}\!.7$–$140\,^{\circ}\!.8$) and probably an encounter with the young AD 1479 (4-rev) dust trail on August 12, $22^{\rm h}25^{\rm m} \pm 10^{\rm m}$ UT ($\lambda_{\odot} = 139\,^{\circ}\!.73 \pm 0\,^{\circ}\!.01$).

6.2 Unexpected old dust trail in 2008

6.2.1 Observation

Observations were again carried out at Atzelsdorf, Austria (Section 6.1.1) from August 07/08 until 12/13. Because of slightly hazy skies, limiting magnitudes did not exceed $lm = 6.00$ (average 5.90; Table 3). Strong interfering moonlight at the end of the period ($k \leq 0.85$) was reducing the dark sky window considerably, resulting in a total effective observing time of only $T_{\rm eff} =$ 12.11 h. In summary, 490 meteors were logged, of which 361 were regarded as PER and 117 as SPO.

2008 marked the beginning of gravitational perturbations of the stream by Saturn (Section 3), culminating in 2009 (Maslov, 2018). Consequently, mean maximum ZHRs were expected to be somewhat higher than usual, at the order of 110–120 (Maslov, 2018).

However, Europe would not benefit from Saturn's influence, as the mean maximum was predicted to recur on August 12, $\sim 12^{\rm h}45^{\rm m}$ UT, amidst daylight hours. Therefore, expectations for both nights of August 11/12 and 12/13 were not high. Indeed, hourly counts after moonset ($22^{\rm h}36^{\rm m}$ UT) on August 11/12 were matching the typical pre-maximum values. Fireballs were only seen during dawn, after official observation ended (one of magnitude -4 and -5 each).

On August 12/13 fieldwork was resumed two hours before moonset ($23^{\rm h}32^{\rm m}$ UT). Despite the mean maximum already lying behind, numerous bright meteors and even fireballs (up to magnitude -4) appeared. Additionally, rates were rising after $23^{\rm h}30^{\rm m}$ UT, and this trend continued during the following hour ($00^{\rm h}30^{\rm m}$ to $01^{\rm h}30^{\rm m}$ UT). At $01^{\rm h}30^{\rm m}45^{\rm s}$ UT a fireball of magnitude -4 appeared, ending up in a terminal flash of -7. At the latest at this moment, it became clear that an unexpected outburst was going on. The final highlight came at $02^{\rm h}00^{\rm m}15^{\rm s}$ UT, when a pair of magnitude -5 and -2 simultaneously turned up, travelling on nearly parallel paths offset by some 15°. From that time on rates were declining again, probably not only as an effect of the advancing dawn. At $02^{\rm h}30^{\rm m}$ UT, shortly after nautical twilight began, the observation ended.

6.2.2 Magnitude distribution and population index

In some way, the magnitude distribution of the 2008 Perseids resembles that of 2007, showing a maximum at magnitude class +4 and a second peak around magnitude class 0, from -1 to +1 (Figure 4; Table 3). Apart from that, bright meteors appeared more abundantly in 2008, mainly as result of the unexpected outburst (Section 6.2.1). Consequently, 35% of the PER logged were brighter than magnitude 0, whereas a similar proportion as in 2007 (1%) was classified as fireballs.

Going along with the higher proportion of meteors of magnitude 0 and brighter a significant lower mean population index than in 2007 was determined ($r =$

Table 3 – Magnitude distribution and population index of 361 Perseids logged from 2008 August 07/08 to 12/13.

Date	lm	−8	−7	−6	−5	−4	−3	−2	−1	0	+1	+2	+3	+4	+5	+6	Σ
07/08	5.90	0	0	0	0	0	0	0	2	1	0	2	0	4	1	0	10
09/10	5.90	0	0	0	0	0	1	0	1	1	2	0	5	11	1	0	22
10/11	5.97	0	0	0	0	0	0	1	1	3	1	2	1	0	0	0	9
11/12	5.95	0	0	0	0	0	3	7	18	21	11	12	20	34	4	0	130
12/13	5.83	0	1	0	1	3	12	10	19	22	26	14	27	49	6	0	190
Σ		0	1	0	1	3	16	18	41	48	40	30	53	98	12	0	361
Mean	5.90		$r = 1.88 \pm 0.07$														
11/12			$r = 1.89 \pm 0.11$														
12/13			$r = 1.85 \pm 0.09$														

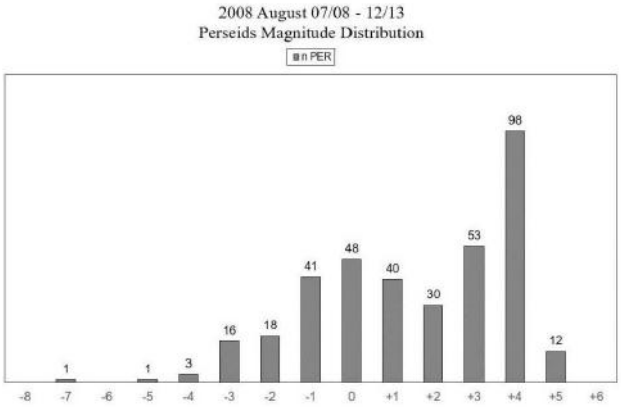

Figure 4 – Magnitude distribution of 361 Perseids logged from 2008 August 07/08 to 12/13.

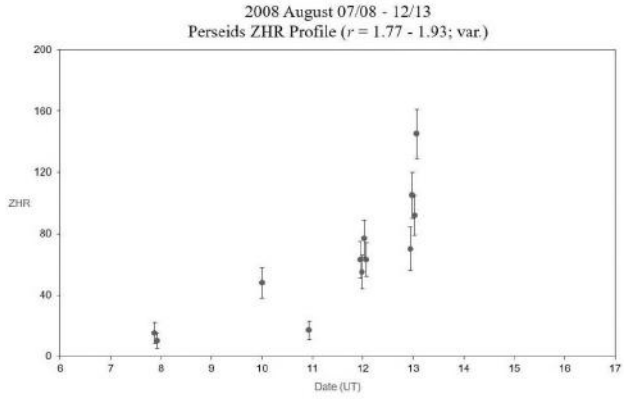

Figure 5 – Perseids ZHR profile from 2008 August 07/08 to 12/13.

1.88 ± 0.07; Table 3). Due to the fact, that in 2008 the bulk of meteors was observed during the nights of August 11/12 and 12/13, corresponding r-values do not show any deviation to speak of (1.89 ± 0.11 and 1.85 ± 0.09 resp.; Table 3).

Concerning the time span encompassing the predicted filament encounter on August 12 (Table 1), calculation of individual population indices yielded higher r-values than the average found for August 11/12: 1.96 ± 0.28 ($00^{\mathrm{h}}00^{\mathrm{m}}$ to $01^{\mathrm{h}}00^{\mathrm{m}}$ UT) and 2.01 ± 0.27 ($01^{\mathrm{h}}00^{\mathrm{m}}$ to $02^{\mathrm{h}}00^{\mathrm{m}}$ UT) respectively.

As for the observed outburst on August 12/13 (Section 6.2.1), the opposite trend can be recognized: during the first partly dark sky period ($23^{\mathrm{h}}10^{\mathrm{m}}$ to $00^{\mathrm{h}}10^{\mathrm{m}}$ UT) the population index of $r = 1.93 \pm 0.21$ was higher than the average, continuously going down to $r = 1.77 \pm 0.13$ throughout the last observing period ($01^{\mathrm{h}}10^{\mathrm{m}}$ to $02^{\mathrm{h}}10^{\mathrm{m}}$ UT).

Concerning the sporadic background, the mean population index within the given period was found to be $r = 2.62 \pm 0.26$.

6.2.3 ZHR profile

The observed outburst of August 12/13 is clearly seen on the activity graph in Figure 5. Based on an individual population index (Section 6.2.2) the ZHR value for the first reasonable dark sky interval ($22^{\mathrm{h}}10^{\mathrm{m}}$ to $23^{\mathrm{h}}10^{\mathrm{m}}$ UT) was of the same order (70 ± 14) as those of August 11/12. At the time, the waxing gibbous moon was still up. During the next hour ($23^{\mathrm{h}}10^{\mathrm{m}}$ to $00^{\mathrm{h}}10^{\mathrm{m}}$ UT), a significant rise to 105 ± 15 could be observed, followed by a decline to 92 ± 13 between $00^{\mathrm{h}}10^{\mathrm{m}}$ to $01^{\mathrm{h}}10^{\mathrm{m}}$ UT. Thereafter the ZHR jumped up by a factor of more than 50% to 145 ± 16 ($01^{\mathrm{h}}10^{\mathrm{m}}$ to $02^{\mathrm{h}}10^{\mathrm{m}}$ UT).

To get out the peak in detail, the activity profile of August 12/13 was examined in the same way as the 2007 data (Section 6.1.3; $r = 1.85$; 10-minute intervals; A5). As a result, the outburst appears to be more prominent, with ZHR values steadily rising by a factor of more than 50% from ∼ 105 to 165 (Figure 6). As an effect of the advancing dawn, the exact time of the relatively broad peak remains somewhat uncertain, probably around $02^{\mathrm{h}}00^{\mathrm{m}} \pm 10^{\mathrm{m}}$ UT. Because of this reason, the width can only roughly be estimated as ∼ 0.°08 (∼ 1.8 h), considering a symmetrical shape.

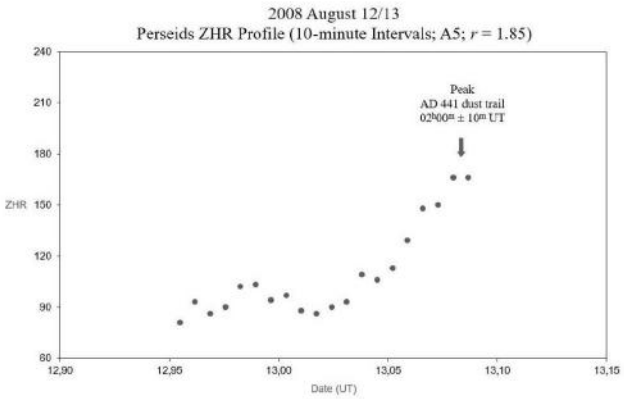

Figure 6 – Perseids ZHR profile of 2008 August 12/13 (10-minute intervals; A5).

Table 4 – Magnitude distribution and population index of 882 Perseids logged from 2010 August 06/07 to 15/16.

Date	lm	−6	−5	−4	−3	−2	−1	0	+1	+2	+3	+4	+5	+6	Σ	r
06/07	6.20	0	0	0	0	1	1	3	3	0	3	6	1	0	18	
07/08	6.39	0	0	1	1	1	3	5	5	5	9	10	3	0	43	
08/09	6.50	0	0	1	1	3	4	6	4	8	10	12	2	0	51	
09/10	6.18	0	1	1	2	1	3	6	2	6	11	10	6	0	49	
10/11	6.49	0	0	1	1	0	5	3	4	8	6	4	2	0	34	
11/12	6.28	0	0	0	4	7	9	13	4	11	14	24	11	0	97	
12/13	6.47	0	1	2	12	22	35	30	36	48	62	81	29	0	358	1.78 ± 0.06
13/14	6.29	0	0	1	4	8	11	11	7	9	17	28	11	0	107	
14/15	6.19	0	0	2	5	9	9	6	9	7	9	21	9	0	86	
15/16	6.41	0	0	0	1	3	2	6	1	0	9	9	8	0	39	
Σ		0	2	9	31	55	82	89	75	102	150	205	82	0	882	
Mean	6.35															1.82 ± 0.04

6.2.4 Discussion

The average population index determined for 2008 was clearly lower ($r = 1.88$) than in 2007 (Section 6.1.2), as was the mean r-value for August 12/13 (1.85). Nevertheless, both values match those yielded during previous returns (Rendtel, 2014). This applies to the sporadic background, too; the mean population index within the given period was found to be $r = 2.62 \pm 0.26$.

Individual population indices during the predicted filament encounter (Section 6.2.2) give no sign to it, as they were significantly higher ($00^{\mathrm{h}}00^{\mathrm{m}}$–$01^{\mathrm{h}}00^{\mathrm{m}}$ UT: 1.96; $01^{\mathrm{h}}00^{\mathrm{m}}$–$02^{\mathrm{h}}00^{\mathrm{m}}$ UT: 2.01) than supposed for resonant meteoroids ($r < 1.80$; Section 6.1.4). Therefore, one may conclude that the encounter did not materialize, at least not during Central European night time hours.

A rather low population index, however, was found during the observed outburst ($01^{\mathrm{h}}10^{\mathrm{m}}$–$02^{\mathrm{h}}10^{\mathrm{m}}$ UT: $r = 1.77$). This refers either to the filament, which seems unlikely with respect to the predicted time (Table 1), or an old dust trail.

Indeed, CBET 1480 (Jenniskens et al., 2008b) gives a likely explanation. Based on calculations by Vaubaillon, the outburst may be the result of an encounter with the AD 441 dust trail, which was predicted to fall just outside Earth's orbit with a close passage at August 12, $23^{\mathrm{h}}34^{\mathrm{m}}$ UT. The low population index found, comparable to the filament, would fit such an old trail, as does the broad peak.

In summary, it can be concluded that during the 2008 return Earth had an encounter with the old AD 441 (12-rev) dust trail on August 13, $02^{\mathrm{h}}00^{\mathrm{m}} \pm 10^{\mathrm{m}}$ UT ($\lambda_{\odot} = 140\,^{\circ}59 \pm 0\,^{\circ}01$), yielding a maximum ZHR of ~ 165. On the assumption of a symmetrical shape, the peak had an estimated width of $\sim 0\,^{\circ}08$ (~ 1.8 h). It occurred at the latest solar longitude of any outburst observed within the 1988–2013 period (Rendtel, 2014). However, during the 1997 return a third peak showed up at a very close position ($\lambda_{\odot} = 140\,^{\circ}35$–$140\,^{\circ}45$); it was last seen in 1999 (Arlt, 1998; Arlt, 1999; Rendtel & Arlt, 1999; Arlt & Händel, 2000). According to Lyytinen (cited in Jenniskens, 2006; p. 298; Fig. 17.29), older dust trails tend to shift the nodes to a later time.

6.3 Additional young dust trail in 2010?

6.3.1 Observation

In 2010, Perseid observations were performed from a southerly location for the first time. Because of excellent weather statistics ($\sim 90\%$ probability of clear skies in August), the Greek Island of Crete was chosen as a suitable observing site. The outcome were ten nights of observing in a row, from August 06/07 to 15/16 (total effective observing time $T_{\mathrm{eff}} = 42.31$ h). Even at sea level, near Frangokástello (24°13′04″E, 35°11′25″N, 0 m; GPS/WGS84) limiting magnitudes were all the time well beyond $lm = 6.00$ (Table 4). However, just at the night of the expected mean maximum (August 12/13) haze moving in from the sea forced a relocation to the mountains. There, between Ímbros and Ásfendos (24°11′24″E, 35°15′02″N, 1100 m; GPS/WGS84), one was rewarded with unspoiled skies ($lm = 6.50$ before dawn). As no moonlight was interfering all the time, the average limiting magnitude for the whole period came to $lm = 6.35$ (Table 4). In summary, 1642 meteors were logged; 882 of them were classified as PER and 677 as SPO.

On August 12/13 observation started at $19^{\mathrm{h}}30^{\mathrm{m}}$ UT, at a time, when the radiant was still rather low in the sky ($h_{\mathrm{Rad}} = 11\,^{\circ}62$). However, observed rates did not meet this fact, as they were surprisingly high. Beautiful and impressive earth-grazing meteors turned up, followed by an obvious decrease in activity after one hour or so. The fall back lasted until around $22^{\mathrm{h}}30^{\mathrm{m}}$ UT; thereafter rates regained strength, culminating just before dawn.

6.3.2 Magnitude distribution and population index

The most striking feature of the 2010 Perseids was the high proportion of meteors of magnitude 0 and brighter (30%), especially within the −1 to −3 magnitude range. Apart from that, PER of magnitude 0 were again overrepresented, as in 2007 and 2008 (Figure 7). 1% were classified as fireballs.

Going along with it, the high percentage of meteors of magnitude 0 and brighter found its expression in the lowest population index ever determined by the author for the period of August 06/07 to 15/16 ($r = 1.82 \pm 0.04$; Table 4). Accordingly, the mean r-value for the night

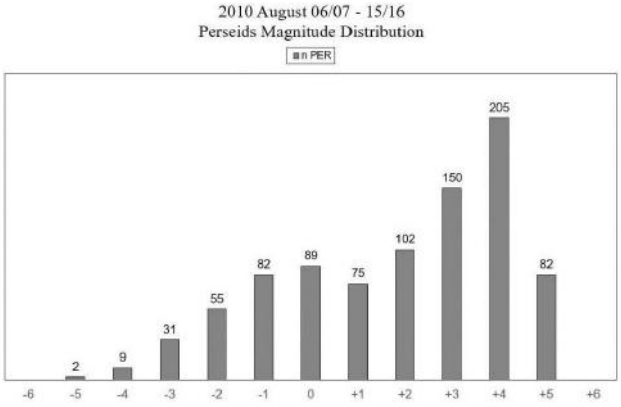

Figure 7 – Magnitude distribution of 882 Perseids logged from 2010 August 06/07 to 15/16.

of August 12/13 (1.78 ± 0.06; Table 4) ranks among the lowest ever found. As for the sporadics, the average population index ($r = 2.46 \pm 0.09$) falls to the low end of the given period, too.

6.3.3 ZHR profile

Due to perfect weather conditions (Section 6.3.1), the activity profile covers the whole period between August 06/07 and 15/16 (Figure 8). It shows a steeper rise than decline, unusual for the Perseids, as a contrary behaviour is the rule (Rendtel, 2014).

Because of the unexpectedly high rates at the beginning of August 12/13 (Section 6.3.1), ZHR calculation included the interval of $20^{\mathrm{h}}00^{\mathrm{m}}$ to $21^{\mathrm{h}}00^{\mathrm{m}}$ UT, despite the low elevation of the radiant (mean altitude $17\overset{\circ}{.}28$). However, as the amount of the total correction factor does not exceed 5.00 ($cf_{\mathrm{tot}} = 3.54$), it was retained. The corresponding ZHR achieved 85 ± 17, not falling far from typical maximum values. If the earliest observing interval ($19^{\mathrm{h}}30^{\mathrm{m}}$ to $20^{\mathrm{h}}30^{\mathrm{m}}$ UT) had been used, it even would have come to 123 ± 23. The following hour ($21^{\mathrm{h}}00^{\mathrm{m}}$ to $22^{\mathrm{h}}00^{\mathrm{m}}$ UT) saw a significant backdrop in the ZHR (62 ± 13), thereafter rates were commuting a value of 75. Only during the last observing hour ($01^{\mathrm{h}}00^{\mathrm{m}}$ to $02^{\mathrm{h}}00^{\mathrm{m}}$ UT), the ZHR steeply rose to 117 ± 12.

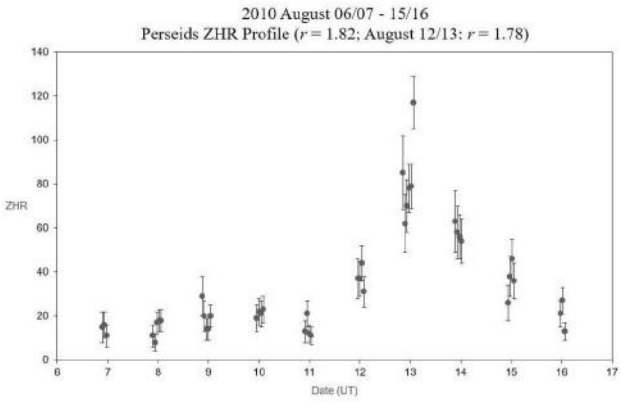

Figure 8 – Perseids ZHR profile from 2010 August 06/07 to 15/16.

6.3.4 Discussion

As mentioned, the mean population index for the investigated period seems to be rather low ($r = 1.82$), as is the value for August 12/13 (1.78) and the sporadics (2.46 ± 0.09). The reason for this is not clear, as the sky quality cannot be blamed ($6.20 \leq lm \leq 6.50$). Nevertheless, a systematic error may be possible. Maslov (2018) points out that in 2010 the Perseid stream still saw a minor gravitational effect by Saturn, like in 2008 (Section 6.2.1). However, this would have affected the whole stream, not only bigger particles (Maslov, personal communication).

Similarly, the first ZHR peak at the beginning of the night of August 12/13 is difficult to explain, as double mean maxima have not been observed with the Perseids so far (Rendtel, 2014). Moreover, the second peak matches the predicted time of the mean maximum (August 13, $\sim 00^{\mathrm{h}}45^{\mathrm{m}}$ UT) better than the first. Therefore, an encounter with the tail of the AD 1479 (4-rev) dust trail may be an explanation, though overcorrection of the ZHR due to the low radiant altitude cannot be excluded. Furthermore, the above average ZHR of the second peak, probably representing the mean maximum, indeed suggests an influence of Saturn.

Summing up, it can be concluded that the 2010 return yielded an above average mean maximum on August 13, $\sim 02^{\mathrm{h}}$ UT ($\lambda_{\odot} \sim 140\overset{\circ}{.}1$) or later, with a ZHR of ~ 115 and a below average population index of $r = 1.78$. At least the ZHR value supports a minor gravitational effect by Saturn. The earlier peak may be the tail of the young AD 1479 (4-rev) dust trail, which appears to have occurred on August 12, $\sim 20^{\mathrm{h}}$ UT ($\lambda_{\odot} \sim 139\overset{\circ}{.}8$) or earlier, but later than forecast (Table 1); the corresponding ZHR was ~ 100.

6.4 Resonant meteoroids in 2015?

6.4.1 Observation

The great success of the 2010 Perseid campaign with respect to the number of logged meteors initiated another one in Crete five years later (observing period from August 09/10 to 15/16). However, the weather in 2015 did not cooperate as well. Consequently, two of the seven nights (13/14 and 14/15) suffered from clouds, especially the second one, but close to the expected mean maximum (August 12/13) skies remained unspoiled.

Depending on the expected sky quality, observations were carried out from two different spots: at sea level, near Thrafterós Potamós ($23°43'19''$E, $35°14'19''$N, 0 m; GPS/WGS84) and from a higher elevation, near Prodrómi ($23°45'34''$E, $35°15'34''$N, 550 m; GPS/WGS84).

Due to minor moonlight interference at the beginning of the period ($k \leq 0.21$), limiting magnitudes were ranging between $lm = 5.90$ and 6.50 (average 6.35; Table 5). Within 26.64 h of total effective observing time 871 meteors were logged, of which 568 were classified as PER and 257 as SPO.

For 2015 increasing gravitational perturbations of the stream by Jupiter were predicted (Section 3), reaching their climax in 2016 (Maslov, 2018). Like other years with minor influence of Jupiter and Saturn, maximum ZHRs were expected to be at the order of 110–120

Table 5 – Magnitude distribution and population index of 568 Perseids logged from 2015 August 09/10 to 15/16.

Date	lm	−8	−7	−6	−5	−4	−3	−2	−1	0	+1	+2	+3	+4	+5	+6	Σ
09/10	6.15	0	0	1	0	0	1	2	2	5	4	4	9	3	2	0	33
10/11	6.38	0	0	0	0	0	1	1	5	5	5	4	6	8	4	0	39
11/12	6.38	0	0	0	0	0	3	4	6	5	1	14	30	18	6	0	87
12/13	6.38	0	1	0	1	4	5	10	23	23	34	42	62	74	18	0	297
13/14	6.30	0	0	0	1	0	3	3	6	5	5	8	13	10	1	0	55
15/16	6.50	0	0	0	0	0	0	0	7	5	6	7	6	18	8	0	57
Σ		0	1	1	2	4	13	20	49	48	55	79	126	131	39	0	568
Mean	6.35		$r = 1.89 \pm 0.05$														
12/13			$r = 1.88 \pm 0.07$														

(Maslov, 2018). This would not favour European longitudes, as the mean maximum was to recur on August 13, $\sim 07^{\mathrm{h}}45^{\mathrm{m}}$ UT. However, the filament passage (August 12, $\sim 23^{\mathrm{h}}00^{\mathrm{m}}$ UT; Table 1) would be detectable.

Moreover, according to Vaubaillon there was a small chance of an encounter with the AD 1862 (1-rev) dust trail on August 12, $17^{\mathrm{h}}32^{\mathrm{m}}$ UT, mainly composed of faint meteors (cf. Jenniskens 2006; not listed in Table 1 because the estimated ZHR was < 50). Hence, observation started as early as $19^{\mathrm{h}}00^{\mathrm{m}}$ UT that day. At the time, the radiant had an elevation of only $9\,^{\circ}\!.05$, but observed rates were above average for 2–3 hours. During the first, earth-grazing meteors turned up, too. At $21^{\mathrm{h}}59^{\mathrm{m}}20^{\mathrm{s}}$ UT a fireball of magnitude −4 appeared, bursting with a terminal flash of −7; it left a persistent train for 45 s. This marked the beginning of a sequence of fireballs (three of magnitude −4 and one of −5) within roughly one hour, but coinciding with a backdrop in activity. For the rest of the night, rates were hovering around typical pre-maximum values; very bright meteors did not appear anymore.

6.4.2 Magnitude distribution and population index

Despite the array of fireballs (Section 6.4.1), the overall magnitude distribution of the 2015 Perseids looks quite normal; a slight positive deviation from the standard function can be seen for the magnitude −1 and the +3 class (Figure 9). Consequently, concerning meteors of at least magnitude 0 and fireballs, calculation yielded similar percentages as the average for the 2007–2010 period (24% and 1% resp.).

In accordance with the magnitude distribution, the average population index for the whole period comes to $r = 1.89 \pm 0.05$; for August 12/13 an r-value of 1.88 ± 0.07 was found (Table 5). Concerning the sporadic background, the population index was determined as $r = 2.82 \pm 0.20$.

With respect to the observed sequence of fireballs, it seemed worth to examine whether it had an influence on the population index. For this reason, the dataset of August 12/13 was divided into three subsets: the $21^{\mathrm{h}}45^{\mathrm{m}}$–$23^{\mathrm{h}}15^{\mathrm{m}}$ UT period, comprising the array of fireballs, and the adjacent periods of $19^{\mathrm{h}}00^{\mathrm{m}}$–$21^{\mathrm{h}}45^{\mathrm{m}}$ UT and $23^{\mathrm{h}}15^{\mathrm{m}}$–$02^{\mathrm{h}}30^{\mathrm{m}}$ UT respectively. Interestingly, the "fireball period" does not show a much divergent value ($r = 1.86 \pm 0.18$), whereas for both adjoining intervals significant deviations become visible ($r = 1.78 \pm 0.15$ and 1.93 ± 0.10 resp.).

6.4.3 ZHR profile

As in 2010 (Section 6.3.3), the ZHR profile shows a steeper rise than decline (Figure 10). To examine the activity early on August 12/13, the first observing interval ($19^{\mathrm{h}}00^{\mathrm{m}}$ to $20^{\mathrm{h}}00^{\mathrm{m}}$ UT) was retained, despite a very high total correction factor of $cf_{\mathrm{tot}} = 5.63$ (mean radiant altitude $11\,^{\circ}\!.40$); it yielded a ZHR of 107 ± 25. During the following hour ($20^{\mathrm{h}}00^{\mathrm{m}}$ to $21^{\mathrm{h}}00^{\mathrm{m}}$ UT), the ZHR decreased to 88 ± 18. At the time, the mean radiant elevation was still as low as $17\,^{\circ}\!.00$, but the cf_{tot}-value had dropped to 3.81. For the rest of the night, ZHRs varied between 71 ± 13 and 93 ± 12, indicating no clear trend.

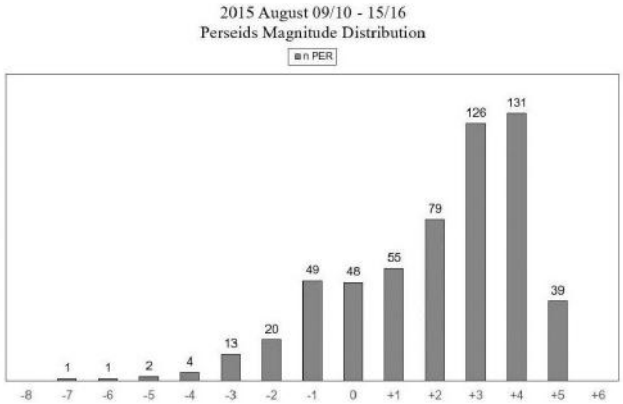

Figure 9 – Magnitude distribution of 568 Perseids logged from 2015 August 09/10 to 15/16.

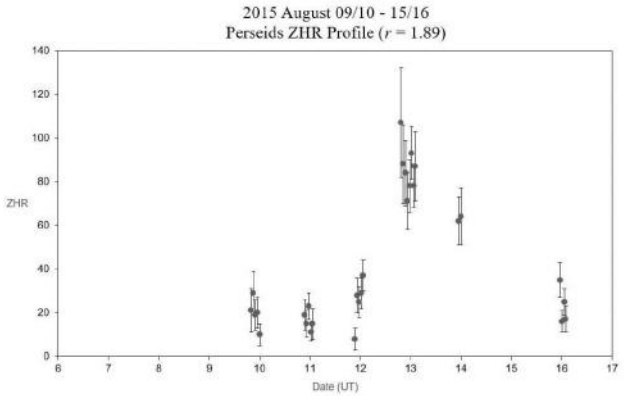

Figure 10 – Perseids ZHR profile from 2015 August 09/10 to 15/16.

Table 6 – Magnitude distribution and population index of 748 Perseids logged from 2016 August 06/07 to 13/14.

Date	lm	−6	−5	−4	−3	−2	−1	0	+1	+2	+3	+4	+5	+6	Σ	r
06/07	6.11	0	0	0	2	0	4	4	4	7	7	13	4	0	45	
09/10	6.30	0	0	0	0	1	1	1	1	3	3	5	1	0	16	
10/11	6.45	0	0	0	0	3	6	6	3	11	13	18	12	0	72	
11/12	6.43	0	2	4	10	21	30	36	34	47	74	106	44	0	408	1.90 ± 0.06
12/13	6.44	0	2	3	3	6	5	9	15	16	17	54	29	0	159	2.11 ± 0.13
13/14	6.65	0	0	1	1	2	2	2	2	6	4	14	14	0	48	
Σ		0	4	8	16	33	48	58	59	90	118	210	104	0	748	
Mean	6.40															2.00 ± 0.05
11/12, 01^h30^m–04^h00^m	6.50	0	0	1	5	11	13	14	24	34	40	60	24	0	226	1.94 ± 0.09
11/12, 04^h00^m–05^h30^m	6.46	0	2	3	4	10	15	17	9	10	29	42	14	0	155	1.78 ± 0.09

6.4.4 Discussion

The above average activity observed early on August 12/13 gave rise to the question if the enhanced rates were real, and what might be the reason for it. To clarify this, one must consider them in context with the observing conditions and the population index as well.

The latter has yielded a typical, almost identical mean value, both, for the whole period ($r = 1.89$) and the night of August 12/13 ($r = 1.88$) as well. Apart from that, individual r-values on August 12/13 started out with 1.78 ± 0.15 and ended up at 1.93 ± 0.10. This could reflect a real trend or merely be an effect of the steadily climbing radiant. On the other hand, the obvious concentration of fireballs within a short timespan (Section 6.4.1) cannot be denied.

The same applies to the ZHRs. The observed activity was higher than expected for the pre-maximum period, but overcorrection due to the low altitude of the radiant might also be an explanation for it.

Anyway, the coincidence of enhanced rates together with a low population index does not support a possible encounter with the AD 1862 (1-rev) trail. More likely seems a signature of the filament, but earlier than expected. According to Jenniskens (2006), predicted times concerning the filament are uncertain by some hours.

Currently it is not clear whether in 2015 resonant meteoroids were responsible for the peak and the concentration of fireballs observed on August 12. If a filament encounter indeed materialized, it came earlier than predicted ($\sim 20^h$ UT; $\lambda_\odot \sim 139\,^\circ\!.6$), yielding a maximum ZHR of 90–100. With respect to the observed concentration of fireballs, which might represent the tail of the filament, the peak appears to be rather broad, as in 2004 (estimated width $\sim 0\,^\circ\!.15$; ~ 4 h) (Section 3).

6.5 Multiple dust trail and filament encounters in 2016

6.5.1 Observation

Within the examined ten-year period 2016 seemed to be the most rewarding one for identifying dust trail and filament encounters, as there were several passages predicted by different authors. Especially Central to Western European longitudes would benefit from this exceptional return (Table 1). For this reason, the author joined a group of Dutch meteor observers (Felix Bettonvil, Sietse Dijkstra, Klaas Jobse, Carl Johannink and Casper ter Kuile), who had selected La Palma, Canary Islands, Spain as the most promising location to observe the 2016 Perseids.

Additionally, there was a strong gravitational effect by Jupiter expected, resulting in a higher activity level of the background component with a ZHR of 150–160 (Maslov, 2018) (Section 3).

During the starting night of August 06/07, observations were carried out from Atzelsdorf, Austria (Section 6.1.1). On La Palma, beginning with August 09/10, first a site beneath the road LP-4 (17°49′59″W, 28°45′01″N, 2140 m; GPS/WGS84) was chosen. From August 10/11 until 13/14, fieldwork was performed on the grounds of the Observatorio del Roque de los Muchachos (17°52′52″W, 28°45′36″N, 2360 m; GPS/WGS84).

In total, 21.72 h of effective observing time yielded 1191 meteors, of which 748 were classified as PER and 355 as SPO. Limiting magnitudes between moonset and dawn were all the time > 6.00; on the last night (August 13/14), atmospheric conditions even surpassed the quality of the standard sky ($6.50 \leq lm \leq 6.70$). However, at the beginning of the session in La Palma, sky transparency suffered somewhat from Calima, a common weather phenomenon during summer months.

Because of the waxing gibbous moon ($k \geq 0.62$), observation on August 11/12 did not start earlier than 23^h30^m UT. Short time before, a brief flurry of medium-bright meteors had caught the attention, but with a glaring moon and the radiant still low in the sky, it easily remained unnoticed. Naturally, observed rates stayed low until moonset (01^h24^m UT); then they were rapidly rising with an obvious peak between 02^h00^m to 03^h00^m UT. At the time, numerous meteors appeared simultaneously, though no one brighter than magnitude −3 was seen. After 03^h30^m UT rates were somewhat receding, interrupted by a fireball of magnitude −5 at $04^h06^m35^s$ UT and the flash of a meteor of magnitude −6 at $04^h14^m20^s$ UT, the latter turning up outside the field of vision. This marked the beginning of an array of fireballs (three of magnitude −4 and one of −5) within less than one hour. Additionally, from that time on activity was on the rise again, well persisting into dawn. At 05^h40^m UT, observation ended, as the limiting magnitude was already down at 5.50.

6.5.2 Magnitude distribution and population index

Overall, the magnitude distribution of the 2016 Perseids fits a standard function, showing a maximum at the magnitude +4 class (Figures 11–13; Table 6). 22% of the PER logged were brighter than magnitude 0, whereas a similar proportion as in previous years (2%) was classified as fireballs.

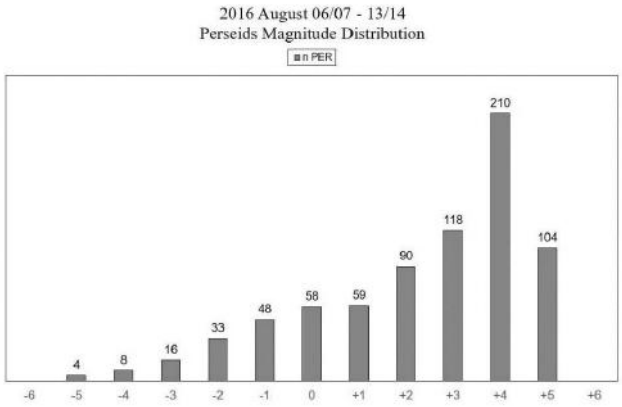

Figure 11 – Magnitude distribution of 748 Perseids logged from 2016 August 06/07 to 13/14.

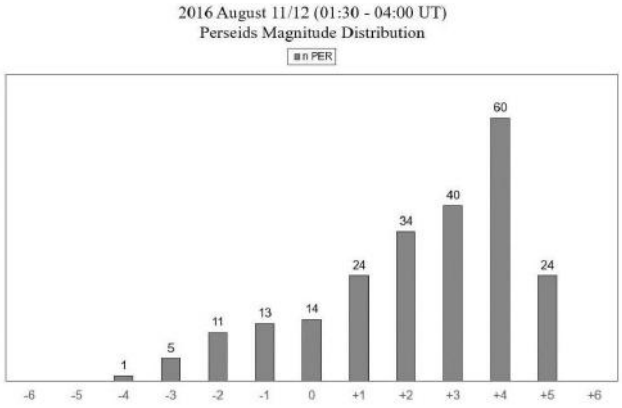

Figure 12 – Magnitude distribution of 226 Perseids logged on 2016 August 11/12, $01^{h}30^{m}$–$04^{h}00^{m}$ UT.

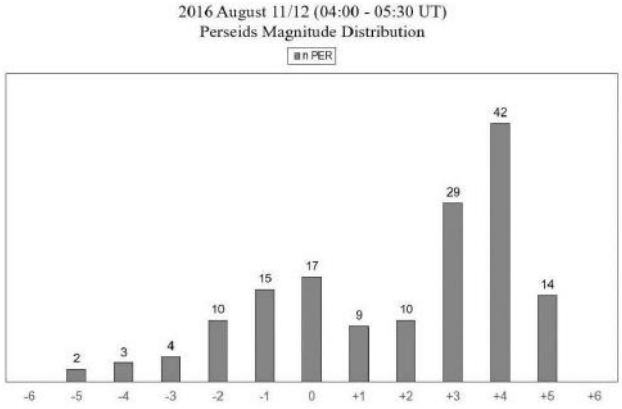

Figure 13 – Magnitude distribution of 155 Perseids logged on 2016 August 11/12, $04^{h}00^{m}$–$05^{h}30^{m}$ UT.

As for August 11/12, a somewhat different pattern becomes visible. Consequently, the $01^{h}30^{m}$–$04^{h}00^{m}$ UT interval (Figure 12) resembles the magnitude distribution of the whole period. The $04^{h}00^{m}$–$05^{h}30^{m}$ UT interval instead, comprising the sequence of fireballs, additionally indicates a bulge within the 0 to −2 magnitude range (Figure 13).

This is reflected by the population indices as well (Table 6). For the $01^{h}30^{m}$–$04^{h}00^{m}$ UT interval, an r-value of 1.94 ± 0.09 came out, whereas the $04^{h}00^{m}$–$05^{h}30^{m}$ UT interval yielded a value of 1.78 ± 0.09. The latter is significantly lower than the mean for August 11/12 ($r = 1.90 \pm 0.06$) and the whole period as well ($r = 2.00 \pm 0.05$).

For the sporadic background the population index was found as $r = 2.74 \pm 0.16$.

6.5.3 ZHR profile

Because of moonlight interference and the low radiant altitude at the beginning of the observing session on August 11/12 (Section 6.5.1), the first interval ($23^{h}30^{m}$ to $00^{h}30^{m}$ UT) was not used for ZHR calculation ($cf_{\mathrm{tot}} = 5.94$). For the second hour ($00^{h}30^{m}$ to $01^{h}30^{m}$ UT), a ZHR of 94 ± 18 was found. Thereafter, ZHRs were steeply rising to 158 ± 16 between $02^{h}30^{m}$ and $03^{h}30^{m}$ UT, followed by a relative backdrop to 122 ± 13 between $03^{h}30^{m}$ and $04^{h}30^{m}$ UT. The last observing interval ($04^{h}30^{m}$ to $05^{h}30^{m}$ UT) finally saw a resurgence of the ZHR to 142 ± 14 (Figure 14).

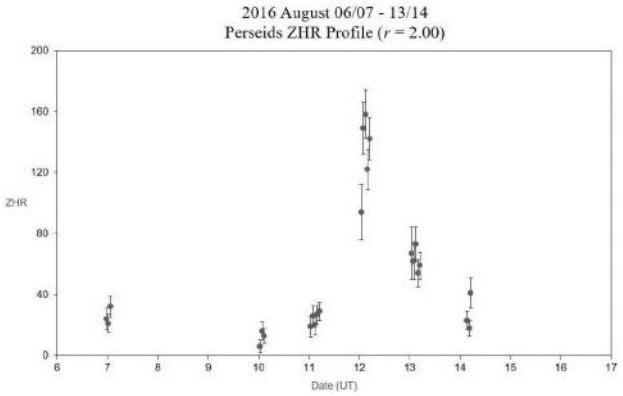

Figure 14 – Perseids ZHR profile from 2016 August 06/07 to 13/14.

As Figure 15 indicates, the activity graph shows two distinct peaks on August 11/12. To get them out more clearly, the profile was examined in the same way as the 2007 and 2008 data (Sections 6.1.3, 6.2.3; $r = 2.00$; 10-minute intervals; A5). The result is depicted in Figure 15. First, a double peak with a maximum ZHR of $\sim$ 170 at $02^{h}45^{m} \pm 10^{m}$ UT can be seen. After a pronounced dip, around $04^{h}00^{m}$ UT, a second peak of comparable strength becomes evident. As the observed rates were still rising at the end of the session, the peak probably occurred after $05^{h}15^{m}$ UT. However, because of the advancing dawn, ZHRs may be slightly over-corrected; therefore, a value of $\sim$ 160 seems to be plausible. With respect to the ZHR level at the beginning of the smoothed profile ($\sim$ 145), the width of the first peak comes to $\sim 0\overset{d}{.}05$ ($\sim$ 1.3 h). On the assumption of a symmetrical shape, that of the second one can only be estimated as $\sim 0\overset{d}{.}08$ ($\sim$ 1.8 h).

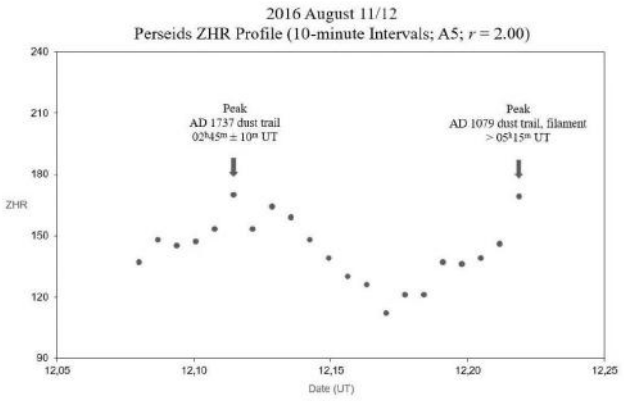

Figure 15 – Perseids ZHR profile of 2016 August 11/12 (10-minute intervals; A5).

6.5.4 Discussion

At a glance, neither the mean population index for the whole period of August 06/07 to 13/14 ($r = 2.00$) nor that for August 11/12 ($r = 1.90$) gives any hint on special events. Going into detail of the 11/12 data, however, reveals two different distributions before and after $\sim 04^{\rm h}00^{\rm m}$ UT, the latter roughly marking the onset of an array of fireballs (Section 6.5.1). Consequently, the population index found for the period until $05^{\rm h}15^{\rm m}$ UT was rather low (1.78), whereas the r-value for the $01^{\rm h}30^{\rm m}$–$04^{\rm h}00^{\rm m}$ UT period (1.94) appears to be slightly higher than the August 11/12 mean.

In accordance with the activity profile, the first peak, found at $02^{\rm h}45^{\rm m} \pm 10^{\rm m}$ UT, may thus be attributed to the very young AD 1737 (2-rev) dust trail, which was not listed in Table 1 because of the uncertain and rather unspecific prediction (August 12, $00^{\rm h}$ to $04^{\rm h}$ UT, according to Vaubaillon; cf. Rendtel, 2015). As for the second peak, which may have persisted into dawn ($> 05^{\rm h}15^{\rm m}$ UT), an encounter with the moderately old AD 1079 (7-rev) dust trail seems to be likely. The passage of AD 1079 trail was forecast to happen around $04^{\rm h}40^{\rm m}$ UT (Table 1).

Due to the rather low population index at that time (see above), one may further assume a blend of the filament (predicted for $04^{\rm h}00^{\rm m}$ to $05^{\rm h}00^{\rm m}$ UT; Table 1) with the AD 1079 trail. In this case, the r-value would speak for the filament and the relatively sharp peak for the dust trail respectively. On the assumption of a symmetrical shape, the width of the second peak was estimated as $\sim 0\,^{\circ}\!.08$ (~ 1.8 h); the first one (see above) had a width of $\sim 0\,^{\circ}\!.05$ (~ 1.3 h).

Concerning the peak of the AD 1479 (4-rev) dust trail, which occurred on August 11/12 before official observation began (Section 6.5.1), it is referred to Miskotte and Vandeputte (2017).

Finally, it can be stated that at least two encounters of Earth with dust trails, one of them probably blended with the filament, were observed on 2016 August 11/12. The resulting peaks occurred at $02^{\rm h}45^{\rm m} \pm 10^{\rm m}$ UT ($\lambda_\odot = 139\,^{\circ}\!.60 \pm 0\,^{\circ}\!.01$) and probably after $05^{\rm h}15^{\rm m}$ UT ($\lambda_\odot > 139\,^{\circ}\!.70$). Corresponding ZHRs were of the order of ~ 170 and ~ 160 respectively.

7 Conclusion

Based on a total number of 2980 Perseids, logged during the five most favourable returns within the examined ten-year period (2007–2016), encounters of Earth with dust trails and the filament were identified from different European longitudes. Detected peculiarities of the mean maximum further complement this work. The results can be summarized as follows:

Dust trail encounters:
Encounters of earth with certain dust trails were observed in 2016 (AD 1737, 2-rev; AD 1079, 7-rev), in 2008 (AD 441, 12-rev) and probably in 2007 (AD 1479, 4-rev). An encounter with the latter in 2010 remains doubtful. As the passage of the AD 1479 trail in 2016 went by almost unnoticed from the given location, it was not treated any further.

Concerning the position of the peaks, they were found to happen on either side of the mean maximum ($\lambda_\odot \sim 140\,^{\circ}\!.1$; see below). The earliest was detected in 2016 (August 12, $02^{\rm h}45^{\rm m} \pm 10^{\rm m}$ UT; $\lambda_\odot = 139\,^{\circ}\!.60 \pm 0\,^{\circ}\!.01$), whereas the latest occurred in 2008 (August 13, $02^{\rm h}00^{\rm m} \pm 10^{\rm m}$ UT; $\lambda_\odot = 140\,^{\circ}\!.59 \pm 0\,^{\circ}\!.01$), comprising a period of $\sim 1^\circ$ in solar longitude. The other peak in 2016 (August 12, $> 05^{\rm h}15^{\rm m}$ UT; $\lambda_\odot > 139\,^{\circ}\!.70$) and that in 2007 (August 12, $22^{\rm h}25^{\rm m} \pm 10^{\rm m}$ UT; $\lambda_\odot = 139\,^{\circ}\!.73 \pm 0\,^{\circ}\!.01$) were lying closer to the maximum of the annual return, as was the possible peak in 2010 (August 12, $< 20^{\rm h}$ UT; $\lambda_\odot < 139\,^{\circ}\!.8$). The 2008 peak was the latest observed within the 1988–2013 period.

Corresponding ZHRs varied greatly, depending on the geometry of the encounter and the assumed strength of any gravitational influence of Jupiter and Saturn respectively. The lowest peak value was found in 2007 (ZHR ~ 95; no influence), whereas the strongest outbursts occurred in 2008 (ZHR ~ 165; minor influence of Saturn) and in 2016 (ZHRs ~ 170 and ~ 160 resp.; strong influence of Jupiter). If any encounter materialized in 2010 (minor influence of Saturn), the corresponding ZHR was ~ 100.

The width of the outbursts showed variations, too. Values found were as narrow as $\sim 0\,^{\circ}\!.05$ (~ 1.3 h) in 2016 (very young AD 1737 trail) and roughly as wide as $\sim 0\,^{\circ}\!.08$ (~ 1.8 h) in 2008 (old AD 441 trail). The young AD 1479 trail (2007) and the moderately old AD 1079 trail (2016) yielded a width of $\sim 0\,^{\circ}\!.05$ (~ 1.3 h) and roughly $\sim 0\,^{\circ}\!.08$ (~ 1.8 h) respectively.

Except for old dust trails, population indices do not seem to vary significantly with the age of the trail. Consequently, r-values found during encounters with the AD 1479 trail and the AD 1737 trail were within the range of the background component (see below). Contrary, the AD 441 trail yielded a population index of $r = 1.77$. A similar value (1.78) was found for the AD 1079 trail, but this may be attributed to the filament as well (see below). However, no outburst caused by the very young AD 1862 (1-rev) trail has been observed within the 2007–2016 period (see Table 1).

Filament encounters:
The most likely encounter with the filament was observed in 2016, though a superposition of the AD 1079

dust trail appears to exist (see above), resulting in a relatively sharp peak of roughly $\sim 0\,^{\circ}\!.08$ (~ 1.8 h) width. Peak time was determined not to be earlier than August 12, $05^{\mathrm{h}}15^{\mathrm{m}}$ UT ($\lambda_{\odot} = 139\,^{\circ}\!.70$), and the ZHR at that time comes to ~ 160. The corresponding population index was found to be as low as $r = 1.78$, comparable to the AD 441 trail (see above).

As the 2015 data suggest, filament passages are not necessarily discernible as a distinct peak. Hence, discrimination is most effective by determination of the population index in accordance with more or less prominent peaks in the activity profile; any concentration of fireballs may give an additional hint. In 2015, the population index at the time of the possible encounter (August 12, $\sim 20^{\mathrm{h}}$ UT; $\lambda_{\odot} \sim 139\,^{\circ}\!.6$) was again as low as $r = 1.78$, coinciding with a maximum ZHR of 90–100. With respect to the observed concentration of fireballs, the peak width was estimated as $\sim 0\,^{\circ}\!.15$ (~ 4 h), broader than in 2016.

Mean maximum:
For the mean maximum period (August 11/12 to 12/13) the average r-value was determined to vary between 1.78 (2010) and 2.11 (2016); the mean comes to 1.94. However, low values may be affected by either old dust trails and/or the filament (see above). Oddly, the only year with a neglectable influence, and in which the mean maximum was recurring during European night times (2010), yielded an untypically low population index of $r = 1.78$. Population indices found for the background component within the given period (August 06/07 to 15/16) were ranging from $r = 1.82$ (2010) to 2.12 (2007). The mean amounts to $r = 1.94$.

In 2007 an extended mean maximum was observed, which lasted for the duration of at least 1.2 days ($\sim$ August 12.9 to 14.1; $\lambda_{\odot} \sim 139\,^{\circ}\!.7$–$140\,^{\circ}\!.8$); corresponding ZHRs were less than average (hovering around 60–70, peak value < 100).

Contrary, during the 2010 return, the maximum ZHR reached an above average value of 110–120 on August 13, $\sim 02^{\mathrm{h}}$ UT ($\lambda_{\odot} \sim 140\,^{\circ}\!.1$), probably reflecting a minor gravitational effect by Saturn.

References

Arlt R. (1998). "Global analysis of the 1997 Perseids". *WGN, Journal of the IMO*, **26**, 61–71.

Arlt R. (1999). "Global analysis of the 1998 Perseid meteor shower". *WGN, Journal of the IMO*, **27**, 237–249.

Arlt R. and Händel I. (2000). "The "new" peak failed: First analysis of the 2000 Perseids". *WGN, Journal of the IMO*, **28**, 166–171.

Cooke B., Moser D., and Moorhead A. (2016). "Spacecraft risk posed by the 2016 Perseid outburst". In *Meteoroids 2016*. 29 pages. (`https://ntrs.nasa.gov/archive/nasa/casi.ntrs.nasa.gov/20160008884.pdf`).

Jenniskens P. (2006). *Meteor Showers and their Parent Comets*. Cambridge University Press, 790 pages.

Jenniskens P., Barentsen G., Johannink C., Jobse K., Dijkstra S., ter Kuile C., Bettonvil F., and Weiland T. (2016a). "2016 Perseid meteors". *CBET*, **4296**. (2016-08-13).

Jenniskens P., Betlem H., de Lignie M., ter Kuile C., van Vliet M. C. A., van 't Leven J., Koop M., Morales E., and Rice T. (1998). "On the unusual activity of the Perseid meteor shower (1989-96) and the dust trail of comet 109P/Swift-Tuttle". *Mon. Not. R. Astron. Soc.*, **301**, 941–954.

Jenniskens P., Lyytinen E., Vaubaillon J., and Maslov M. (2008a). "Perseid meteors 2008". *CBET*, **1464**. (2008-08-09).

Jenniskens P. and Nakano S. (2010). "2010 Perseid meteors". *CBET*, **2416**. (2010-08-17).

Jenniskens P., Sato I., Lyytinen E., and Vaubaillon J. (2007). "Perseid meteors 2007". *CBET*, **1019**. (2007-08-02).

Jenniskens P. and Vaubaillon J. (2010). "2010 Perseid meteors". *CBET*, **2401**. (2010-08-04).

Jenniskens P., Vaubaillon J., Maslov M., Moser D., and Cooke B. (2016b). "2016 Perseid meteors". *CBET*, **4293**. (2016-08-09).

Jenniskens P., Webb C. I., Kitting C., Peterson C. L., Miskotte K., and Vaubaillon J. (2008b). "Perseid meteors 2008". *CBET*, **1480**. (2008-08-26).

Maslov M. (2018). "Perseids 1901-2100: predictions of activity". (`http://feraj.ru/Radiants/Predictions/1901-2100eng/Perseids1901-2100predeng.html`) . (accessed 2018 November 14).

McBeath A., editor (2006-2014). *2007-2015 Meteor Shower Calendars*. International Meteor Organization.

Miskotte K. and Vandeputte M. (2017). "The magnificent outburst of the 2016 Perseids, the analyses". *MeteorNews*, **2**, 61–69.

Rendtel J. (2008). "Filament and dust trail encounters and the mean Perseid maximum 2000-2007". *WGN, Journal of the IMO*, **36**, 68–76.

Rendtel J., editor (2014). *Meteor Shower Workbook 2014*. International Meteor Organization, Potsdam.

Rendtel J., editor (2015). *2016 Meteor Shower Calendar*. International Meteor Organization.

Rendtel J. and Arlt R. (1999). "First results of the 1999 Perseid meteor shower". *WGN, Journal of the IMO*, **27**, 250–255.

Rendtel J. and Arlt R., editors (2014). *Handbook for Meteor Observers*. International Meteor Organization, Potsdam.

Handling Editor: Javor Kac

Preliminary results

Results of the IMO Video Meteor Network — February 2018, and testing of new cameras

Sirko Molau[1], *Stefano Crivello, Rui Goncalves, Carlos Saraiva, Enrico Stomeo, Jörg Strunk, Javor Kac*

During 2018 February, cameras of the IMO Video Meteor Network recorded over 16 500 meteors in about 8 300 hours of observing time. New cameras are presented that appear useful for meteor observations and can be recommended following the discontinuation of the manufacturing of CCTV cameras using Sony ExView HAD CCD sensor.

Received 2019 January 29

1 Introduction

The meager weather continued during the second month of 2018. The effective observing time was slightly higher than in 2018 January and higher than the output of the previous two years, but as often there were significant regional differences. Cameras in Portugal and Germany enjoyed more than twenty observing nights, whereas observers in other countries had make do with less. Some observers in Eastern Europe could not even manage ten observing nights.

Overall, 76 active video cameras recorded more than 16 500 meteors in 8 300 hours of effective observing time (Table 2 and Figure 1). 29 cameras observed during twenty or more observing nights. The average yield of 2.0 meteors per hours matches the February mean of the last few years and points to the upcoming annual minimum in meteor activity.

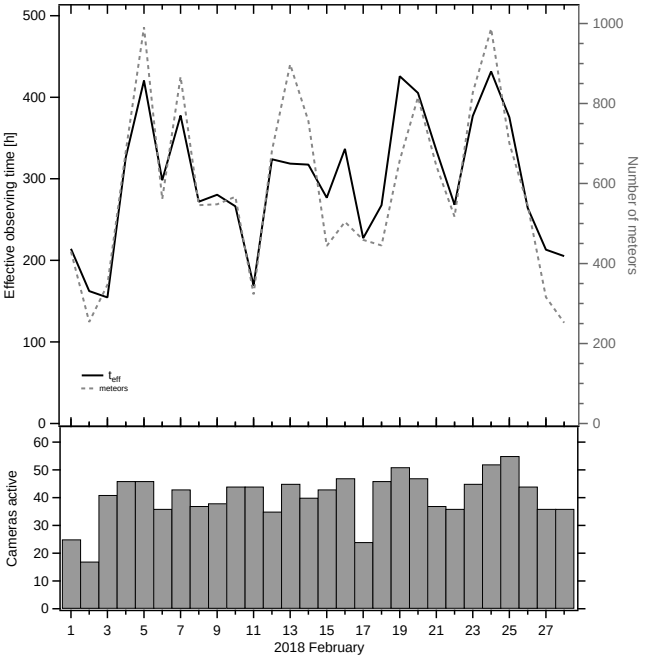

Figure 1 – Monthly summary for the effective observing time (solid black line), number of meteors (dashed gray line) and number of cameras active (bars) in 2018 February.

2 Testing new cameras

In the absence of relevant meteor showers, we want to have a quick look at the observing equipment. Until now, most observers have relied on Mintron or Watec cameras for the video observation of meteors. Both are based on the Sony ExView HAD CCD sensor. Following Sony's 2015 announcement of the discontinuation of the manufacturing of CCD chips and subsequently ceasing production (Carroll, 2015), these cameras will sooner or later disappear from the environment and we will need a replacement. HD cameras get an ever-higher consumer market share, but meteor detection software still tends to be tailored for a standard video signal. This is why the first author was particular curious, when Russian amateur Dmitrii Rychkov approached him in August 2018 and asked for Sirko's opinion on a new video camera with a CMOS sensor. He had assembled a camera from components similar to those used in the commercial camera "RunCam Night Eagle" (which was designed for Drones and other scale model devices) and adapted it to the needs of video meteor observers, e.g. by giving it a convenient CCTV-like body with a c-mount adapter.

In mid-September the test camera Dimcam1 was ready to use at Sirko's site. It replaced his Mintron-based camera Mincam1 which had been suffering from severe hardware problems for weeks. First light testing immediately showed promise, since despite the lower price the camera was at least half a magnitude more sensitive than Mincam1, and it also displayed a more "comfortable" line-based noise pattern (probably because of the rolling shutter). During the first few clear nights, the camera was already recording the same number or more meteors than the image-intensified camera Avis2, which has the highest long-term average meteor count of all IMO Network cameras. That was also confirmed by the camera parameters measured: Whereas Avis2 reached a limiting magnitude of 6.7 with field of view of 1204 square degrees, the test camera achieved magnitude 6.5 at 1550 square degrees. The small differ-

[1]Abenstalstr. 13b, 84072 Seysdorf, Germany.
Email: sirko@molau.de

IMO bibcode WGN-471-molau-vidfeb
NASA-ADS bibcode 2019JIMO...47...38M

Table 1 – Observing results of the cameras Avis2 and Dimcam1 in the 4th quarter of 2018.

	Avis2			Dimcam1		
Month	Nights	Time [h]	Meteors	Nights	Time [h]	Meteors
October 2018	26	192.5	2463	24	170.5	2467
November 2018	16	91.6	806	13	83.5	1041
December 2018	24	82.4	420	23	49.6	412
Sum	66	366.5	3689	60	303.6	3920

ences between the cameras should almost cancel each other out. In fact, Dimcam1 recorded more meteors than Avis2 in the 4th quarter of 2018, because the camera observed in south eastern direction, whereas Avis2 pointed in the meteor-poor north-western direction.

However, the tests also revealed a few teething problems for Dimcam1:

- Due to the housing design, the camera had so small a back focus, that the powerful Computar lens could only be mounted without the aberration filter and this had an adverse impact on the image quality. Bright stars were blurred to large blobs (Figure 2, left).
- The image was distorted, because the 16:9 sensor was mapped without correction to a 4:3 video signal.
- The camera had no control for settings (e.g. integration time, gain, gamma) and no auto-iris connector.
- The video signal did not have a fixed frame rate of 25 frames/s. Subsequent video frames were often identical, which lead to problems in meteor detection and velocity determination.

After Sirko provided his feedback, Dmitrii soon presented an improved camera with a new firmware version, and a few days ago Sirko received the new camera version for testing. Since Sirko had hardly any clear skies since then, he could not yet test the camera in detail, but the first results with Dimcam2 are very promising. If we forget the auto-iris connector for a moment, all teething problems are cured. The image is not distorted anymore, the frame rate is fixed at 25 resp. 30 frames/s, and Computar lenses can now be mounted including the aberration filter and this improves the image quality (Figure 2, right). The limiting magnitude increased by 0.3 magnitude and now matches the image-intensified camera Avis2. The field of view, however, has reduced by about 1/3 to 970 square degrees, since the image has to be clipped at the left and right side to obtain an undistorted 4:3 aspect ratio. Last but not least, the camera got an OSD control to adjust different parameters (PAL/NTSC, gain, integration time, zoom, ...).

In short – the new camera fits excellent to the requirement of video meteor observers and is a dignified successor of Mintron and Watec. It is not only more sensitive, but with a price below 150€ also clearly cheaper.

Unfortunately, there is a problem in providing the modified camera commercially, since the manufacturer of the electronics will offer building components only in larger quantities. Hence, Dmitrii is investigating an alternative camera with smaller sensor, but roughly similar parameters. For urgent cases, he still has a handful of original cameras with new firmware available. Alternatively you may buy the "RunCam Night Eagle 2 Pro Astro Edition" which has the same CMOS sensor and firmware as the test camera. However, then you have to solve the camera housing and the mounting of c-mount lenses on your own.

Figure 2 – Meteors in Orion, recorded with Dimcam1 (left) and Dimcam2 (right). Both cameras were equipped with an identical 8-mm $f/0.8$ Computar lens.

References

Carroll J. (2015). "Sony rumored to discontinue production of CCD sensors". https://www.vision-systems.com/articles/2015/03/sony-rumored-to-discontinue-production-of-ccd-sensors.html .

Handling Editor: Javor Kac

Table 2 – Observers contributing to 2018 February data of the IMO Video Meteor Network. Eff.CA designates the effective collection area; the overall number of nights is the number of nights with at least one camera operating, the overall observing time and number of meteors are sums over all cameras.

Code	Name	Location	Camera	FOV [°²]	Stellar LM [mag]	Eff.CA [km²]	Nights	Time [h]	Meteors
ARLRA	Arlt	Ludwigsfelde/DE	Ludwig2 (0.8/8)	1475	6.2	3779	23	167.5	529
BIATO	Bianchi	Mt. San Lorenzo/IT	Omsl1 (1.2/4)	6435	4.0	1705	7	11.2	75
BOMMA	Bombardini	Faenza/IT	Mario (1.2/4.0)	5794	3.3	739	13	75.1	196
BREMA	Breukers	Hengelo/NL	Mbb3 (0.75/6)	2399	4.2	699	16	160.7	237
BRIBE	Klemt	Herne/DE	Hermine (0.8/6)	2374	4.2	678	2	10.9	18
		Bergisch Gladbach/DE	Klemoi (0.8/6)	2286	4.6	1080	20	187.7	353
CARMA	Carli	Monte Baldo/IT	Bmh2 (1.5/4.5)*	4243	3.0	371	16	111.6	395
CASFL	Castellani	Monte Baldo/IT	Bmh1 (0.8/6)	2350	5.0	1611	12	86.4	164
CINFR	Cineglosso	Faenza/IT	Jenni (1.2/4)	5886	3.9	1222	14	24.3	169
CRIST	Crivello	Valbrevenna/IT	Arci (0.8/3.8)	5566	4.6	2575	17	119.4	265
			Bilbo (0.8/3.8)	5458	4.2	1772	16	117.7	247
			C3P8 (0.8/3.8)	5455	4.2	1586	15	99.2	177
			Stg38 (0.8/3.8)	5614	4.4	2007	17	124.8	308
ELTMA	Eltri	Venezia/IT	Met38 (0.8/3.8)	5631	4.3	2151	9	67.0	130
FORKE	Förster	Carlsfeld/DE	Akm3 (0.75/6)	2375	5.1	2154	17	158.0	326
GONRU	Goncalves	Foz do Arelho/PT	Farelho1 (0.75/4.5)	2286	3.0	208	21	153.6	86
		Tomar/PT	Templar1 (0.8/6)	2179	5.3	1842	23	218.9	589
			Templar2 (0.8/6)	2080	5.0	1508	22	214.7	441
			Templar3 (0.8/8)	1438	4.3	571	20	194.8	210
			Templar4 (0.8/3.8)	4475	3.0	442	22	209.2	455
			Templar5 (0.75/6)	2312	5.0	2259	23	193.8	373
GOVMI	Govedič	Središče ob Dravi/SI	Orion2 (0.8/8)	1447	5.5	1841	11	56.5	53
			Orion4 (0.95/5)	2662	4.3	1043	4	4.0	8
HERCA	Hergenrother	Tucson/US	Salsa3 (0.8/3.8)	2336	4.1	544	21	202.1	288
HINWO	Hinz	Schwarzenberg/DE	Hinwo1 (0.75/6)	2291	5.1	1819	23	187.8	305
IGAAN	Igaz	Budapest/HU	Hupol (1.2/4)	3790	3.3	475	9	30.9	20
JONKA	Jonas	Budapest/HU	Husor (0.95/4)	2286	3.9	445	8	42.1	44
			Husor2 (0.95/3.5)	2465	3.9	715	5	29.9	29
KACJA	Kac	Kamnik/SI	Cvetka (0.8/3.8)*	4914	4.3	1842	5	21.4	38
			Rezika (0.8/6)	2270	4.4	840	6	25.0	63
			Stefka (0.8/3.8)	5471	2.8	379	4	20.9	31
		Kostanjevec/SI	Metka (0.8/12)*	715	6.4	640	12	48.9	87
KOSDE	Koschny	La Palma/ES	Icc9 (0.85/25)*	683	6.7	2951	2	10.5	83
			Lic2 (3.2/50)*	2199	6.5	7512	3	6.8	60
LOJTO	Łojek	Grabniak/PL	Pav57 (1.0/5)	1631	3.5	269	8	62.4	172
MACMA	Maciejewski	Chełm/PL	Pav35 (0.8/3.8)	5495	4.0	1584	10	34.7	40
			Pav36 (0.8/3.8)*	5668	4.0	1573	13	59.5	86
			Pav43 (0.75/4.5)*	3132	3.1	319	8	36.9	25
			Pav60 (0.75/4.5)	2250	3.1	281	12	61.8	73

Table 2 – Observers contributing to 2018 February data of the IMO Video Meteor Network – continued from previous page.

Code	Name	Location	Camera	FOV [°²]	Stellar LM [mag]	Eff.CA [km²]	Nights	Time [h]	Meteors
MARRU	Marques	Lisbon/PT	Cab1 (0.75/6)	2362	4.8	1517	27	233.5	502
			Ran1 (1.4/4.5)	4405	4.0	1241	23	212.6	445
MOLSI	Molau	Seysdorf/DE	Avis2 (1.4/50)*	1230	6.9	6152	22	141.2	675
			Escimo2 (0.85/25)	155	8.1	3415	17	148.2	149
			Mincam1 (0.8/8)	1477	4.9	1084	20	134.5	415
		Ketzür/DE	Remo1 (0.8/8)	1467	6.5	5491	21	157.3	573
			Remo2 (0.8/8)	1478	6.4	4778	21	162.0	608
			Remo3 (0.8/8)	1420	5.6	1967	21	174.0	386
			Remo4 (0.8/8)	1478	6.5	5358	22	175.7	634
MORJO	Morvai	Fülöpszállás/HU	Huful (1.4/5)	2522	3.5	532	10	68.0	48
MOSFA	Moschini	Rovereto/IT	Rover (1.4/4.5)	3896	4.2	1292	16	81.3	105
NAGHE	Nagy	Piszkéstető/HU	Hupis (0.8/3.8)	5615	4.0	1524	2	1.8	7
OCHPA	Ochner	Albiano/IT	Albiano (1.2/4.5)	2944	3.5	358	4	23.3	12
OTTMI	Otte	Pearl City/US	Orie1 (1.4/5.7)	3837	3.8	460	11	59.7	65
PERZS	Perkó	Becsehely/HU	Hubec (0.8/3.8)*	5498	2.9	460	7	26.9	77
ROTEC	Rothenberg	Berlin/DE	Armefa (0.8/6)	2366	4.5	911	19	156.3	152
SARAN	Saraiva	Carnaxide/PT	Ro1 (0.75/6)	2362	3.7	381	24	210.3	207
			Ro2 (0.75/6)	2381	3.8	459	24	215.6	400
			Ro3 (0.8/12)	710	5.2	619	25	220.3	427
			Ro4 (1.0/8)	1582	4.2	549	24	200.9	124
			Sofia (0.8/12)	738	5.3	907	23	173.6	235
SCALE	Scarpa	Alberoni/IT	Leo (1.2/4.5)*	4152	4.5	2052	13	61.3	77
SCHHA	Schremmer	Niederkrüchten/DE	Doraemon (0.8/3.8)	4900	3.0	409	24	203.5	338
SLAST	Slavec	Ljubljana/SI	Kayak1 (1.8/28)	563	6.2	1294	2	5.1	6
			Kayak2 (0.8/12)	741	5.5	920	1	1.4	1
STOEN	Stomeo	Scorze/IT	Min38 (0.8/3.8)	5566	4.8	3270	16	80.7	284
			Sco38 (0.8/3.8)	5598	4.8	3306	17	83.5	267
STRJO	Strunk	Herford/DE	Mincam2 (0.8/6)	2354	5.4	2751	23	193.5	597
			Mincam3 (0.8/6)	2338	5.5	3590	22	162.4	190
			Mincam4 (0.8/6)	2306	5.0	1412	20	149.6	187
			Mincam5 (0.8/6)	2349	5.0	1896	22	192.5	375
			Mincam6 (0.8/6)	2395	5.1	2178	21	165.4	293
TEPIS	Tepliczky	Agostyán/HU	Huago (0.75/4.5)	2427	4.4	1036	15	87.8	98
			Humob (0.8/6)	2388	4.8	1607	9	50.3	66
WEGWA	Wegrzyk	Nieznaszyn/PL	Pav78 (0.8/6)	2286	4.0	778	14	75.4	96
YRJIL	Yrjölä	Kuusankoski/FI	Finexcam (0.8/6)	2337	5.5	3574	13	116.3	151
ZAKJU	Zakrajšek	Petkovec/SI	Tacka (0.8/12)	714	5.3	783	11	56.6	45
* active field of view smaller than video frame						Overall	28	8 310.9	16 565

The International Meteor Organization

www.imo.net

Follow us on Facebook InternationalMeteorOrganization

Follow us on Twitter @IMOMeteors

Council

President: Cis Verbeeck,
Bogaertsheide 5, 2560 Kessel, Belgium.
e-mail: cis.verbeeck@scarlet.be

Vice-President: Juraj Tóth,
Fac. Math., Phys. & Inf., Comenius Univ.,
Mlynska dolina, 84248 Bratislava, Slovakia.
e-mail: toth@fmph.uniba.sk

Secretary-General: Robert Lunsford,
14884 Quail Valley Way, El Cajon,
CA 92021-2227, USA. tel. +1 619 755 7791
e-mail: lunro.imo.usa@cox.net

Treasurer: Marc Gyssens, Heerbaan 74,
B-2530 Boechout, Belgium.
e-mail: marc.gyssens@uhasselt.be
BIC: GEBABEBB
IBAN: BE30 0014 7327 5911
Bank transfer costs are always at your expense.

Other Council members:

Megan Argo, Jodrell Bank Centre for Astrophysics,
Alan Turing building, University of Manchester,
Oxford Road, Manchester, M13 9PL, UK.
e-mail: megan.argo@gmail.com

Javor Kac (see details under WGN)

Detlef Koschny, Zeestraat 46,
NL-2211 XH Noordwijkerhout, Netherlands.
e-mail: detlef.koschny@esa.int

Masahiro Koseki, 4-3-5 Annaka, Annaka-shi,
Gunma-ken 379-0116, Japan.
e-mail: geh04301@nifty.ne.jp

Sirko Molau, Abenstalstraße 13b, D-84072 Seysdorf,
Germany. e-mail: sirko@molau.de

Jean-Louis Rault, Société Astronomique de France,
16, rue de la Vallée, 91360 Epinay sur Orge,
France. e-mail: f6agr@orange.fr

Jürgen Rendtel, Eschenweg 16, D-14476 Marquardt,
Germany. e-mail: jrendtel@aip.de

Paul Roggemans, Pijnboomstraat 25, 2800 Mechelen,
Belgium, e-mail: paul.roggemans@gmail.com

Galina Ryabova, Res. Inst. of Appl. Math. & Mech.,
Tomsk State University, Lenin pr. 36, build. 27,
634050 Tomsk, Russian Federation.
e-mail: ryabova@niipmm.tsu.ru

Damir Šegon, J. Rakovca 3, 52100 Pula, Croatia.
e-mail: damir.segon@pu.t-com.hr

Commission Directors

Visual Commission: Rainer Arlt (rarlt@aip.de)
Generic e-mail address: visual@imo.net
Electronic visual report form:
http://www.imo.net/visual/report/electronic

Video Commission: Sirko Molau (video@imo.net)

Photographic Commission: Bill Ward
(William.Ward@glasgow.ac.uk)
Generic e-mail address: photo@imo.net

Radio Commission: Jean-Louis Rault (radio@imo.net)

Fireballs: Online fireball reports:
http://fireballs.imo.net

Outreach Officer

Jure Atanackov, e-mail: jureatanackov@gmail.com

Webmaster

Karl Antier, e-mail: webmaster@imo.net

WGN

Editor-in-chief: Javor Kac
Na Ajdov hrib 24, SI-2310 Slovenska Bistrica,
Slovenia. e-mail: wgn@imo.net;
include METEOR in the e-mail subject line

Editorial board: Ž. Andreić, M. Argo, D.J. Asher,
F. Bettonvil, J. Correira, M. Gyssens,
C. Hergenrother, T. Heywood, J.-L. Rault,
J. Rendtel, C. Verbeeck, S. de Vet, D. Vida.

IMO Sales

Available from the Treasurer or the Electronic Shop on the IMO Website	€	$
IMO membership, including subscription to WGN Vol. 47 (2019)		
Surface mail	26	32
Air Mail (outside Europe only)	49	60
Electronic subscription only	21	25
Proceedings of the International Meteor Conference on paper		
1990, 1991, 1993, 1995, 1996, 1999, 2000, 2002, 2003, per year	9	12
2007, 2010, 2011, per year	15	20
2012, 2013, 2014, 2015 per year	25	34
Proceedings of the Meteor Orbit Determination Workshop 2006	15	20
Radio Meteor School Proceedings 2005	15	20
Handbook for Meteor Observers	15	20
Meteor Shower Workbook	12	16
Electronic media		
Meteor Beliefs Project ZIP archive	6	8

2019 total lunar eclipse fireball

A magnitude -5 sporadic fireball that fell during the totality of the Moon eclipse on 2019 January 21 at $06^{\mathrm{h}}18^{\mathrm{m}}$ CET. It was photographed from the Plose mountain near Brixen, South Tyrol (Italy), at 2010 m above sea level, using Canon EOS 20Da at ISO 800, $t = 15$ s, with a Sigma zoom lens 3.5/10-20 mm, at $f = 20$ mm and $F = 4.5$. Photo courtesy: Peter C. Slansky.